وزارة التعليم العالي والبحث العلمي

BADJI-MOKHTAR-ANNABA UNIVERSITY
UNIVERSITE BADJI-MOKHTAR-ANNABA

جامعة باجي مختار- عنابة

Faculte des sciences de l'ingenieur **Annee 2006**

Departement de Genie Civil

THESE

Presentee en vue de l'obtention du diplome de DOCTORAT D'ETAT

COMPORTEMENT D'UNE ARGILE AU TRIAXIAL STANDARD SOUS CHARGEMENT MONOTONIQUE ET CYCLIQUE "APPLICATION AUX OUVRAGES DE SOUTENEMENT FLEXIBLE"

Option

Geotechnique

Par

MUSTAPHA HIDJEB

ENCADREUR :	**AHMED BOUMEKIK**	**Professeur**	**Universite de Constantine**

DEVANT LE JURY

PRESIDENT :	**M.F HABITA**	**Professeur**	**Universite de Annaba**
EXAMINATEURS :	**Y HADIDANE**	**M.Conference**	**Universite de Annaba**
	L MOKRANI	**M.Conference**	**Universite de Setif**
	A BELOUAR	**M.Conference**	**Universite de Constantine**

ACKNOWLEDGEMENTS

The author wishes to express his gratitude to Pr A.Boumekik

to whom he is indebted for his guidance and help during

his supervision of this work..

RESUME

THESE PRESENTEE
POUR LE DIPLOME DE DOCTORAT D'ETAT

Titre **:**

LE COMPORTEMENT DES OUVRAGES DE SOUTENEMENT SOUS L'EFFET DE CHARGEMENT CYCLIQUE

Auteur **:**

HIDJEB MUSTAPHA

Institution **:**

UNIVERSITE BADJI MOKHTAR - ANNABA

1 PROBLEMATIQUE

Les ouvrages de soutènement sont souvent soumis à des sollicitations cycliques.

Leur comportement dépend principalement du comportement du sol se trouvant de part et d'autre de l'ouvrage. Dans cette recherche, nous avons opté pour une approche expérimentale.

En effet, nous avons procèdé, en laboratoire, à la caractérisation de l'argile sous chargement monotonique et sous chargement cyclique.

Dans la deuxième partie de cette recherche nous avons, par la méthode des éléments finis et en utilisant le modèle Mohr- coulomb, étudié le comportement d'un rideau de palplanches avec butons soutenant les parois d'une grande excavation.

L'effet du chargement cyclique sur le comportement du rideau de palplanche est étudié en comparant le comportement d'un rideau, réalisé dans une argile dont les caractéristiques mécaniques ont été obtenues par chargement monotonique, au comportement du même rideau de palplanche, réalisé dans la même argile, mais dont les caractéristiques mécaniques ont été obtenues par chargement cyclique.

2 PRESENTATION DU SUJET

La recherche exposée dans cette thèse a pour objet l'étude du comportement des ouvrages de soutènement sous l'effet de chargement cyclique.

Sachant que celui ci dépend principalement du comportement du sol se trouvant de part et d'autre de l'ouvrage nous avons procédé à une étude expérimentale de ce sol.

Des échantillons ont été soumis à un chargement triaxial monatonique alors que d'autres ont été soumis à un chargement triaxial cyclique. Ces derniers ont alors été à leurs tour soumis à un chargement monotonique.

Cette approche expérimentale permet de déterminer l'effet du chargement cyclique sur la résistance résiduelle au cisaillent du sol d'une part et d'autre part son effet sur certains paramètres telle la cohésion et l'angle de frottement interne de l'argile.

La deuxième partie de cette thèse sera consacrée à une étude paramétrique du comportement d'un rideau de palplanche soutenant une excavation profonde.
L'influence de la variation de la cohésion interne C' sera examinée.

Le chapitre1 présente une étude bibliographique sur les différents facteurs influants sur le comportement de l'argile (vitesse de chargement, pression interstitielle, mode de chargement, fréquence, etc.…).

Le chapitre 2 est consacré à la description du dispositif d'essai : appareillage utilisé, échantillon de sol et mode opératoire. L'étude expérimentale nécessite l'utilisation de 2 appareils triaxiaux : l'un statique et l'autre cyclique, sous condition non-drainée avec mesure de la pression interstitielle.

Le chapitre 3, pressente sous forme de courbe les résultats d'essais concernant :
- 8 essais triaxiaux sous chargement monotonique en mode déplacement contrôlé (quatre en compression et quatre en traction)
- 12 essais triaxiaux sous chargement cyclique en mode chargement contrôlé
- 9 essais triaxiaux sous chargement monotonique en compression en mode déplacement contrôlé.

L'analyse et l'interprétation de ces résultats ont montré que le comportement cyclique de l'argile est caractérisé :
- A la rupture, la résistance au cisaillement est inversement proportionnelle au nombre de cycle
- La résistance en traction et en compression est pratiquement similaire.
- Les courbes de chemin de contrainte (p,q) s'éloignent de l'origine sauf pour le premier cycle où le phénomène inverse est observé.

Des essais en chargement monotonique ont été effectués sur des échantillons ayant déjà subit un chargement cyclique, dans le but de caractériser l'effet du chargement cyclique sur la cohésion, l'angle de frottement interne et la résistance au cisaillement.

Les résultats obtenus ont été exploités au chapitre 4 pour analyser le comportement d'un rideau de palplanches par simulation en éléments finis sur le logiciel Plaxis en utilisant le modèle de rupture Mohr-Coulomb.
La comparaison des courbes de réponse pour les 2 cas de chargement a permis de mettre en évidence l'effet sur l'ouvrage du comportement cyclique du sol par rapport au comportement monotonique :
- réduction des zones de déformation plastique
- une diminution des déformations verticales (tassement en amont du rideau et soulèvement en fond de fouille).
- une diminution des déplacements horizontaux du rideau
- à l'exception des zones situées aux extrémités, il y'a diminution des moments fléchissants sollicitant le rideau.

Mots clés : Rideau de palplanche, argile, résistance au cisaillement, chargement cyclique.

ABSTRACT

THESIS SUBMITTED
FOR DOCTORAT D'ETAT DEGREE

Title**:**

THE BEHAVIOUR OF RETAINING STRUCTURES UNDER CYCLIC LOADING

Author:

HIDJEB MUSTAPHA

Institution:

BADJI MOKHTAR UNIVERSITY-ANNABA

In the present work the behaviour of retaining structures under cyclic loading is investigated.

The case of sheet pile wall in deep excavation in clay was considered.

An important question in design problems is the static strength possessed by the soil following a cyclic disturbance. Cyclic loading of soil samples may result in softening so that the stress-strain properties are altered.

To investigate this, samples (used for cyclic loading) were reloaded statically under displacement controlled conditions to determine any strength loss caused by cyclic loading

Therefore the stress-strain strength behaviour of clay under cyclic loading has been receiving increasing attention in recent years. Earthquake loading induces cyclic shear and normal stresses in the soil on both sides of the sheet pile retaining walls of the excavations.

Compared to thee monotonic loading, under earthquake loading drainage paths for excess pore pressure dissipation in clay of the deep excavation are comparatively long.

Considerable excess pore water pressure may develop as a result. Accordingly it is reasonable and conservative to assume completely undrained conditions.

In the second part of this work an analysis of the behaviour of the sheet pile supporting the walls of the excavation, has been carried out.

The results obtained from the experimental investigation were used in a finite element simulation using commercial software (Plaxis). Mohr- Coulomb model was used

Key words: Retaining structures, clay, shear strength, cyclic loading.

Content

NOTATION

A Skempton's parameter for changes in pore pressure due to changes in deviatoric stresses.

B Skempton's pore pressure parameter for changes in pore pressure due to changes in ambient stresses.

B_B,B_M Skempton's pore pressure parameter calculated from base and mid- height pore pressure measurements.

C' Effective cohesion intercept.

C_u Undrained shear strength from slow monotonic tests.

C_v Coefficient of vertical consolidation.

C_F Clay fraction (D = particle diameter < 0.002mm)%.

D Deviatoric stress.

F Frequency

E_S Secant modulus. It is the ratio of the maximum applied tensile or compressive shear stress to the corresponding developed amount of axial strain.

LL Liquid limit.

N Number of cycles.

OCR Apparent overconsolidation ratio**:** P_{mean} (œd)/ σ_o'

P_{mean} œdometer mean total stress: (P+ $2k_oP$)1/3

P final œdometer pressure prior to sampling.

k_o Coefficient of lateral earth pressure at rest.

U_B,U_M Pore pressure measured at the base and mid-height of the sample.

U_{Bo}, U_{Mo} Initial base and mid-height pore pressure respectively. They are Measured under isotropic total stress conditions immediately prior to testing.

ΔU_B, ΔU_M Excess pore pressure measured at the base and mid-height of the sample .

U_{MC} Mid pore pressure corrected for the variation in mean total stress by a factor of –D/3 in compression and D/3 in tension.

U_{BC} Base pore pressure corrected for the variation in mean total stress by a factor of –D /3 in compression and D/3 in tension.

ΔU_{MC} Excess mid pore pressure corrected for the variation in mean total stress.

by a factor of –D/3 in compression and D/3 in tension.

ΔU_{BC} Excess base pore pressure corrected for the variation in mean total stress. by a factor of –D/3 in compression and D/3 in tension.

ΔU $\Delta U_M - \Delta U_B$

σ'_{ax} Axial effective stress.

σ'_{lat} lateral effective stress.

σ_1' Major principal effective stress.

σ_2' Intermediate principal effective stress.

σ_3' Minor principal effective stress.

σ_1 Major principal total stress.

σ_2 Intermediate principal total stress.

σ_3 Minor principal total stress in triaxial compression it is equal to the cell pressure.

ϵ_A Axial strain.

ϵ_{dA} Double amplitude axial strain: $\epsilon_{dA} = \epsilon_{Amax} - \epsilon_{Amin}$

τ Shear stress.

τ/Cu Cyclic total stress ratio.

τ/σ_o' Cyclic effective stress ratio.

σ_o' Initial effective stress calculated from initial mid pore pressure.

σ_v Œdometer vertical total stress.

σ_L Œdometer lateral total stress.

ϵ_{Ap} Permanent or residual axial strains (i.e. axial strain that remains at the end of each unloading).

$\Delta\sigma_3$ Change in the minor principal total stress. In triaxial compression testing it is equal to the change the cell pressure

$\Delta\sigma_1$ Change in the major principal total stress.

Φ' Maximum angle of shearing resistance with respect to effective stress.

Subscripts

max: maximum

min: minimum

Figures

Tables

+
+

General Introduction

The aim of the present work is to assess the behaviour of retaining structures under cyclic loading.

To investigate this, the case of a sheet pile wall in a deep excavation in clay was considered.

An important question in design problems is the static strength possessed by the soil following a cyclic disturbance. Cyclic loading of soil samples may result in softening so that the stress-strain properties are altered.

To investigate this, samples (used for cyclic loading) were reloaded statically under displacement- controlled conditions to determine any strength loss caused by the cyclic loading.

It is widely recognised that the behaviour of soil subjected to cyclic loading differs from that associated with monotonic loading.

Thus it is impossible to predict the quantitative behaviour of any soil under cyclic loading from the results of conventional loading tests.

Therefore the stress-strain strength behaviour of clays under cyclic loading has been receiving increasing attention in recent years. Earthquake loading induces cyclic shear and normal stresses in the soil on both sides of a sheet pile retaining walls of deep excavations.

Depending upon the drainage conditions, there will usually be either a volume decrease or a generation of excess pore pressure if the volume changes are delayed or prevented, due to long drainage paths or if the loading imposes high shear stresses or high frequencies.

Compared to the monotonic loading, under earthquake loading the drainage paths for excess pore pressure dissipation in clay of a deep excavation are comparatively long. Considerable excess pore water pressure may develop as a result. Accordingly, it is reasonable and conservative to assume completely undrained conditions

It is also accepted that the failure of clay under reversed triaxial cyclic loading is a consequence of accumulating strains and pore water pressure.

Although accurate pore water pressure measurements are of paramount importance for a better understanding of the behaviour of clay under cyclic loading, few studies of clay soils have included accurate measurement of pore water pressure, because of the low permeability of clays and the corresponding long response time for pore water pressure measurement.

In the present investigation, load- controlled cyclic triaxial tests on undrained samples of Cowden clay were carried out. In order to gain some understanding of the fundamental behaviour of the saturated clay in terms of effective stresses, the acquisition of accurate pore pressure measurements throughout each cycle has been one of the major objectives of this investigation.

For this purpose a low frequency of approximately 1cycle/hour has been used and, as well as the Bell and Howell transducer which was used for base pore pressure measurements, a miniature pressure transducer mounted at mid-height of the specimens, was used for mid-height pore water pressure.

In the second part of this work and in order to study the behaviour of a sheet pile wall supporting a deep excavation has been carried out.

The results obtained from the experimental investigation were used in a finite element simulation using commercial software (Plaxis). Mohr-Coulomb model was used.

CHAPTER 1

LITERATURE REVIEW

1.1 Monotonic tests

1.1.1 Rate effects on shear strength

In 1846 a French engineer, A. Collin, as reported by Schimming et al (1966) (1) recognised the time-dependent nature of soil strength. He made reference to “instantaneous” and “permanent” soil strengths, which he defined respectively as the resistance to temporary forces with duration less than 30 seconds and permanent forces not significantly altered after a considerable lapse of time. Collin used a double shear device and observed that permanent strength of clay may be in the range 24% to 34% of the instantaneous strength.

Since 1948, When Casagrande and Shannon (2) initiated a study of soil dynamics, the number of investigators with interests in the effects of rate of loading on soils has grown considerably.

The work carried out at M.I.T, and Harvard University from 1943 to 1964 by Casagrande and Shannon (1948) (3), Taylor et al (1953), and others as reported by B. schimming et al (1966) (1) show that all cohesive soils display an increase in the applied strain rate.

Bjerrum, Simon et al (1958) (4), performed several series of consolidated undrained triaxial tests with pore pressure measurements on Fornebu clay, with strain rates varying from 1.66to 0.00006 %.

They observed that the maximum deviator stress decreased with increasing time to failure and there was a corresponding reduction in the true angle of internal, friction. They concluded that the decrease of strength must partly be a result of this reduction as the rate of

loading decreased. They also concluded that increase in pore pressure at failure with time may also be partly responsible for the decrease in shear strength.

Crawford (1959) (5) performed several strain-controlled triaxial compression tests with pore pressure measurements on undisturbed samples of sensitive marine clay, with times to failure varying from 6 to 600 minutes. He found that these tests demonstrated a significant influence of the strain rate on deviator stress and that the angle of shearing resistance in terms of effective stress increased from 17.5° to 23° as time to failure increased and that the cohesive intercept decreased at the same time.

Anderson et al (1980) (6) carried out a series of undrained strain-controlled monotonic triaxial tests on an undisturbed plastic marine clay (Drammen clay) at a strain rate of 0.05 %/min. They reported that although the undrained shear strength of the Drammrn clay in tension was only 50% to 60% of the compression strength, the effective stress parameters C' and Ø' were approximately the same. They suggested that this difference in undrained strengths may be the result of the anisotropic preconsolidation and the different stress paths.

Craig (1982) (7), conducted a series of undrained triaxial compression tests on saturated remoulded Derwent clay using lubricated end platens and constant rates of load increase.

By plotting the results in terms of time to failure, and taking 100 minutes as a base, he observed a linear relation between strength and the logarithm of time to failure (between 0.002 and 270 minutes) and that a ten-fold decrease in time to failure caused a % increase in shear strength. He also reported that, for strain-controlled tests, the increase in shear strength could be as much as 10%, or higher.

Mokrani (1983) (8) conducted a series of load and displacement-controlled triaxial tests on Derwent and Cowden clays. From Mokrani's results, the following results can be made:

- Load controlled tests: decreasing time to failure from 16300 to 0.23 seconds caused about a 34 % increase in the maximum deviator stress of the Derwent clay, while decreasing time to failure from 14210 to 0.1 seconds caused about 45% increase in the maximum deviator stress of the Cowden clay.
- Displacement-controlled tests: For Cowden clay decreasing the time to failure from 8410 to 18.22 seconds caused about 12 % increase in the maximum deviator stress.

Mokrani suggested that the observed difference in strength between load and displacement-controlled tests may, in part, be due to the fact that under load control the specimen experiences an accelerating rate as failure is approached, which increase the strength, while in a displacement-controlled test, the stress rate is kept constant throughout the duration of the test.

While it is evident that the most obvious way of examining the influence of strain rate on undrained shearing resistance is to perform tests on identically prepared samples at different controlled strain rates, the time requirement associated with slow rates of testing is of a major inconvenience. To overcome this problem, two other methods of testing can be introduced.

A – step-changing procedure: Richardson and Whitman (1983) (9) introduced this technique in which the strain rate applied to a sample is step-changed during a test.

Each strain rate would be applied only long enough to establish the stress-strain relationship for that stage of the test. They reported that the stress-strain curves from step-changing procedures on remoulded samples do not agree precisely with results from constant rate tests.
However, they suggested that these errors should be no more serious than those arising from the non-homogeneity of natural soils.

B – Kenny (1966), as reported by Graham (1983) (10) developed the step-changing and relaxation method suitable for the determination of the strain rate effect from a single sample. The difference between the two methods is that the sample tested with the second method would go through a period a relaxation after each strain rate application.

Graham et al (1983) (10) used the step-changing and relaxation method to perform triaxial compression and extension tests as well as simple shear tests on slightly overconsolidated post-glacial clays.
They reported a linear relation between strength and logarithm of rate. They also reported that undrained shear strengths decrease with decreasing logarithm of strain rate.

L.Callisto et al (1998) (11) performed triaxial and true triaxial tests on Pisa clay. The samples were subjected to drained triaxial stress paths. They observed that stiffness was strongly dependent on the direction of the stress path.

1.1.2 Rate effects on pore pressure behaviour

Crawford (1959) (5) reported that there was a significant influence of the strain rate on pore water pressure at failure, and that the high pore pressure in a slow test may be due to a secondary consolidation effect because more time was allowed for "structural breakdown ". He added that a number of tests in which the deviator stress was held constant for several hours in which the strain was held constant were carried out. He reported that under constant deviator stress the pore pressure continued to rise, whereas under a constant strain condition, the pore pressure decreased. He concluded that pore pressures are dependent on strain and may be considerably influenced by sample disturbance and isotropic conditions.

Discussing the data reported by M.I.T and Harvard University, Whitman (1960) (12) suggested that as rate increases, gradients of pore water pressure will be set up within the undrained triaxial samples.

Thus, the pore water pressure within the central zone may be time dependent. He also suggested that the mineral may, under rapidly applied loads, have a resistance to compression approaching that of water. Such behaviour, he concluded, would be the result of structural viscosity. If so, he continued, then the excess pore water pressures set up during undrained shear in soft saturated soils would decrease as the strain rate increases.

1.2 Cyclic loading tests

1.2.1 Introduction

The behaviour of clay subjected to cyclic loading is imported in the foundation design of offshore gravity platforms.

Wave action on a platform causes a great number of large cyclic horizontal forces and moments which are transmitted to and carried by the soil foundation.

Extensive programs of laboratory tests have been carried out by numerous researchers such as Bjerrum (1973) (13), Anderson et al (1976, 1980) (14, 6) to study the effects of cyclic loading on small elements of clay in the triaxial and simple shear apparatus.

They found that the behaviour of clay depends upon a wide range of factors, including the type of test, wave form, frequency, number of cycles and tress history.

Two types of stress-controlled loading are encountered in the literature of triaxial cyclic loading on clay, namely with:-cyclic testing with and without re-orientations of the principal axes (i.e. reversed and repeated cyclic testing).

Repeated cyclic loading involves triaxial cyclic testing where the axial deviator stress is always compressive and is cycled between a lower (usually zero) and an upper limit. This type of test is considered to be appropriate to problems related to pavement subgrades and earthquake effects.

A better simulation of wave action on off-shore structures may be obtained by performing reversed cyclic triaxial tests. By subjecting triaxial specimens to an alternating compression /tension deviator stress, the major principal stress rotates through 90°, i.e. the direction of the major and minor principal stresses change position in each cycle. Rate effects are also observed in cyclic loading tests. However, it is believed that rate effects are much more important in reversed cyclic tests than in one-way loading (compression only) tests.

1.2.2 Effect of cyclic stress ratio τ/c_u

For comparative purposes it has been found convenient to express the cyclic loading stress as a ratio of the undrained station compression strength of the soil. Researchers have found that the larger the cyclic stress ratio, the lower the number of cycles required to induce failure.

The failure criterion is generally based on specified cyclic strain amplitude.

Craig (1982) (7) observed that progressively faster rates of testing result in increasing undrained shear strength due to viscosity effects.

By using Khaffaf's work (1978) (14) on Derwent clay, he showed that there is a difference in interpretation of the results of cyclic tests at different frequencies when using a unique C_u measured in a compression test carried out at a strain rate of about 0.1%/min, and when using strengths obtained from monotonic compression tests with different times to failure.

Craig reported that using a unique value for C_u is inconsistent with considerations of rate effects associated with changes in cyclic loading frequency. To justify his argument he reported Khaffaf's data on Derwent clay in terms of an adjusted strength $C_u^{[1]}$, where a rate factor of 1.06 obtained from the monotonic compression test with different times was used.

Proctor and Khaffaf (1984) (15) reported the original results at ε_{dA}=5% expressed in terms of a unique c_u. Using a rate factor of 1.06 taken from Craig (1982) (7) and a reference time to failure of 200 minutes, Proctor and Khaffaf presented plots of the ratio τ/c_u versus the number of cycles to failure.

They observed that the curves for the adjusted results are brought closer together despite variations in waveform associated with their pneumatic loading equipment which provides a "degraded square" wave.

1.2.3 Effect of frequency and wave form

The load shape and frequency are two of the many factors which may influence the results of cyclic loading tests.

Seed and Chan (1966) (16) subjected samples of San Francisco Bay mud to reversed rectangular loading at a frequency of 2 Hz.

Thiers and Seed (1969) (17) similarly loaded identical samples at a frequency of 1Hz. Stress-controlled undrained triaxial tests were performed in each case. concluded that the cyclic behaviour is dependent upon frequency

Plotting the cyclic stress ratio versus the number of cycles to failure, they found that decreasing the frequency from 2Hz to 1 Hz causes 20% to 25% reduction in the cyclic strength.

Fisher et al (1976) (18) studied the effects of two different frequencies, 1Hz and 1/15Hz, on reversed cyclic triaxial tests on plastic clay.

They found that the strains in compression were approximately the same, while the strains in extension were different. The specimen tested at 1/15Hz experienced twice as much strain in tension than the specimen tested at 1Hz. Their explanation of this behaviour was based on the anisotropic stress-strain behaviour of the clay tested.

Takahashi et al (1980) (19) reported a series of stress-controlled repeated cyclic tests on low plasticity clay from the lower Cromer Till.

The samples loaded over 450 seconds to the maximum shear stress generated higher pore pressures than those loaded to the maximum shear stress in 50 seconds, so the effective stress path migrated more rapidly towards the failure line. They concluded that the rate of axial strain development showed a corresponding dependence on cyclic period.

Khaffaf (1978) (14) performed reversed load-controlled and strain controlled cyclic triaxial tests on the four different materials listed in Table 1.1.

Table 1.1 Index Properties (Khaffaf 1978)

Soil Characteristics	Soil Type				
	Derwent clay (Soil A)	Derwent clay (Soil B)	Derwent clay (Soil C)	Grimwith Clay (Soil D	Grimwith Clay Original
Liquid limit %	46	34	33	25	38
Plastic Limit %	20	15	15	14	18
Plasticity Index (%)	26	19	18	11	20
Clay Fraction (D< 0.002mm) %	45	30	27	18	33
Activity	0.58	0.63	0.67	0.61	0.61
Sp . gravity of solids	2.68	2.73	2.72	2.61	2.65
C_v (m^2/year) of	0.84	0.93	1.03	3.30	1.10

Remoulded soil σ_v'= 480 kN/m^2					

The frequency ranged between 0.0083Hz and 5Hz. He reported that, for the load-controlled tests on Derwent clay where a "degraded square" was used, increasing the frequency from 0.0083Hz to 1Hz caused approximately 20% increase in cyclic strength for 10% double amplitude axial strain (ϵ_{da}). For controlled tests on Grimwith clay, Khaffaf showed that the higher the frequency, the smaller the strains for any given number of cycles of fixed shear stress $\pm\tau$, resulting in the number of cycles to failure increasing with frequency.

Khaffaf also noted that there was a significant increase in frequency effect with increasing clay fraction which he attributed to the fact that fatter clays demonstrated greater creep strains. For the strain-controlled tests on Derwent clay, he reported that the higher the frequency, the lower the number of cycles required to induce a prescribed cyclic tress level. He also reported that the slight difference in behaviour between strain and load-controlled tests might be due to the different stress-strain paths strength of the two test modes.

A. Thammathiwat et al (2004) (21) carried out a series of triaxial tests on undisturbed specimen of Bangkok clay. They were subjected to cyclic loading under a constant mean total principal stress by varying the frequencies at 0.1Hz, 05Hz and 1.0Hz and cyclic stress ratio at 0.2, 0.25, 0.30, 0.35, and 0.40.

They concluded that a general trend showed that the slow loading tests require longer time to cause failure than the rapid loading test.

1.2.4 Effects of stress history

Khaffaf (1978) (14) compared the behaviour of different types of clay for over-consolidation ratios of 1 and 7.5. This study led Khaffaf to the conclusion that, under a given stress ratio τ/C_U'[2] an over-consolidated clay can sustain a much larger number of cycles before developing a prescribed double amplitude axial strain than a normally-consolidated clay.

Anderson et al (1976) (14) conducted tests on Dramen clay using both simple shear and triaxial apparatus. They reported that over- consolidated clays are more easily deteriorated under cyclic loading than are normally consolidated clays. This observation contradicts that of Khaffaf. The latter suggested that this might be due to different laboratory testing techniques.

Fig 1.1 Effective stress paths for undrained triaxial tests (Andersen 1980)

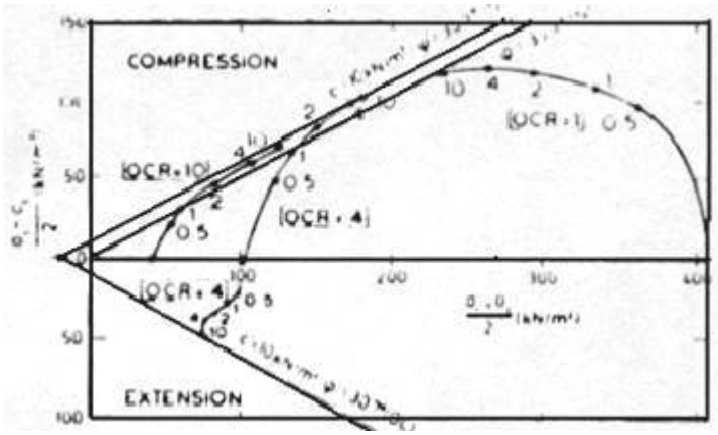

Khaffaf (1178) (14) explained that there are two main techniques for preparing over-consolidated clay. The first, which was used by Anderson et al, consists of consolidating the clay to a common maximum pressure and then unloading it to several different pressures to produce different OCR (s). The specimen with the highest OCR would have the highest moisture content and the lowest undrained shear strength, $C_{U.}$

The second method which was used by Khaffaf followed a different stress path. The samples were consolidated to different pressures and then swelled back to one common minimum pressure, resulting in the fact that the specimen with the highest OCR had the lowest moisture content and the highest undrained shear strength C_U values (for OCR=1, the value of C_U is the minimum).

Khaffaf argued that Andersen's over-consolidated samples deteriorated more easily than normally-consolidated ones because, although he was using the same total stress ratio (τ/C_U), different effective stress ratios (τ/σ_0') were being applied.

A. Thammathiwat et al (2004) (20) observed that the cyclic strength increased substantially as the initial static stress was increased.

1.2.5 Pore water pressure behaviour under cyclic loading

Andersen et al (1976) (14) performed a series of repeated and reversed cyclic loading tests on Drammen clay, using the triaxial and simple shear apparatus. They found that, for normally-consolidated samples, an increase in the water pressure from the first cycle was observed. For over-consolidated Drammen clay, an Initial net negative pore water pressure was observed

It is believed that, under undrained conditions, the normally consolidated clay, although no longer be able to consolidate, would attempt to do so. Such behaviour would result in an equivalent pore water pressure rise and a net positive excess pore water pressure increase prom the first cycle.

On the other hand, for over-consolidated clay the initial application of the cyclic shear stress would result in attempted dilation of the densely packed particles, generating a reduction in the pore water pressure. However, as the cyclic action continues, the clay will attempt to consolidate and, since no volume change is allowed, this would result in a positive water pressure increment superimposed on the initial pore water pressure. This change in the total pore water pressure increment from negative to positive is achieved when the compressive tendency under cyclic action has overcome the dilation of the soil produced on first loading.

Khaffaf (1978) (14) found the net change in pore pressure under a rev-versed cyclic loading is greater than that under repeated cyclic loading.

Koutsoftas (1978) (21) performed a series of reversed cyclic triaxial tests to a prescribed magnitude of double amplitude axial strain on normally and over-consolidated plastic and silty clays of the Holocene age. The cyclic tests were followed by undrained triaxial tests to failure. They found that the excess pore water pressure generated in normally consolidated specimens during the static tests that followed the cyclic tests were larger than those for over consolidated specimens.

Takahashi et al (1980) (20) carried out a series of repeated and reversed cyclic triaxial tests on remoulded low plasticity sandy clay from the Lower Cromer Till. They used a sinusoidal waveform for the reversed cyclic tests and a triangular waveform for the repeated tests.

The pore water pressure was measured by means of a piezometer probe mounted flush with the cylindrical surface at the mid-height of the sample.

The effective stress paths for a reversed cyclic test carried out at a cyclic stress ratio of 0.75 and with a cycle period of 30 minutes. The sample for this test was normally consolidated. The corresponding stress-strain and pore pressure-strain data for cycles 1, 5 and 8 and Plots of the maximum and minimum axial strains and pore water pressures versus the number of cycles.

Takahashi et al suggested that the migration of the effective stress paths towards the origin was a consequence of pore pressure generation.

A. Thammathiwat et Al (2004) (20) observed that excess pore water pressure increased as the number of loading cycles increased.

1.2.6 Effects of cyclic loading upon static shear strength

An increase in pore water pressure softens a clay sample during cyclic loading. The cumulative increase in pore water pressure will cause a reduction in effective stress and, consequently, a reduction in undrained shear strength will recur.

Thiers and Seed (1968) (21) performed a series of reversed cyclic triaxial tests on undrained San Francisco Bay mud. They found that the static strength was reduced by 10% after 200 cycles if cyclic strain (defined as the amount of double amplitude axial strain obtained at a specified stress level and a specified number of cycles) was 3%, but for cyclic strains less than 1.5% the strength was unaffected. They then continued their study on San Francisco Bay mud and observed that, when the peak cyclic strain was less than one half the static failure strain, the static strength after cyclic loading was at least 80% of the original strength.

Andersen et al (1980) (6) investigated the effects of undrained triaxial cyclic loading on Drammen clay by carrying out undrained static tests on samples with “cyclic loading history”. They found that the undrained static strength had, in general, decreased as a result of cyclic loading; the decrease, however, increased with cyclic shear strain and number of cycles. The loss of strength was less than 25% as long as cyclic shear strain was less than ± 3% after 1000 cycles.

Koutsoftas (1978) (21) performed a series of reversed cyclic undrained triaxial tests on two types of marine clay. They found that, for double amplitude cyclic strains less than 4-5%, the loss in undrained shear loading was less than 10%. The reduction in strength was explained by a reduction in the effective stress due to pore water pressure generated during cyclic loading.

Guy Lefebvre et al.(1989) (24) investigated the behaviour under cyclic (repeated) loading, and the post-cyclic static strength of a sensitive clay from the Hudson Bay region. The strain rate and structure effects were also studied by carrying out monotonic and cyclic triaxial tests at both slow and rapid strain rates or frequencies, and at confining pressures

above and below the apparent preconsolidation pressure. The stability threshold for both structured and normally consolidated Grande Baleine clay is about 60–65% of the original undrained shear strength measured at the same strain rate as that used in the repeated loading test. The undrained shear strength and the failure envelope remain essentially unchanged if the repeated preloading is kept below the threshold. The clay structure remains unaltered by this preloading

S.Teachavorasinskun et Al (2002) (25) studied the shear modulus and damping of soft Bangkok clays measured using cyclic triaxial apparatus.

The degradation curves of the equivalent shear modulus fell into the ranges reported in the literature, for clay having similar plasticity. The damping ratios varied from about 4–5% at small strains (0.01%) to about 25–30% at large strains (10%). The effects of load frequency and cyclic stress history on the shear modulus and damping ratio were also investigated. An increase in load frequency from 0.1 to 1.0 Hz had no influence on the shear modulus characteristic, but it did result in a slight decrease in the damping ratio. The effects of the small amplitude cyclic stress history on the subsequently measured shear modulus and damping ratio were almost negligible when the changes in void ratio were taken into account.

A. Thammathiwat et Al (2004) (21) observed because excess pore water pressure increased as the number of loading cycles increased. Consequently the shear resistance decreased; at least until the excess pore water pressure dissipated.

1.3 Conclusion

It can be deduced from the literature, that one of the ways to investigate the behaviour of clay situated behind retaining walls will be an investigation of this soil in a triaxial cell.

The use of the triaxial cell to study the behaviour of clay will be:

a) under undrained monotonic conditions
b) under undrained cyclic conditions

The shear strength of the soil loaded under monotonic conditions of samples already submitted to cyclic loading will be compared to those that have never been submitted to any loading before.

The shear parameters of the clay obtained from the two cases will be used in order two evaluate their effects on the behaviour of the retaining structures of a large excavation.

CHAPTER 2:

TESTING APPARATUS AND TESTING PROGRAM

2.1Testing apparatus

2.1.1 Introduction

The main laboratory equipment used in this research consisted of a conventional 102mm diameter sample triaxial cell, a conventional triaxial loading machine, an electro-servo hydraulic system and a cyclic cell pressure apparatus.

Bell and Howell diaphragm transducers measured cell and base pore water pressure. A miniature Druck transducer was used for mid-sample pore water pressure measurement.

2.1.2 The Triaxial Cell

The circular base of the triaxial cell has a central pedestal on which the specimen is placed. A central ceramic disc, 25mm in diameter and 3mm thick, was fitted into the base platen. The ceramic disc allows the pore water to communicate with the saturated duct in the cell base.

Two highly polished 102mm diameter end platens made of aluminium to reduce the weight of the assembly were used. The bottom platen has a central hole in which the porous ceramic is fitted.

A special end fitted (universal ball joint, which can transmit both tension and compression between the top platen and the end of the load cell but with minimum restraining moment.

The purpose of this rod is to facilitate the remote screw attachment of the load cell with the universal joint on top of the platen.

A collar was fastened around the universal joint from which two small rods protruded. The rods impinging on the vertical rod (screwed to the) prevented rotation of the joint and

allowed screw connection. The main features of the triaxial body are a transparent Perspex cylinder, a top plate and a bottom aluminium annulus.

The assembly is held together with six hollow tie rods. The bottom annulus is sealed against the base by means of a greased O-ring set in the base.

The top-platen has a central metal bearing through which the loading ram passes (to prevent leakage of cell water). Also in the top plate are an air release valve and a hole for the passage of the miniature "Druck" transducer cable.

The load cell, which is made of stainless steel, can transmit an axial load up to 27 kN (equivalent to a deviator stress of about 3450 kN/m^2). For strain gauges connected in a Weatstone Bridge arrangement were sealed in the load cell.

The upper end of the loading ram was designed to screw into a universal joint attached either to the ram of the servo-hydraulic system or to the loading machine.

2.1.3 Lubricated End Platens

To ensure as uniform a distribution of radial strains as possible throughout the sample, frictionless end platens were used Mc Dermott (1965) (26).The platen/specimen interfaces were lubricated by free end, which consisted of thin rubber discs, with a film of high vacuum silicon grease between rubber and plate.

2.1.4 The Electro-Servo hydraulic system

The servo hydraulic system is composed of a hydraulic power supply, an actuator containing both a load cell and L.V.D.T. (Linear variable differential transformer) controlled by a servo valve and an electronic control console. The system can be used either in load or in position control.

A - The actuator and the hydraulic power supply unit

The actuator consists of a cylinder and a piston with a ram that is connected to the sample. Attached to the ram is an L.V.D.T which is an electronic device for position measurement.

B - Electronic control console

- **The mini controller :**

The mini controller provides a compact and flexible method for controlling the servo-hydraulic system. The unit is capable of controlling a simple machine or multi-actuator rigs.

Controls that are required during initial setting up are located on the top of the module and are reached by pulling the complete controller unit forward. A single controller is dedicated to control a single machine offering load or position control.

- **Dynamic function generator:**

The function generator provides the varying component of the signal controlling the hydraulic actuator via the servo-amplifier and servo valve. A variety of wave-forms including sinusoidal, ramp, triangle and square wave may be selected, the frequency and amplitude of which can be set by the operator.

The generator is a digital type and is able to hold any output wave-form for an indefinite period at any point by depressing the hold push button.

Frequency range and selection is basically 0.0001 to 1000 Hz in 7 decades stages by pushbutton control. A 10-turn potentiometer provides overlapping fine frequency control of each range setting

- **Signal channel selector and peak monitor unit**

The signal channel selector contains six pushbuttons to allow selection of up to six controller signals and a toggle switch marked ”input/output” which determines whether the controller input, or conditioned output signal, is displayed. The selector output may be connected to any suitable recording or display device.

- **Time/cycle counter unit**

This electro-mechanical counter counts the cycles from the function generator and can stop the generator when a preset number of cycles has been reached. The counter is capable of counting at up to $f < 20$ Hz, with an accuracy of $\pm$ 1 count.

2.1.5 Conventional Triaxial Loading Machine

Monotonic tests were carried out using a testing machine designed by Wykenham Farrance Ltd.

The main features of the loading machine are a loading frame and a ram driven by an electric motor through a gear box which may be set at 30 different speeds.

2.1.6 The Rotating Mercury Pot system

For the purpose of this research, an apparatus capable of cycling the cell pressure has been designed by the author. The main features of the apparatus were an electric motor, a gear box and a rotating arm holding a self-compensating mercury pot which is connected to a static pot.

The system (mercury pot and arm) is driven by a small electric motor via a gear box. The motor has a constant speed of 0.5 revolution/ minute.

The gear box has four different reduction rates and a neutral position.

The chosen rate of reduction is obtained by means of an external lever.

For further reduction of the speed, a V belt and two pullies with a 2 to 1 diameter ratio were used.

The rotating system consists of a mercury pot and a counterweight.

The mercury pot was hung from a small steel rod, screwed to a movable aluminium block which could be positioned over the full half length of the arm.

The arm was 200cm long and made of aluminium. Whenever possible, aluminium was used in order to reduce the overall weight of the apparatus.

A block of steel clamped onto the other end of the arm was used as a counterweight. By sliding both the mercury pot and counterweight along the arm, a large range of amplitudes of sine wave form could be obtained (the double amplitude can be varied from 0 to about 200 kN/m^2 and the frequency from 1/60 to 1/60.000 Hz). The principal of operation of the rotating mercury system is the same as that of the self-compensating mercury system described by Bishop and Henkel (1967) (27). Two pairs of mercury pots placed in series were used.

2.1.7 Time/cycle counter

A micro switch activated by a stabilised 24 volts D.C. power supply, connected to an electro-mechanical counter was used to count the number of cycles produced by the rotating mercury system.

2.1.8 Experimental Measurements

The cell pressure was applied by means of the apparatus described in section 3.6.

A Bell and Howell diaphragm transducer activated by a 10 volts D.C. power supply was used for the measurement of the cell pressure.

The output was recorded on a digital voltmeter, solartron (L.M.14120.20) with a selector switch in the circuit to allow the reading of six channels.

A - Pore pressure measurements

Two types of pressure transducers were used for pore pressure measurement: Bell and Howell and miniature Druck transducers.

- **Bell and Howell transducer**

This type of transducer was used for cell pressure and base sample pore pressure measurements. This electrical diaphragm transducer was housed in a brass block which, in turn, was connected by suitable channel and tube to the porous drain situated in the base platen. The transducer was energised by means of a constant input of 10 volts D.C. and monitored on the D.V.M.

The disadvantage of this system as far as pore pressure is concerned is the response time. Being remote from the sample there is a time lag between a pore pressure generated in the This lag is mainly a function of the permeability of the porous drain.

Khaffaf (1975) (28) found the system adequate for normal”static” testing but inadequate for cyclic work.

- **Miniature Pressure Transducer**

The mid-height pore water pressure measurements were made by means of a miniature pressure transducer developed by Druck Ltd.

The transducer has a diffused silicon strain gauge diaphragm as the sensing member and incorporates a porous ceramic disc.

The transducer can stand a maximum pressure of 600kN/m^2 and is energised by a supply of 10 volts D.C. It can be saturated with de-aired water by immersion in boiling water.

The advantages of the use of the "Druck" transducer in triaxial testing, as reported D.W. Hight (1982), are listed below:

B - Measurements of axial strain

The mean axial strain was calculated from the axial displacements of the loading ram, measured by means of a dial gauge mounted on the loading ram with the spindle moving relative to a fixed point directly on the cell body. The sensitivity of the dial gauge was 0.01 mm/division.

C - Measurements of the axial load

The load cell was energised by a constant supply of 10 volts D.C. from the electronic console of the electro-servo-hydraulic system and the amplified signal was monitored on the digital display of the console.

2.2 Material tested and experimental procedures

2.2.1 Material tested

Cowden clay was used in this investigation. It is a glacial Till, dark brown in colour, obtained from the Cowden site on north Humberside. The index properties, as reported by G.B.Kachachi (1983) (29), are as follows:

Liquid limit	= 44%
Plastic limit	= 19%
Plasticity index	= 25%
Clay fraction (D < 0.002mm)	= 32%
Activity	= 0.78

C_V remoulded soil (σ_V' = 480 kN/m^2) =1.5 m^2/yr

2.2.2 Preparation of Cowden clay in the Œdometer

One final consolidation pressure of 600kN/m^2 was used for preparing remoulded samples of Cowden clay for both static and cyclic triaxial tests. The preparation procedure was as described below:

The clay material was broken into small fragments and placed in a large bin. Distilled water was added until the clay was completely submerged. The clay was left for two days in order to soak, and was then placed in a large mixing machine and mixed thoroughly to a slurry by adding more water until the water content was approximately twice that of the liquid limit so that the viscosity was sufficiently low to allow the removal of air by applying a vacuum above the slurry

The composite cell body was bolted to the base and sealed by means of a large diameter o-ring. The inside of the cell was cleaned and smeared with a thin film of silicone grease to reduce vertical friction.

The vertical consolidation pressure was applied by means of hydraulic pressure across a flexible jack. The cell allowed top and bottom drainage, both of which were provided from porous plastic sheets set above and at the bottom of the clay.

The vertical drainage from the top of the clay bed was provided by a hollow spindle passing through the hydraulic jack and cell lid, leading to a Klinger valve. Drainage from the bottom of the cell was via a small sintered bronze disc set flush into the base, also connected to a Klinger valve. The top and bottom porous plastic sheets were boiled for 30 minutes before use to ensure full saturation.

The clay slurry was poured in a series of 50 mm layers into the œdometer.
After addition of each layer, air was removed by applying a vacuum to the surface for a period of about 30 minutes through a Perspex lid sealed with a greased o-ring on top of the cell body.

When the required height of slurry was obtained, the cell was topped up with distilled water and the saturated porous plastic sheet was placed on top of the slurry.

The rubber jack was then lowered into position and the cell lid was bolted onto the body. An initial head of water (40 cm) was applied to the rubber jack by means of a bottle of water while top and bottom drains were open.

This low pressure was kept for at least 24 hours and when the drainage ceased it was increased slowly to ensure uniform consolidation.

When the clay was considered stiff enough, it was found necessary to release the pressure and remove the cell cover in order to scribe level the surface of the clay.

A 13mm thick Perspex platen with a central drainage hole was then placed on the top of the clay to provide equal strain conditions at higher consolidation pressure. The pressure was then applied in increments ($\Delta P/p = 1.0$) up to the finale required pressure.

After each pressure increment, enough time was allowed for full consolidation to occur. When drainage had ceased, and the clay was considered fully consolidated, the top and bottom drains were closed so that neither air nor water was drawn back.

After completion of the consolidation process and opening the cell, eight 102mm internal diameter thin walled cutting tubs, cleaned and greased on the inside to ease later

extraction, were positioned in a circular pattern, in order to overcome inconsistency of different radii caused by the non-uniformity in the pressure distribution during consolidation.

A thick platen was put on top of the sampling tubes and, by means of a hydraulic jack; they were pushed simultaneously into the bed of clay.

The sampling tubes were extracted manually from the bed of clay.

In order to preserve the moisture content, the specimens were pushed up the tubes for a further 3cm and sealed at both ends with paraffin wax. The tubes were wrapped in cellophane and stored in plastic bags until required for testing.

2.2.3 Setting up a specimen in the triaxial testing apparatus

A 102 x 102 mm sample diameter was set up in the triaxial cell according to the following procedure:

The end platens were cleaned with acetone and slightly smeared with high vacuum silicone grease. Care was taken not to block the sintered ceramic disc in the base platen. The top and bottom plates were then covered with sheets of rubber membrane.

The rubber membrane covering the base platen had a central hole to allow intimate contact between the base of the sample and the ceramic disc.

To make sure no air was trapped between the platens and rubber membrane, and to remove excess grease, the two end platens were placed over each other and a weight of 10kg was placed on top of them for approximately one hour.

Meanwhile, the sample was removed from the tube by means of a sample extractor and trimmed to the required height in a 102 m high oversized brass cylinder. The sample was then placed in position between the top and bottom platens.

A rubber membrane, 0.33mm thick, checked for any blow holes was stretched inside a cylinder former slightly larger than the specimen and then sucked to take the shape of the former. The former was then placed over the sample and when the suction was released, the membrane came into contact with the specimen.

Three o-rings were sprung into position around the bottom platen.
For mid-pore water pressure measurements a miniature pressure transducer was installed.

Prior to the tests de-aired water was flushed through the Druck transducer de-airing chamber. (Note that air was dissolved before flushing by maintaining a high positive high pressure within the system when not in use.)

In this study the installation procedure of the miniature pressure transducer was the same as that described by D.W. Hight (1982) (30).

Details of the transducer installed at the periphery of the sample are given in

For installation, a hole was cut in the rubber membrane at sample mid-height and the miniature "Druck" transducer was inserted into a rubber grummet as an additional support for the transducer.

The rubber grummet was made by pouring a solution into a mould. The rubber grummet and mould

To ensure an intimate contact between the sample periphery and the porous stone (of the transducer), a pad of saturated Kaolin (3 to 5 mm thick) was placed on the porous stone.

The assembly ("Druck" transducer/rubber grummet) was then carefully inserted into the hole of the rubber membrane. Great care was taken at this stage to avoid any penetration of the sample, which would increase interference effects.

The rubber grummet/transducer assembly was sealed with two small o-rings. The puncture in the rubber membrane around the rubber housing was sealed with a rubber solution. Three o-rings were then positioned around the top platen.

A vertical rod, slightly higher than the sample/platen assembly shown in Figure 4.5, was screwed into the base of the cell beside the sample. A ring was fastened around the universal joint from which two rods protruded.

The cell was cleaned, the base sealing o-ring was applied in its groove and some grease was applied. The body was lowered into position and bolted down with six tie rods. The cell was then filled with water.

2.3 Data acquisition and testing program

2.3.1 Data Acquisition

The dial displacement gauge, the load cell, the base and mid height pore pressure, and the cell pressure readings were manually recorded at suitable time increments throughout each test.

The data were reduced by means of a micro computer. The computer program applied corrections for changes in the sample area. It was developed to carry out data reduction for either monotonic or cyclic (displacement or load controlled) loading tests. The computer also has a plotting facility which was used to produce all the graphs presented in this study

2.3.2 Testing Program

Undrained monotonic and cyclic triaxial tests were performed on remoulded Cowden clay. The clay was normally consolidated in a œdometer to a pressure of 600 kN/ m^2. All the tests were carried out on samples of 102 mm diameter by 102 height. In this investigation, both base and mid-height pore pressure measurements were made.

A. Monotonic compression tests

A set of four displacement-controlled triaxial compression tests (comp.1 to comp.4) was carried out. Details of these tests are shown in Table 2.1.

B. Monotonic tension tests

Also performed were four displacement-controlled triaxial tests (Tens.1 to Tens.4). Details are shown in Table2.2.

C. Cyclic Tests

Three sets of load-controlled triaxial tests were carried out. The details of these three sets are shown in Table 2.3.

D. Monotonic (tension or compression tests) on cyclically loaded samples

All samples of series B and C were subjected to monotonic (compression or tension) loading after termination of cyclic loading. Details of these tests are given in Table 2.4.

Table 2.1 Monotonic Compression Tests

Test Code	Œdometer Consolidation Pressure	Cell Pressure	Strain rate	U_{M0} (2)	U_{Bo} (3)	σ_o' (4)	OCR
	kN/m^2	kN/m^2	kN/m^2	$\%/m^2$	kN/m^2	kN/m^2	
Comp. 1	600	500 (1)	0.012	428.3	449.6	81.9	4.9
Comp. 2	600	500	0.012	421.1	420.5	77.9	5.1
Comp. 3	600	400	0.06	337.3	335.3	66.3	6.0
Comp. 4	600	400	0.30	334.4	325	65.5	6.1

Table 2.2 Monotonic Tension Tests

Test Code	Œdometer Consolidation Pressure	Cell Pressure	Strain rate	U_{Mo} (2)	U_{Bo} (3)	σ_o' (4)	OCR
	kN/m^2	kN/m^2	kN/m^2	$\%/m^2$	kN/m^2	kN/m^2	
Tens. 1	600	500 (1)	0.012	410	409.2	89	4.5
Tens. 2	600	500	0.012	404.7	403.5	96.	5.1
Tens. 3	600	400	0.06	310.8	308.4	89.5	4.5
Tens. 4	600	400	0.3	334.4	333.6	65.6	6.1

Table 2.3 Cyclic loading tests

Test code	Œdometer pression kN/m^2	Cell Pess kN/m^2	Freq Hz	U_{Mo} kN/m^2	U_{Bo} kN/m^2	$Cu^{(4)}$ kN/m^2	τ/Cu comp	τ/Cu Tens	σ_o' kN/m^2	OCR	$(C_{da})_{max}$ %
A.1	600	400	0.00027	323.3	330.8	70	0.3	- 0.46	67.7	5.9	5
A.2	600	400	0.00027	320.3	316	70	0.3	- 0.46	79.7	5	1.5
A.3	600	400	0.00027	304.2	300.5	70	0.3	- 0.46	95.6	4.2	1.0
B.1	600	400	0.00027	334.1	333.2	70	0.4	- 0.57	67.1	6.0	5
B.2	600	400	0.00027	320.3	315.3	70	0.4	- 0.57	79.7	5	2
B.3	600	400	0.00027	323.7	322.9	70	0.4	- 0.57	76.3	5.2	2
B.4	600	400	0.00027	323.9	3.23.9	70	0.4	- 0.57	76.1	5.2	2
B.5	600	400	0.00027	320.6	302	70	0.4	- 0.57	97.4	4.1	2
C.1	600	400	0.00027	318.6	317.3	70	0.59	- 0.59	81.4	4.9	5
C.2	600	400	0.00027	317.5	317.3	70	0.59	- 0.59	72.5	5.4	5
C.3	600	400	0.00027	318.7	318.7	70	0.59	- 0.59	81.3	4.9	5
C.4	600	400	0.00027	315	314	70	0.59	- 0.59	85	4.7	5

(4) Cu is the mean of value of the undrained shear strength measured in monotonic tests at a straz in rate of 0.012%/minute

Table 2.4 Monotonic loading tests on cyclically loaded samples

Test Code (1,2,3)	Cell Pressure kN/m^2	Strain Rate %/min	U_{Mo} kN/m^2	U_{Bo} kN/m^2	σ_0' (after cyclic loading) kN/m^2	OCR
B.1.C	400	0.012	360.8	362.1	33.8	11.8
B.2.C	400	0.012	348.1	346.5	45.5	8.8
B.3.C	400	0.012	346.5	348.5	46.7	8.6
B.4.C	400	0.012	340.9	340.1	53.6	7.5
B.5.C	400	0.012	335.5	338.5	63.8	6.3
C.1.T	400	0.012	369.3	369.3	29.8	13.4
C.2.T	400	0.012	368.1	365.7	30	13.3
C.3.C	400	0.012	376	374.9	24.1	16.6
C.4.C	400	0.012	376.5	373.7	22	18. 2

1 – The first letter refers to the test series
2 – The number in the middle refers to the test number
3 – The last letter refers to the type of loading
(i.e. C for compression and T for tension)

2.4 Conclusion

The main laboratory equipment that will be used in this research consiste of:

- a conventional 102mm diameter sample triaxial cell
- a conventional triaxial loading machine,
- an electro-servo hydraulic system and
- cyclic cell pressure apparatus.

Bell and Howell diaphragm transducers measured cell and base pore water pressure. A miniature Druck transducer was used for mid-sample pore water pressure measurement.

Testing Program

Undrained monotonic and cyclic triaxial tests were performed on remoulded Cowden clay. The clay was normally consolidated in a œdometer to a pressure of 600 kN/ m^2.
The following tests will be carried out.

- Monotonic compression tests
- Monotonic tension tests
- Cyclic Tests
- Monotonic (tension or compression tests) on cyclically loaded samples

CHAPTER 3

DISCUSSION OF RESULTS AND CONCLUSIONS

3.1Discussion of results

3.1.1 Introduction

In this investigation only samples of 102 mm in height by 102 mm in diameter were used. The "free" ends (lubricated end platens) technique was used because of its simplicity and reliability in maintaining a much greater uniformity of stress and deformation throughout a monotonic compression test.

However, in an extension test, the effectiveness of the lubricated end platens may be limited to the early stages of the test (up to about 3% axial strain) as, at large stresses, the sample forms a neck.

In the present work, both base and mid-height pore pressure measurements were carried out. The mid-height pore pressure measurements were carried out by means of a piezometer probe "Druck-transducer" mounted flush with the cylindrical surface of' the sample at mid-height.

3.1.2 Monotonic Tests

A. Pore water pressure behaviour in compression tests

A set of 4 displacement-controlled compression tests was carried out. Data such as B (Skempton's pore water pressure parameter), rate of testing, cell pressure, moisture content, œdometer consolidation pressure, initial effective stress [1] for each test are given in Table 3.1.

For convenience, pore water pressure results are presented in Figures 3.1 to 3.4, in terms of plots of excess pore water pressure ΔU_M and ΔU_B (ΔU_M = excess pore pressure measured at the mid-height of the sample; ΔU_B = excess pore pressure measured at the base) against axial strain at different strain rates.

The author believes that due to its quick response and adjacent position to the sample, the miniature "Druck" transducer consistently measures accurately the pore water pressure existing at the transducer/clay interface and that the base (Bell and Howell) transducer may be inaccurate in fast tests due to its remoteness and slow response. Even in slow tests a difference between the pore water pressure developed at the base and mid-height can occur due to non-uniform Stress/strain conditions.

These real differences will be greater in faster tests and the observed difference may be even greater due to inaccuracies in measurements of the Bell and Howell transducer.

Figures 3.1 to 3.4 show combined plots of ΔU_M, ΔU_B and D (deviator stress) versus axial strain (ϵ_A) for the tests Comp.1, Comp.2, Comp.3, Comp.4. I t can be deduced from Figures 3.2 to 3.4 that ΔU, the magnitude of the difference between mid-height and base pore pressure generation is larger at small strains ($\epsilon_A < 3\%$) than at large strains.

Fig 3.1 Deviator stress & excess mid-base PWP vs axial strain for test comp.1

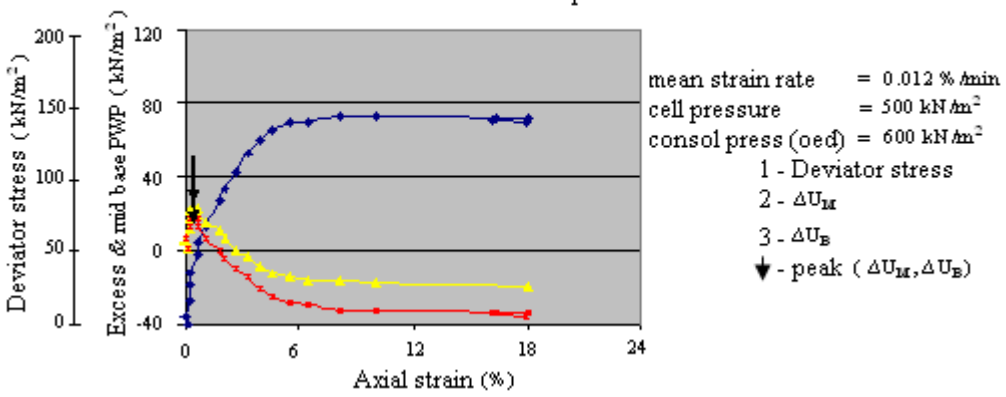

Fig 3.2 Deviator stress & excess mid-base PWP vs axial strain for test comp. 2

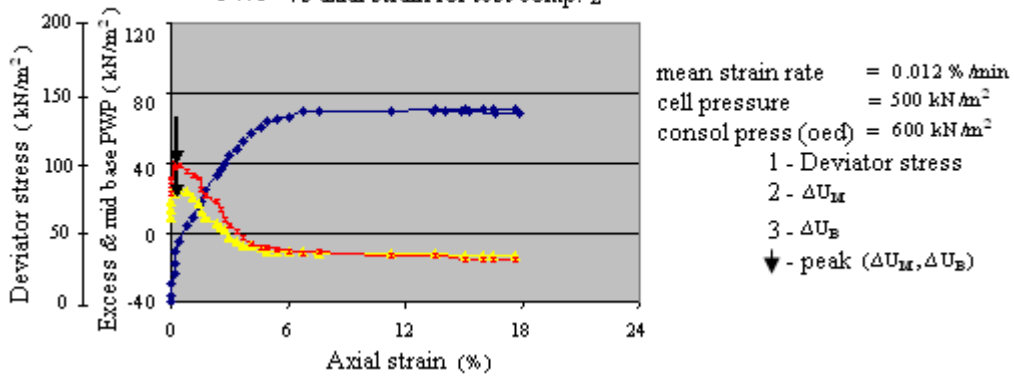

Fig 3.3 Deviator stress & excess mid-base PWP vs axial strain for test comp.3

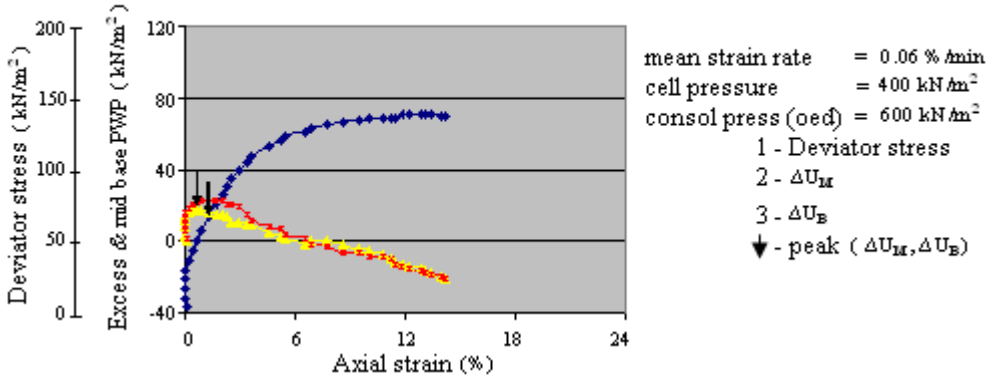

Fig 3.4 Deviator stress & excess mid-base PWP vs axial strain for test comp. 4

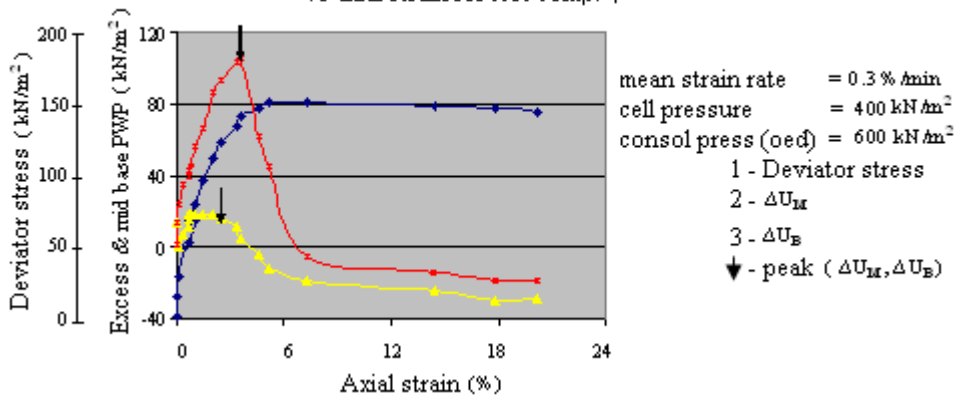

This is believed to be due to the rapid rate of change of the deviator stress at the start of the test. However, in Figure 3.1, for test Comp.1, large values of ΔU are observed throughout the test. This is considered to be erroneous and may be due to the low B values (see Table 3.1) associated with this test. Table 3.1 shows that, while tests Cornp.2, Comp.3 and Comp.4 achieved a fully saturated condition ($B_M = B_B = 1$), test Comp.1 achieved $B_M = 0.93$ and $B_B = 0.9$. Bearing in mind the high compressibility of the soil skeleton, these values probably indicate a significantly large loss of saturation.

A combined plot of excess mid-pressure (ΔIJ_M) versus axial strain (ϵ_A) for the whole set is presented in Figure 3.5. Curves for tests Comp.1 and Comp.2 peak at about. 1% axial strain, whereas curves for tests comp. 3 and Cornp.4 show peaks at about 2% and 2.8% axial strain respectively .

It can also be seen that tests Comp.1 and Comp. 2 had higher peak ΔIJ_M than tests Comp. 3 and Comp. Also indicated by an arrow for each test is the excess pore pressure at maximum deviator stress. It. is seen that tests Comp. I, Comp. 2 developed higher excess pore pressure at maximum deviator stress than test Comp. 3. However, test Comp.4, although run at the fastest strain rate of 0.3%/min shows higher excess pore pressure at maximum deviator stress than test Comp.3.

All compression tests presented in Figure 3.5 show a dilatant behaviour which is a feature associated with an overconsolidation state.

Fig 3.5 Excess mid & base PWP vs axial strain for tests comp.1 to comp.4

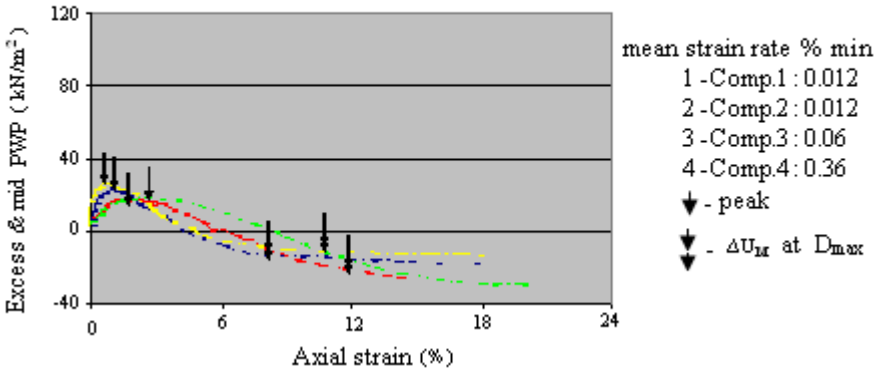

This is discussed in section 3.2.3. The author believes that, due to the difference in the initial effective stress (σ_o') from one Sample to another, resulting from the sample preparation process (effects of the sampling process are discussed in Section 3.4), a better comparison of pore water pressure behaviour could be obtained by "plotting $\Delta U_M/\sigma_0$' versus axial strain (ϵ_A), as shown in Figure 3.6 (test Comp.1 has not been included in Figure 3.6 because of its low B values.) It is seen that all the curves show similar peak values of $\Delta U_M/\sigma_o$'.

Fig 3.6 $\Delta U_M/\sigma$ 'o vs axial strain for tests comp.2 to comp.4

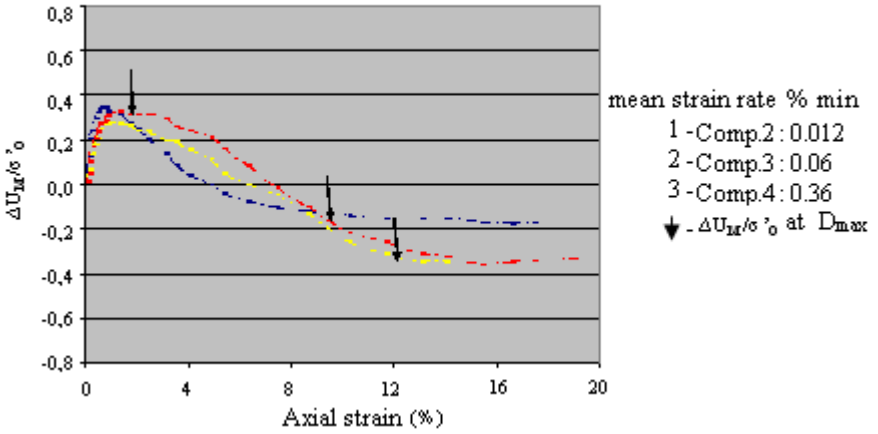

This behaviour is iI1ustrated Figure 3.7, where $\Delta U_M/\sigma_0$' is plotted against strain rate. It is also seen in Figure 3.6 that $\Delta U_M/\sigma_o$' at maximum deviator stress (D_{max}) is lower in test Comp.3 than in test comp.2, whereas test Comp.4 developed higher $\Delta U_M/\sigma_o$' at D_{max} than test Comp 3.

Fig 3.7 $(\Delta U_M/\sigma'_0)_{peak}$ vs strain rate for compression tests.

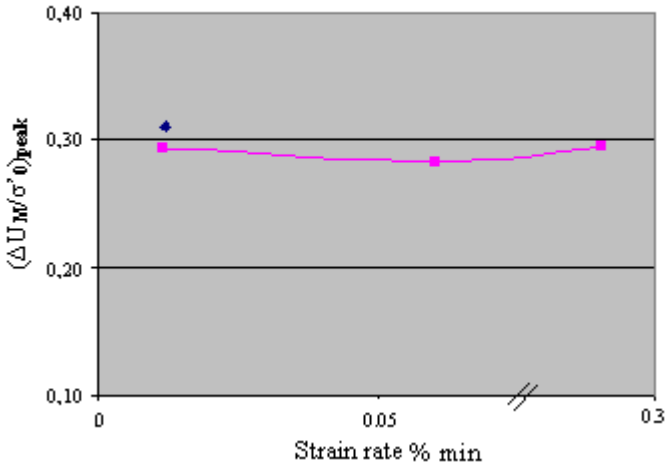

The latter observations, as illustrated in Figure 3.8, were rather unexpected as this contradicts the idea that increasing the strain rate suppresses pore pressure at failure, resulting in an increase in shear strength (e.g.: Bjerrum et al (1958) (14), Crawford (1959) (5). Comp.2

Fig 3.8 $(\Delta U_M/\sigma'_0)_{Dmax}$ vs strain rate for compression tests.

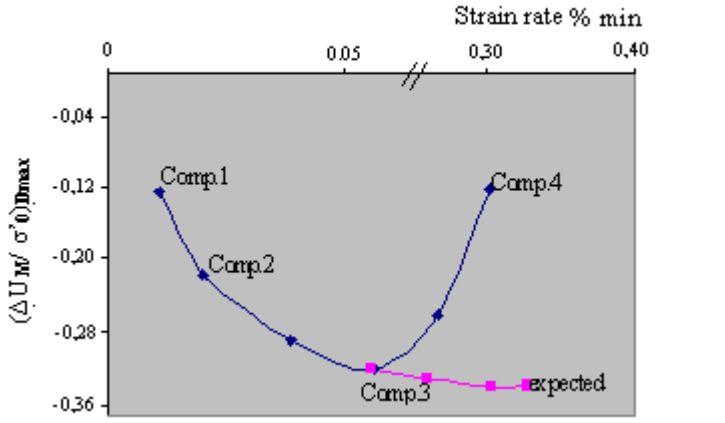

Mokrani, (1983) (8), carried out a series of 4 displacement.-controlled tests on Cowden clay consolidated in the œdometer to a pressure of 400 kN/m^2, using mean strain rates of 0.086, 0.8, 7.5 and 36 %/min. For mid-pressure measurement, Mokrani inserted the "Druck'' transducer into a hole bored in the sample at mid-height.

He suggested that while pore pressure measurements carried out at 7.5 % /min and 36 %/min were erroneous, accurate pore water pressures were collected in the remaining two tests (curves a and b in Figure 3.9). These two, strain rates (0.086 and 0.8%/min) are quite fast compared with those used by the author, i.e. 0.012 and 0.3 %/min.

Fig 3.9 Excess PWP vs axial strain.
(after Mokrani 1983)

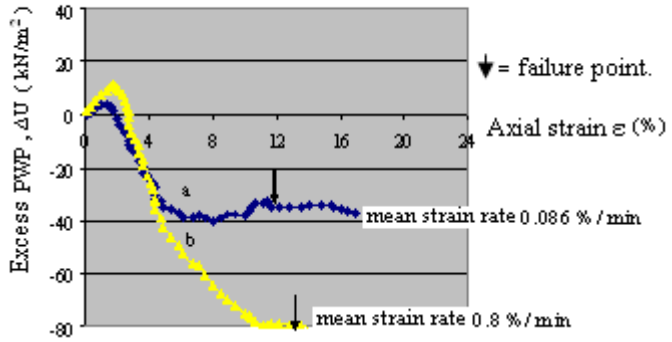

Mokrani observed that, at failure, the slowest test (curve a) developed a higher excess pore pressure than the faster test (curve b).

This is in agreement with the observation made earlier by the author (compare test. Comp.3 with test Comp. 2) and complies in principal with the idea that increasing strain rate induces a decrease in pore pressure at failure.

At low strain "(1- 2.5 %)" however, Mokrani found that the faster test curve (b) showed a higher peak ΔU_M, which he attributed to the fact that at small strains and, bearing in mind that the soil structures at the start, of the test were similar in both cases, the pore water pressure was only dependent upon the magnitude of the load applied.

The above observation is in contradiction with that of the author (see Figure 3.5). However, the author believes that such a contradiction might well be reconciled if Mokrani's plots were made on the normalized basis used in Figure 3.5.

The mid-pore pressure measurements produced by Mokrani may have been erroneous due to the technique used.

He inserted the miniature transducer into the middle of the sample. This inevitably disturbed the soil structure around the transducer.

He reported that some samples, after being dried out, had holes (previously drilled to accommodate the transducer) with a depth bigger than the length of the body of the pore pressure transducer, suggesting that the pore pressure measurements may have bee in error, caused by some air being trapped in the hole as a result of non or bad contact between the ceramic disc or the "Druck" transducer and the clay.

Furthermore, Mokrani's samples were not reconsolidated in the triaxial cell and no initial effective stress or initial pore water pressure data were provided, so an objective comparison on a normalised basis was impossible.

B. Pore pressure behaviour in tension tests

A set of 4 strain-controlled tests was performed. Details of this series of tests are given in **Table 3 .2**.

Again, the author believes that while mid-height pore pressure measurements were accurate, base pore pressures, especially at high strain rates were erroneous. Pore water pressure results are plotted in terms of excess pore pressure ΔU_M and ΔU_B (ΔU_M excess pore pressure measured at the base in tension; ΔU_B = Excess pore pressure measured at the base in tension) against axial strain (ϵ_A). Figures 3.10 to 3.13 show plots of ΔU_M, ΔU_B and deviator stress (D) versus axial strain (ϵ_A) for tests Tens.l, Tens.2, Tens.3, Tens.4. It is seen that at low strains (ϵ_A > -3%) tests Tens. 1 to Tens .3 showed higher excess pore pressures at mid-height than at the base, while at larger strains the opposite occurred.

Results of test Tens.4, as seen in Figure 3.13, show the same overall behaviour observed in the other tests, except that higher excess pore pressures occur at mid-height than at the base developed up to (-7.4%) axial strain.

Plots of mid-height pore pressures versus axial strain (ЄA) for all tension tests are shown in Figure 3.14. Also shown by an arrow in this figure are the excess pore water pressures at maximum deviator stress for each test.

It is seen that ΔU_M at maximum deviator stress in curves for tests Tens. 1 and Tens .2 are higher than in tests Tens.3 and Tens.4. Test Tens. 4, although run at the fastest strain rate of 0.3%/min, developed higher excess pore pressure at maximum deviator stress than test Tens .3, run at 0.03 %/min.

This is believed to be mainly due to the low initial effective stress (σ_o') in test Tens. 4 (see Table 3.2) resulting from the sampling process.

Fig 3.10 Deviator stress & excess mid-base PWP vs axial strain for test tens.1

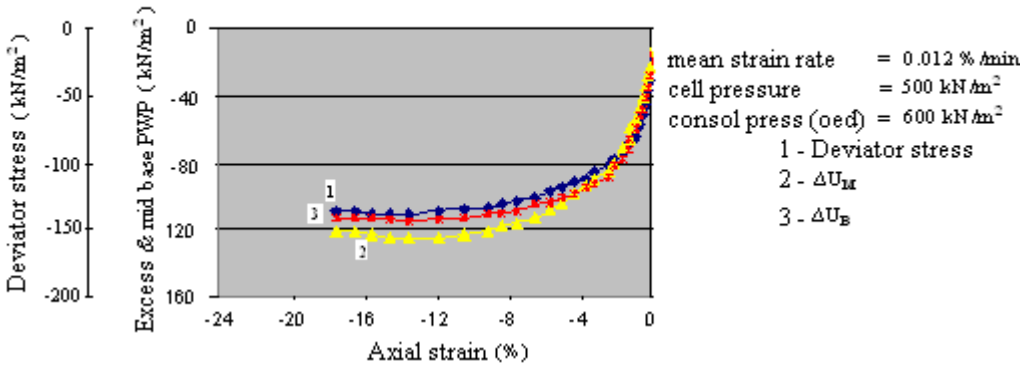

Fig 3.11 Deviator stress & excess mid-base PWP vs axial strain for test tens. 2

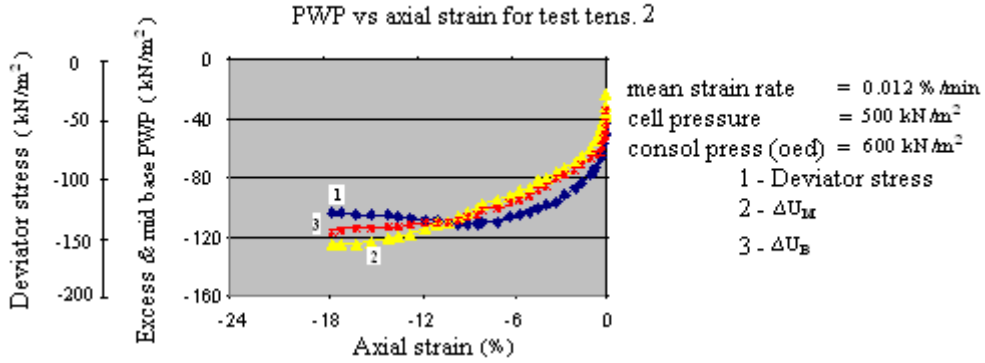

Fig 3.12 Deviator stress & excess mid-base PWP vs axial strain for test tens. 3

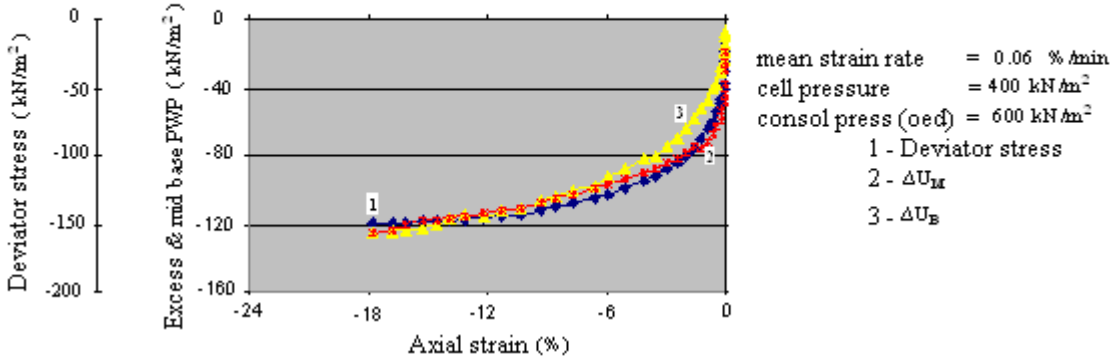

Fig 3.13 Deviator stress & excess mid-base PWP vs axial strain for test tens. 4

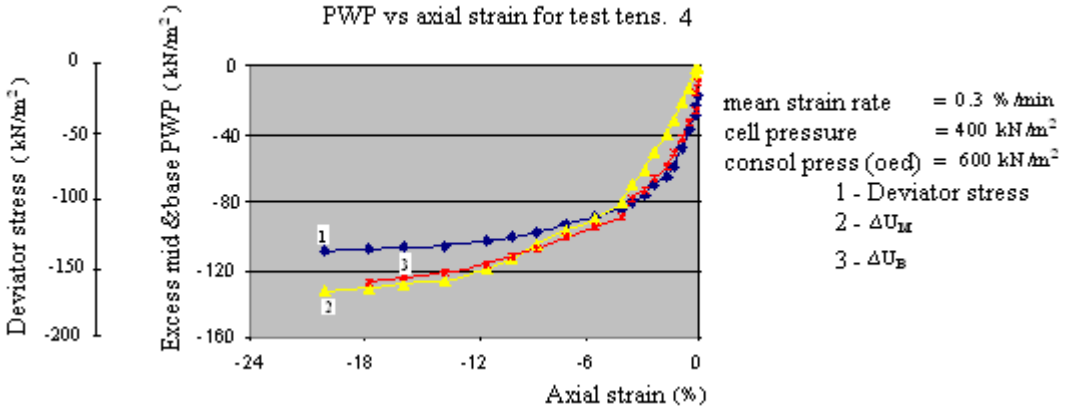

Fig 3.14 Excess mid & base PWP vs axial strain for tests tens.1 to tens.4

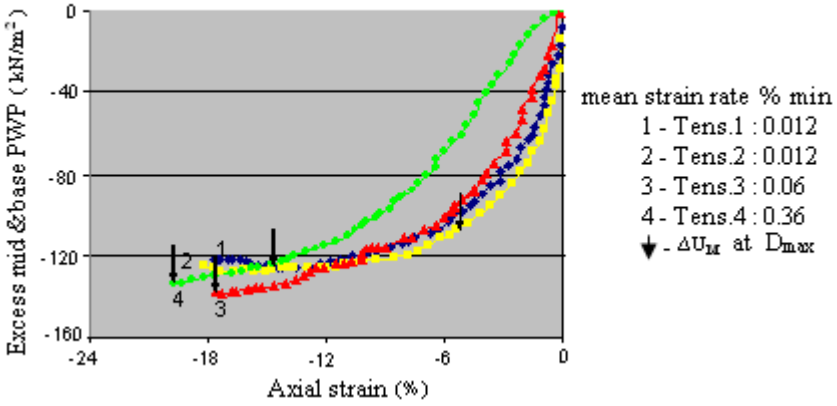

Figure 3.15 shows plots of $\Delta U_M/\sigma_o'$ versus (ϵ_A) for all tension tests except those for test Tens.1, which had low B values (see Table 3.2). It is seen that $\Delta U_M/\sigma_o'$ at maximum deviator stress decreases with increasing strain rate, which is in agreement with the idea of pore pressure at failure decreasing with increasing strain rate.

Fig 3.15 ($\Delta U_M/\sigma'_0$) vs axial strain for tension test 2 to test 4.

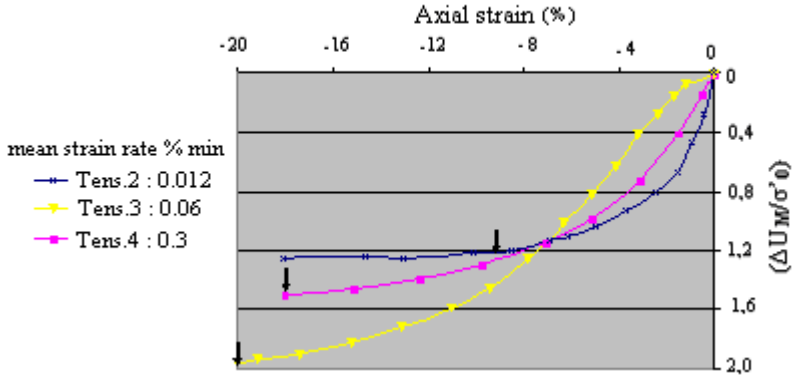

Table 3.3 shows excess mid-pore pressure measured at the end of testing for all monotonic tests, corrected for the ambient effect by a factor of -D/3 in compression and +D/3 in tension (ΔU_{MC}). It is seen that, in terms of ΔU_{MC}, rate effect on dilation is not clear.

However, when the final pore water pressure is expressed in terms of a ratio ($\Delta U_{MC}/\sigma_O'$), it is clear that, both in compression and tension increasing strain rate results in an increasing dilation.

The large difference in pore pressure response in compression and tension may be due to differences in stress paths. A comparison of pore pressure response under the two modes of loading can be obtained in terms of the Skempton's pore pressure parameter A.

Skempton's original equation for an undrained triaxial compression test is:

$$\Delta U = B\left[\Delta\sigma_3 + A\left(\Delta\sigma_1 - \Delta\sigma_3\right)\right] \qquad (1)$$

where ΔU is the excess pore water pressure developed by increments of major and minor total stresses, $\Delta\sigma_1$and $\Delta\sigma_3$. A and B are the Skempton pore pressure parameters. If the soil is fully saturated (B =1) and there is no change in the cell pressure, $\Delta\sigma_3 = 0$, and knowing that: $\left(\Delta\sigma_1 - \Delta\sigma_3\right) = D$

Equation (1) becomes: $\Delta U = A.D$ (2)

Hence $A = \Delta U / D$

For tension tests where $\Delta\sigma_3 = -D; \Delta\sigma_1 = 0$

And $\Delta\sigma_3.\Delta\sigma_3 = +D$

Equation (1) becomes: $\Delta U = -B.D + A.B.D$

If B = l then $\Delta U = D\left(A - 1\right)$

Hence $A = \Delta U / \left|AD\right| + 1$ (3)

Figure 3.16 shows plots of the parameter A versus axial strain (ϵ_A) for all monotonic tests. It should be noted that for tests Comp.1 and Tens.1 which had low B values (see Tables 3.1 and 3. 2) the A parameter was calculated using equation (1) with B_M= 0.93.

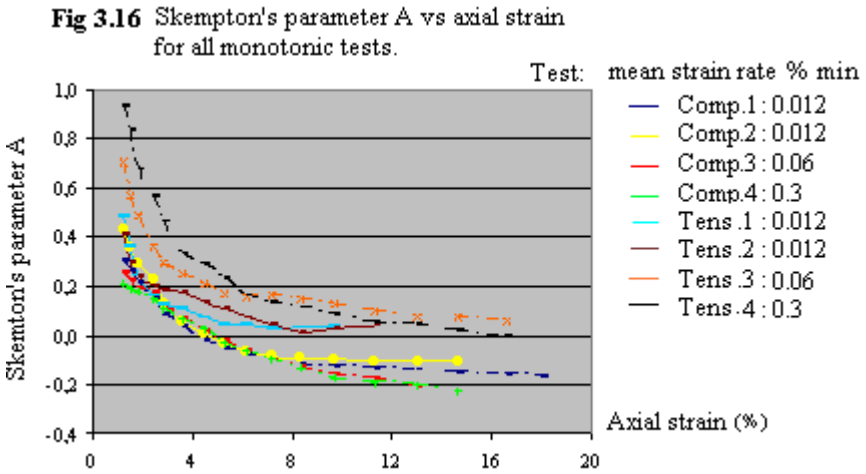

Fig 3.16 Skempton's parameter A vs axial strain for all monotonic tests.

It is seen in Figure 3.16 that a low strain rate of 0.012 %/min (Comp.1,2; Tens.1,2), the qua1itative behaviour of the parameter A versus axial strain are similar in tension and compression. In compression, variation of the strain rate from 0.012%min to 0.03%/min and 0.3%/min has a slight effect on the behaviour of the A parameter.

A similar behaviour is observed at large strains (ϵ_A < - 8%) in tension.

However, at smaller strains (ϵ_A > - 8%) in tension, increasing the strain rate from

0.012%/min to 0.03%/min and 0.3%/min had greater effect on the behaviour of the A parameter.

For further investigation of the effects of the variation of the mean total stress on the pore pressure behaviour the author suggests that, in future, monotonic compression and tension tests with constant mean total stress should be carried out.

C. Rate effect on stress-strain properties in monotonic tests

It is widely accepted ,Andersen (1980) (6) that the undrained shear strength (Cu) measured in compression is higher than that measured in tension. However, it is seen, in Tables 3.1 and 3.2, that the compressive undrained shear strength is almost equal to the extension shear strength.

This may be due to the fact that the initial effective stresses associated with the tension tests are higher than those of the compression tests. In fact it is seen in Tables 3.1 and 3.2 that:

$$\left(D_{\max}/\sigma_0'\right)_{compression} = 1.72 \qquad \text{and} \qquad \left(D_{\max}/\sigma_0'\right)_{tension} = 1.44$$

which implies that, for equal initial effective stress: $\left(CU\right)_{compression} \succ \left(CU\right)_{tension}$

Figures 3.17 and 3.18 are combined plots of deviator stress versus axial strain for all compression and tension tests respectively.

.

Fig 3.17 Deviator stress vs axial strain for tests comp.1 to comp.4

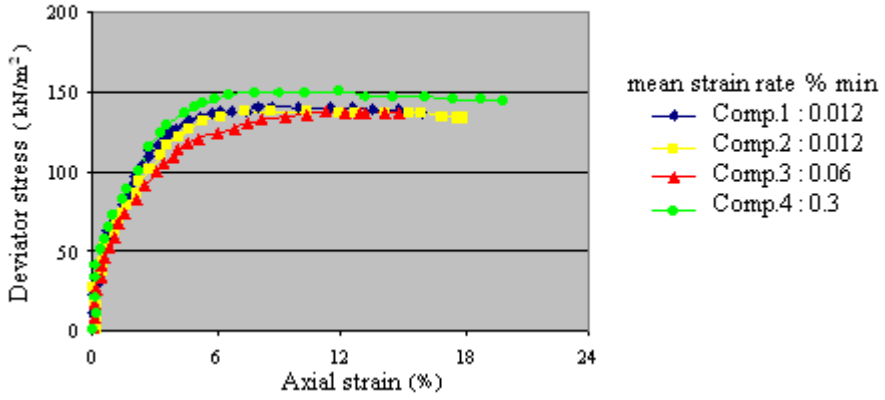

It is seen in Figure 3.17 that, despite the increase from 0.012%/min (Comp.1, Cmp.2) to O.06 %/min (Camp.3), no clear effect on D_{max} is observed. Similarly, for test Tens.4, Figure 3.18 does not show any increase compared with D_{max} from the very slow tests, Tens.1 and Tens.2.

This is believed to be due to the initial effective stress σ_0' associated with tests Comp.3 and Tens.4 (Tables 3.1 and 3.2) which can dominate the strain rate effect

Fig 3.18 Deviator stress vs axial strain for tests tens.1 to tens.4

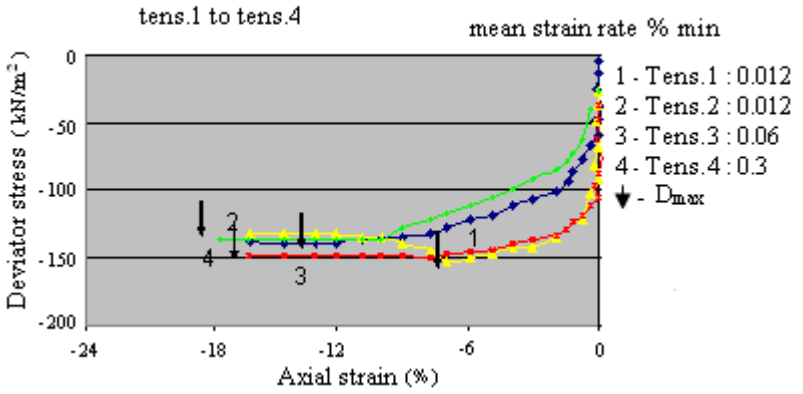

Figure 3.19 shows semi-logarithmic plots of maximum deviator stress versus displacement rate for all monotonic tests. The best straight lines passing through the different points (except test Comp.3 and test Tens.4, which did not show a strain rate effect on shear strength) using the least squares method, give an increase of 6.6 % and 10% per log cycle in the maximum deviator stress in compression and tension, respectively,(i.e. 6.6 % and 10% of the deviator stresses measured at a displacement rate of'0. 000l mm/s).

Fig 3.19 Max. deviator stress vs displacement rate for monotonic tests.

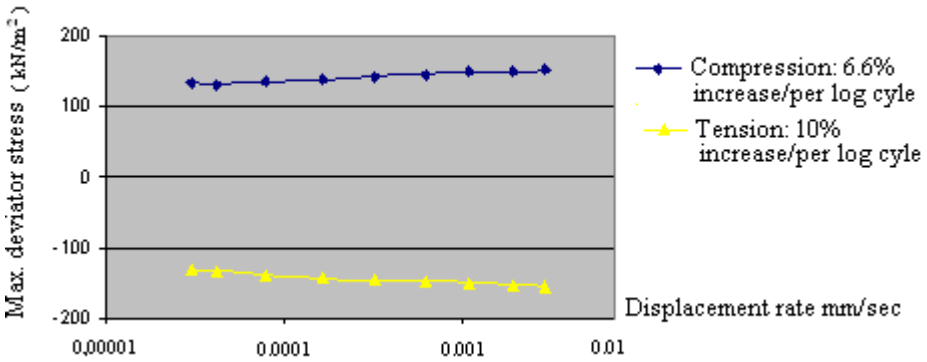

Mokrani (1983) (8), (Figure 3.20), reported for his displacement controlled compression tests on Cowden clay a 3.2 % increase in D_{max} per log cycle (i.e. 3.2% of D_{max} measured at a displacement rate of 0,01mm/s).

Fig 3.20 Mximum deviator stress vs displacement-rate at failure for the displacement controlled tests on cowden clay. (after Mokrani 1983).

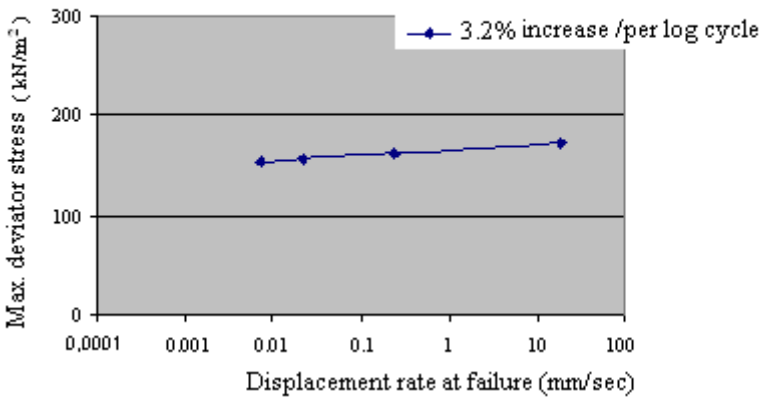

This is shown in Figure 3.21, where semi-logarithmic plots of the ratio of the maximum deviator stress to the initial effective stress (D_{max}/σ_o`) versus displacement rate are presented.

Fig 3.21 D_{max}/σ_o' vs displacement rate for all monotonic tests

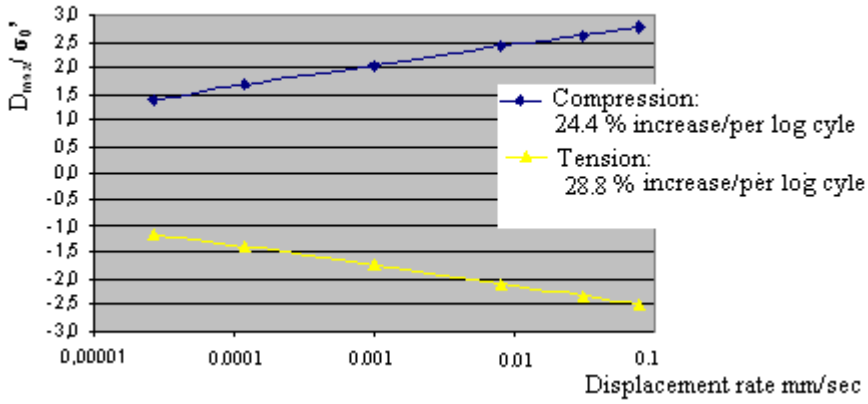

The best straight lines passing through the points drawn using the least squares method show an increase of 24.4% and 28.8% in D_{max}/σ_o` per log cycle in compression and tension respectively (i.e. 24.4% and 28.8% of D_{max}/σ_o' measured at a displacement rate of 0.0001 mm/s.)

It is also interesting to note the stress strain behaviour of tests Tens.3 and Tens.4. The deviator stresses in the tests (Figure 3.18) did not show a clear failure point. In fact, the deviator stresses continued to increase, although very slowly right to the end of the loading process. It is believed that this may be due to the continuous dilation effect observed in these two tests.

The pore water pressure behaviour discussed in Sections 3.2.1 and 3.2.2 clearly suggest that samples used for monotonic testing were lightly over-consolidated. This, as was mentioned in Section 3.2.1, is due to the sampling process (no further reconsolidation in the triaxial cell was carried out).

The over-consolidation ratios (OCRs) for the monotonic tests given in Tables 3.1, 3.2, were computed by dividing the maximum effective stress in the œdometer P_{max}', assuming k_0= 1/2 for normally consolidated clays, by the initial effective stress in the triaxial cell.

D. Effective stress analysis

Figure 3.22 shows plots of shear stress $(\sigma'_{ax} - \sigma'_{lat})/2$ [2] versus mean effective stress $(\sigma'_{ax} + \sigma'_{lat})/2$ for the very slow monotonic tests (0.012%/min.). The effective failure envelope for the compression tests assuming C'=0 and Ø'=26.4°, while that for the tension tests with the same assumption of C'=0 had Ø'=28.4)°. For the same clay, G.Kachachi, (1983), suggested, for his slow monotonic compression tests and assuming C' = 0, an effective failure envelope with Ø' = 27°.

The effective stress paths for the remaining tests, together with one very slow test, are presented in Figure 3.23.

Because of the limited amount of data available, it is difficult to define accurately the effective failure envelope for the monotonic tests.

However, if, for the compression tests (Comp.3, Comp.4), where no clear yielding line is observed, it is assumed that C'=0, it can be seen that increasing the strain rate from 0.012 to 0.06 and 0.3%/min, results in Ø' increasing from 26.4°to 29.4° and 34.3°.

Fig 3.22 Effective stress paths for tests Comp.1,2 and Tens. 1,2

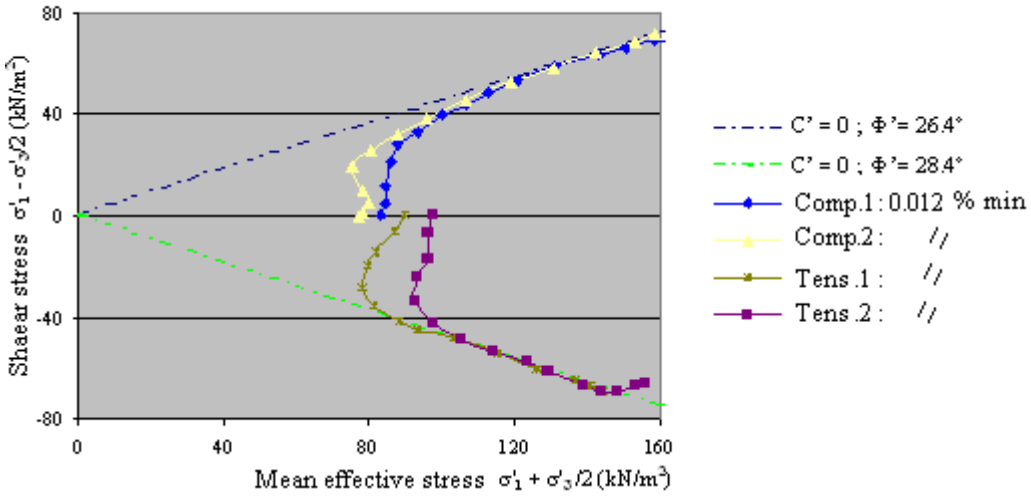

Fig 3.23 Effective stress paths for tests comp. 1,3,4 and tens.1,3,4

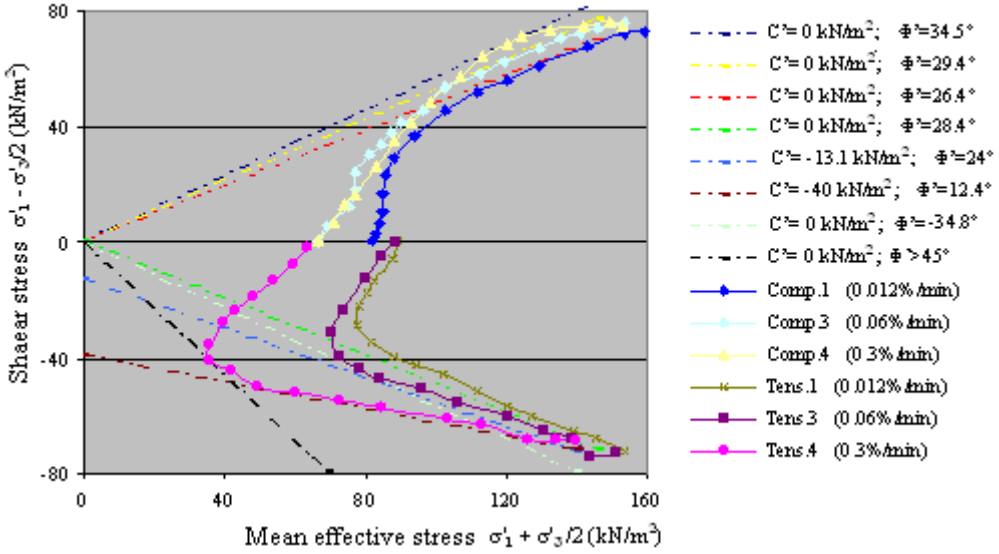

In tension, if the same assumption (i.e. C'=0) is made, the resulting effective failure envelopes are highly improbable as, for test Tens.3, Ø' =34.8° and for test Tens.4, Ø' would be even greater than 45° which, in fact, implies a negative value of the minor principal effective stress.

However, if the effective failure envelopes are drawn along the apparent yield lines, it can be seen that increasing the strain rate from 0.012 to 0.06 and 0.3 %/min would give an increase in C' from 0 to 13.1 and 40 kN/m^2 and a decrease in Ø', from 28.4° to 24° and to 12.4° respectively.

Although these failure envelopes are improbable, they were drawn for comparison with the cyclic tests. The true effective failure envelopes may in fact be curved. The outward displacement of the effective stress paths of tests Comp.3, Comp.4 from that of test Comp.1 and tests Tens,3, Tens.4 from Tens.1 implies that C' and Ø' are affected by the rate of shearing.

The author believes that at strain rates of 0.03 and 0.3%/min correct "failure" pore pressures were still measured. If these are higher than the true values due to pore water

pressure gradients, then the effective stress paths would be closer to the origin than they should be.

Figure 3.24 shows the effective stress paths for two displacement controlled compression tests carried out by D.W.Hight (1982) (31). The two tests were carried on anisotropically consolidated samples of Lower Cromer till (C_V= 1-2 m^2/year sheared at strain rates of 0.014%/min and 0. 3%/rnin.

Fig 3.24 Effective stress paths measured during undrained shear of lower cromer till after D.W Hight (1982)

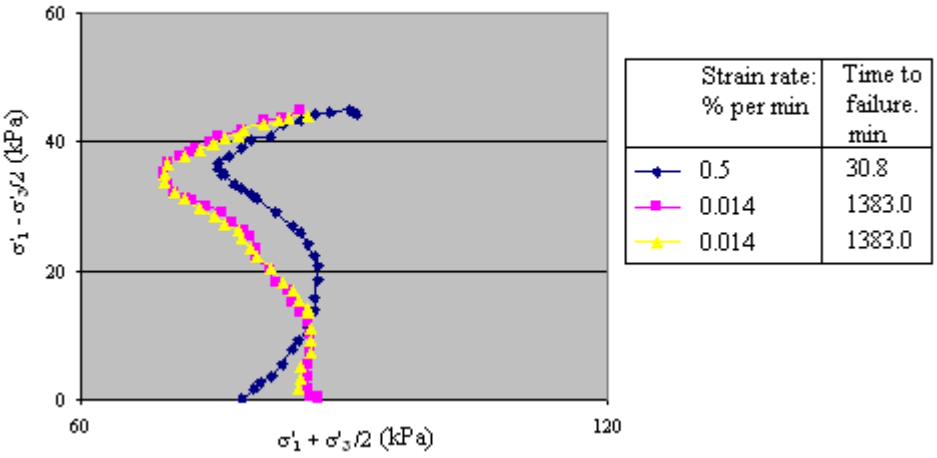

The pore pressures used to derive the effective stress paths were measured with a miniature transducer. Also shown in Figure 3.24 is the effective stress path derived from pore pressures measured at the base of the sample for the test carried out at the strain rate of 0.014%/min. It is seen that the effective stress path for the fastest test lies below those of the slowest test.

This is in contradiction with the observation made by the author (see Figure 3.23) well-established principal of shear strength increasing with strain rate.

The author believes that this may be due to the difference in the sample preparation procedures used by the author and Hight, and may also be explained by the difference in initial effective stresses of the samples.

3.1.3 Cyclic reversal triaxial tests

A. Axial strain

Figure 3.25 shows plots of double amplitude axial strain ϵ_{da}[3] versus the number of cycles for all cyclic tests. It should be noted that axial strain data for tests A.1 to, A.3 and B.1 were only obtained for the first and last two cycles.

Tests of series A and B, although not intended, were loaded about an initial tensile deviator stress. This was because the upthrust the samples experienced due to the connection of the loading ram to the top platen was not compensated. This resulted in the total stress ratio τ/C_u and the initial effective stress ratio τ/σ_0' applied in tension being higher than in compression.

The parameters τ/C_u and τ/σ_0'are the ratios of maximum shear stress applied in the reversed cyclic triaxial test during a cycle to the static undrained shear strength (C_u) and to the initial effective stress respectively.

$$\epsilon_{da} = \left|\epsilon_{D\max}\right| + \left|\epsilon_{-D\max}\right|$$

(ϵ_{Dmax}) and (ϵ_{Dmax}) are the axial strains associated with the maximum deviator stress in compression and tension respectively. It should be noted that under cyclic loading the same value of (C_u) as used to calculate τ/C_u applied in tension and compression.
The undrained shear strength was obtained from the monotonic tests carried out at a strain rate of 0.012%/min.
It is suggested in Section 3.2.3 that, for samples with equal initial effective stresses,

$$(C_u)_{comp} \succ (C_u)_{tens}$$

It can therefore be deduced that

$$(C_u)_{tens} = (C_u)_{tcomp} \times (\tau / C_u)_{comp}$$

and

$$(C_u)_{comp} / (C_u)_{tens} = 1.18$$

The total stress ratio applied in tension was, in fact, about 18% higher than in compression. The author believes that if the same value of (C_u) was used to calculate the cyclic stress ratio τ/C_u in compression and tension (i.e. symmetrical loading), a tendency for greater ϵ_A in the tensile mode than in compression may be observed.

As tests of series A and B were asymmetrically loaded, the parameters $(\tau/Cu)_{mean}$ and $(\tau/\sigma_0')_{mean}$ were used. They are the mean values of τ/Cu and τ/σ_o' applied in compression and tension respectively

$$(\tau / C_u)_{mean} = \left[(\tau / C_u)_{comp} + (\tau / C_u)_{tens}\right] / 2$$

$$(\tau / C_u)_{mean} = \left[(\tau / C_u)_{comp} + (\tau / C_u)_{tens}\right] / 2$$

It is seen in Figure 3.25 that tests A.1 and B.1, winch were run at: $(\tau/Cu)_{mean}$ of ± 0.38 and ± 0.48 respectively, developed larger ϵ_{da} than the remaining tests of series A and B which had (τ/C_u)mean of ± 0.38 and ± 0.48 respectively.

Fig 3.25 Double amplitude axial strain (%) vs nimber of cycles.

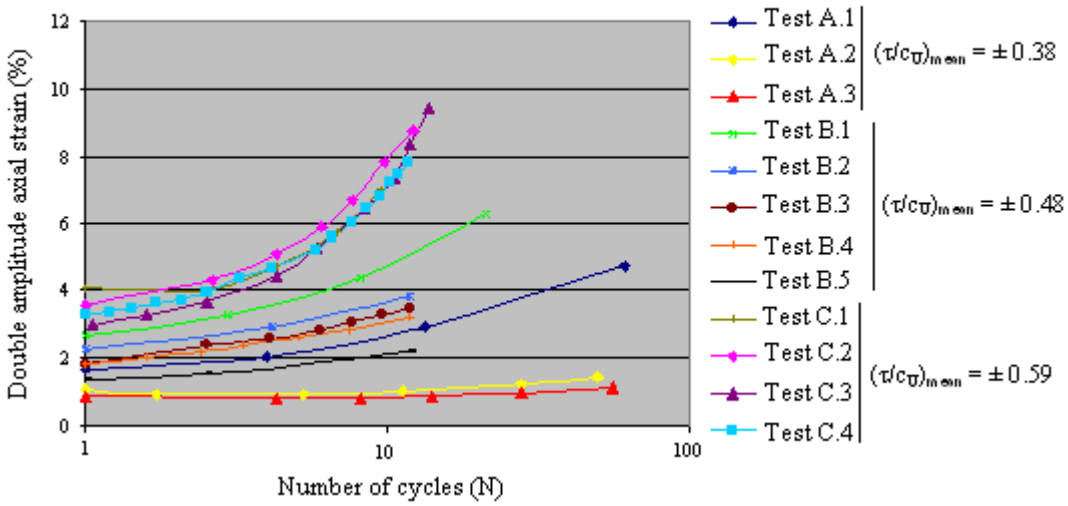

This may be due to the low initial effective stresses associated with these two tests (see Table 3.4). However, with these two exceptions, the greater the $(\tau/Cu)_{mean}$, the smaller the number of cycles required to cause a specified ϵ_{da}.

The close similarity in the variation of ϵ_{da} with the number of cycles between test C.4, which was first loaded in tension before compression, and any other test of series C (i.e. tests C.1 to C.3) where the opposite sequence was applied, suggests that there is apparently no significant effect of the sequence of loading on the double amplitude axial strain.

An alternative view of the results, which is the relation between $(\tau/Cu)_{mean}$ and the number of cycles at different double amplitude axial strains (2% and 5%), is shown in Figure

3.26. It is seen that increasing $(\tau/Cu)_{mean}$ from ±0.38 to ±0.48 and then to ±0.5 9, reduced the number of cycles to cause 2% and 5 % ϵ_{da} from 3 to 2 and then to 1 and from 28 to 6 and then to 4 respectively. Also shown in Figure 3.26 are the 2% ϵda results from tests A.1 and B.5.

It is seen that test B.3, run at $(\tau/Cu)_{mean}$= ±0.48, had a higher resistance to cyclic loading than test A.1 run at $(\tau/Cu)_{mean}$= ±0.38).

Similarly, the 5% ϵ_{da} results from test C.2 [(τ/C_U) = ± 0.59] had a lower resistance to cyclic loading than any test of series C (i.e. C.1, C.3, C.4), although all tests of series C were tested with similar $(\tau/C_U)_{mean.}$= ±0.59.

Fig 3.26 τ/c_U vs number of cycles

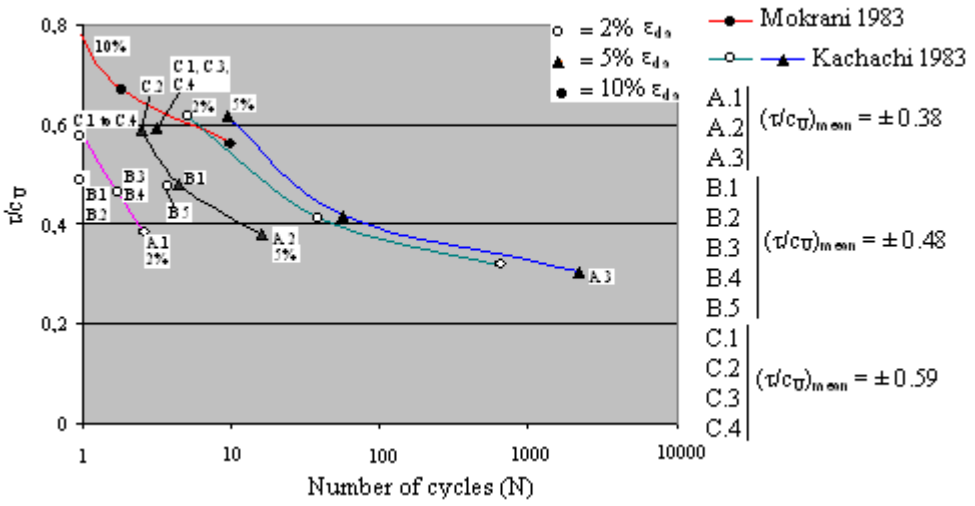

These inconsistencies in cyclic resistance are believed to be due to the fact that samples with different initial effective stresses are compared on the basis of $(\tau/C_U)_{mean}$ and that a consistent behaviour could be obtained provided that the above comparisons are made on an initial effective stress basis (see Figure 3.28). In fact, it is seen in Table 3.4 that A.1 had a higher $(\tau/\sigma_o')_{mean}$= ± 0.39 than test B.5 which had $(\tau/\sigma_o')_{mean}$=± 0.35.

Similarly test C.2 had $(\tau/\sigma_o')_{mean}$= ± 0.57, while tests C.1, C.3, C.5 had $(\tau/\sigma_o')_{maen}$=±0.5.

Also plotted in Figure 3.26 are data from tests carried out by G.Kachachi (1983) (29). Kachachi's samples were consolidated in the œdometer to a pressure of 480 kN/m^2 and had overconsolidation ratios varying from 1 to 3. The frequency was 0.1 Hz. It is seen that increasing $(\tau/Cu)^{[4]}$ from 0.31 to 0.62 decreased the number of cycles required to cause 2% and 5% ϵ_{da} from 2500 to 7 and from 10150 to 15 respectively.

Mokrani, (1983) (8), Figure 3.26, using the same soil as Kachachi (Cowden clay consolidated in the œdometer to 480kN/m^2) and a frequency of 0.02Hz, reported that increasing τ/Cu from ± 0.5 7 to ±0.67 and then to ± 0.76 decreased the number of cycles to cause 10% ϵ_{da} from 3 to 2 and then to 1 respectively.

It can be concluded from Figure 3.26 that at the same total stress level, Kachachi's and Mokrani's Samples show higher resistance to cyclic loading than those of the author.

The main reason for the difference in response to cyclic loading is believed to be due to the effect of frequency.

The main reason for the difference in response to cyclic loading is believed to be due to the effect of frequency.

Khaffaf (1978) (15) performed a series of reversed triaxial tests on clay, Covenham clay and modified Grimwith clay, with plasticity indices of 21%, 22% and18% respectively, using a range of frequencies from 1 Hz to 1/120 Hz. Khaffaf found that cyclic strength decreases with decreasing frequency, as shown in Figure 3.27.

Fig 3.27 Reversed cyclic stress ratio vs number of cycles at double amplitude strain=10 % different materials and frequencies. (after Khffaf 1978).

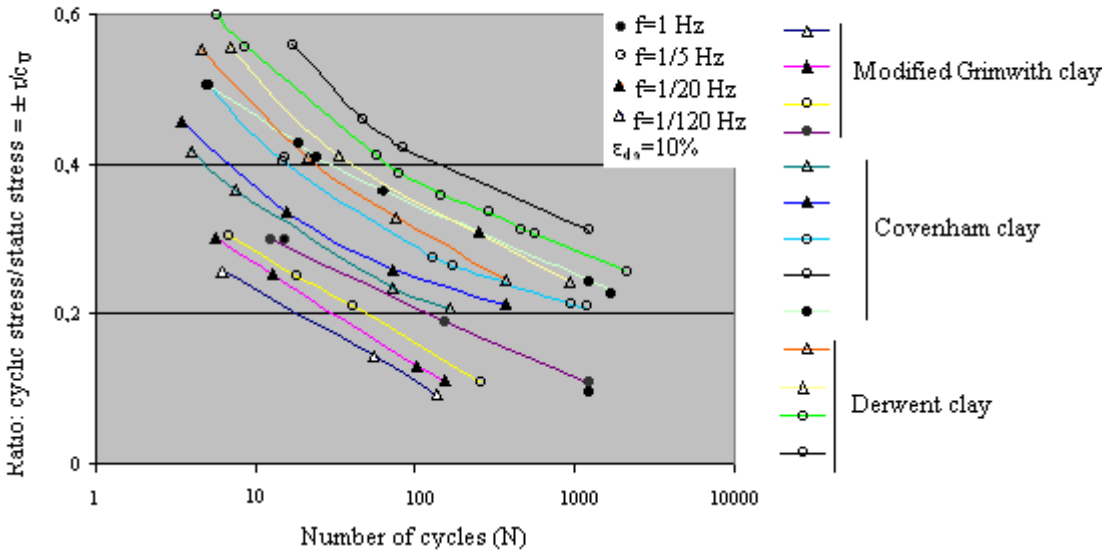

Procter and Khaffaf (1978) (15)argued that greater loading rates inhibit the development of strains which otherwise, in a slower or static test, would develop as creep strains. Thus, increased frequency retards the weakening process.

Khaffaf (1975) (28)reported that the larger the cyclic stress ratio, the lower the number of cycles required to induce deformations and failure. Khaffaf found that the ratio of $(\tau/Cu)^{(4)} > \pm 0.6$ applied to any of the clays he tested in his study (North Sea clay, Covenham clay, Alvingham clay and Amsterdam clay with plasticity index values of 21%, 22%, 19% and 18% respectively) will cause failure to occur almost immediately, while for $\tau / Cu^{(4)} < \pm 0.2$, failure would not occur even after 10.000 cycles.

To overcome the difficulties in data interpretation on the basis of $(\tau/ Cu)_{mean}$, the author's results are re-assessed on the basis of $(\tau /\sigma_o')_{mean}$, This is shown in Figure 3.28, where plots of the initial effective stress ratio $(\tau/\sigma_o')_{mean}$ versus the number of cycles required to cause 2% and 5% are presented. Kachachi's data are also shown in Figure 3.28.

It is seen that for test B.3, which had $(\tau/\sigma_o')_{mean}=\pm 0.44$, two cycles were required to develop ϵ_{da} = 2%, while for test B.2 which had $(\tau/\sigma_o')_{mean}=\pm 0.43$, only 1 cycle was required to reach a similar value of ϵ_{da} = 2%. Similarly, for test B.1, which had $(\tau/\sigma_o')_{mean} =\pm 0.5$, 6 cycles were required to develop 5% ϵ_{da} while for tests C.1 and C.3, which also had $(\tau/\sigma_o')_{mean}=\pm 0.5$, only 4 cycles were needed to develop the same double amplitude of axial strain of 5 %. These differences are believed to be very small and in the range of experimental error.

It can be concluded from Figure 3.28 that, with the exception of tests B.1 and B.2, the higher $(\tau/\sigma_o')_{mean}$ the smaller the number of cycles required to reach a specified ϵ_{da} (i.e. 2% and 5%). As, on the basis of $(\tau /Cu)_{mean}$, it is seen that Kachachi's samples show higher resistance to cyclic loading than those of the author. This may well be due to frequency effect,

as suggested before.

Khaffaf (1978) (15) compared the behaviour of different types of clay for overconsolidation ratios of 1 and 7.5.

This study led Khaffaf to the conclusion that, under a given cyclic stress ratio, τ/Cu[(4)] an overconsolidated clay can sustain a much higher number of cycles before developing a prescribed double amplitude axial strain than a normally consolidated clay, as shown in Figure 3.29. Khaffaf did not resaturate and reconsolidate his samples in the triaxial cell and his overeonsolidation ratios refer to OCR in the œdometer.

Thus related to the triaxial cell, his samples would be lightly overconsolidated (i.e.OCR=3) and heavily overconsolidated (i.e. OCR=20).

Fig 3.28 τ/σ'_0 vs number of cycles

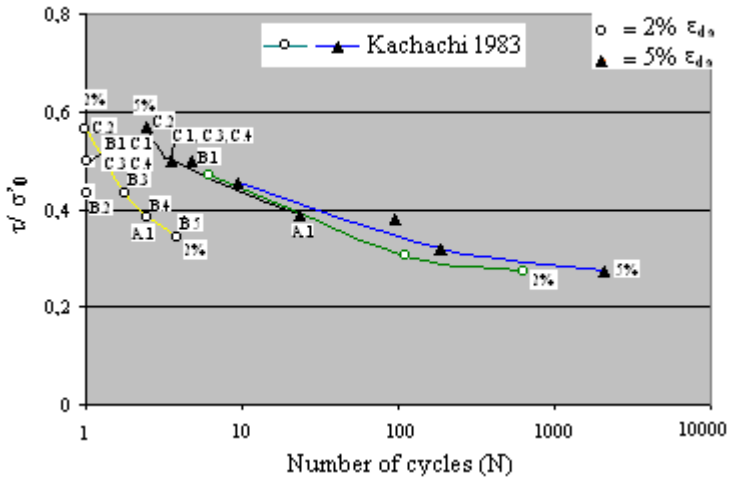

Fig 3.29 Reversed cyclic stress ratio vs number of cycles at different double amplitude strain (after Khaffaf 1978)

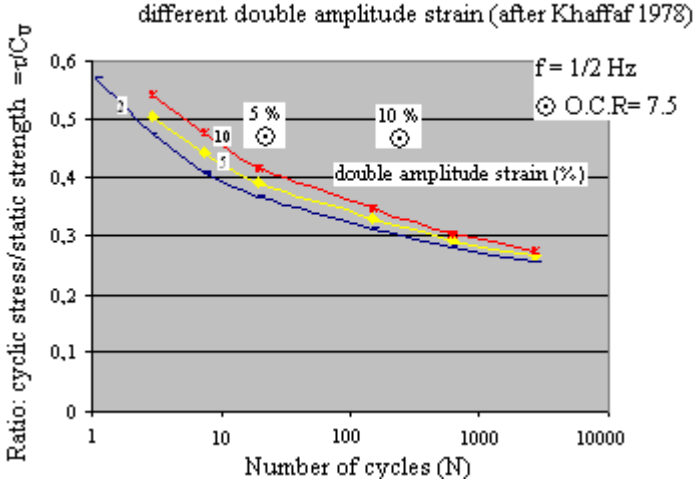

Figures 3.30 (a-c), 3.3l (a-e) and 3.32(a-d) show semi-logarithmic plots of axial strain (ϵ_A) at maximum deviator stress in compression and tension versus the number of cycles, for tests of series A, B anti C respectively. Also presented in these figures are plots of the residual or permanent strains (ϵ_{Ap}) versus N

The permanent strain is the axial strain that remains at the end of each unloading (i.e. D = 0). It is seen in Figure 3.30 (a, b) that $|\epsilon_A|$ is larger in tension than in compression.

This tendency to favour a tensile mode of deformation is believed to be mainly due to the large difference in the total stress ratio $(\tau/Cu)_{mean}$ to which the soil was subjected in compression and tension. The reason for this asymmetry is referred to above.

In fact, the total stress ratio (τ/Cu) applied to samples of series A was approximately 53% higher in tension than in compression (see Table 3.4). A comparison of the axial strain developed in compression and tension versus the number of cycles for test A.3, shown in Figure 3.30(c) would be difficult as only very small (ϵ_A) were recorded for this test.

Furthermore, strain data for the first cycle of this test was impossible to obtain because or an electrical failure which occurred at the start of the test.

It can also be observed in Figure 3.30(a-c) that tests A1 to A.3, although run at the same $(\tau/Cu)_{mean}=\pm 0.38$, show different resistance to cyclic loading. This is due to the fact that, although these tests had the same $(\tau/Cu)_{mean}$, they had different $(\tau/\sigma_o')_{mean}$. In fact, a comparison in terms of $(\tau/\sigma_o')_{mean}$ shows that the lower the ratio $(\tau/\sigma_o')_{mean}$ the higher the resistance to cyclic loading.

Figures 3.31 (a-e) show the strain data for tests B.1 to B.3. Despite the asymmetric loading (the total stress ratio in tension was approximately 42% higher in tension than in compression, see Table 3.4), at the beginning of each test (1st cycle), the axial strains developed in compression were similar to those in tension.

However, as the number of cycles increases, this equality disappears and ϵ_A becomes larger in tension than in compression.

A much more symmetrical overall axial strain behaviour with only all tendency for greater (ϵ_A) in the tensile mode is observed in Figure 3.32(a-d) for tests C.1 to C.4, which were symmetrically loaded, as shown in Table 3.4.

This is in agreement with Mokrani (1983). As observed earlier for the double amplitude axial strain, the sequence of loading has no apparent effect on the development of (ϵ_A).

This is shown in Table 3.5, where values of (ϵ_A) developed at $\pm D_{max}$ for three different cycles for the compression/tension tests C.1 to C.3 and the tension/compression test C.4 are presented.

It can also be seen, in Figure 3.32(a-d) that, in tests with a symmetrical total stress ratio τ/Cu, the amount of axial strain recovered on unloading (i.e. D=0) in tension is generally similar to that in compression and that the axial strain recovery is approximately constant.

The axial strain recovery is defined as the difference in axial strain developed at D_{max} (in tension or compression) and D=0 kN/m^2.

Fig 3.30.a Axial strain vs number of cycles for test A.1

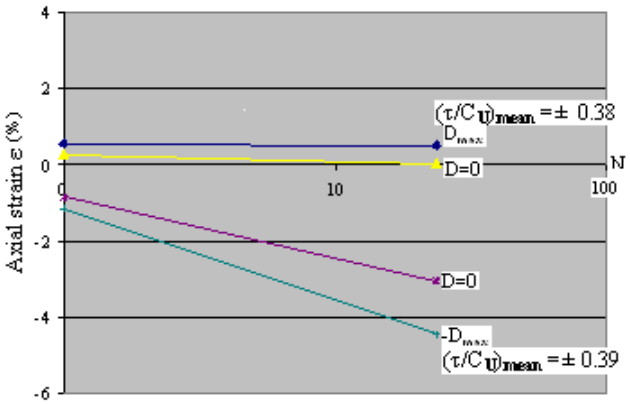

Fig 3.30.b Axial strain vs number of cycles for test A.2

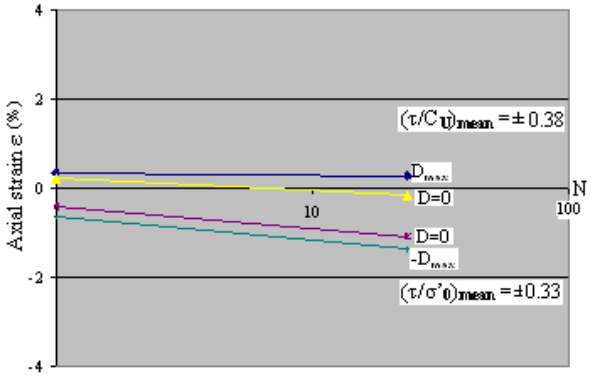

Fig 3.30.c Axial strain vs number of cycles for test A.3

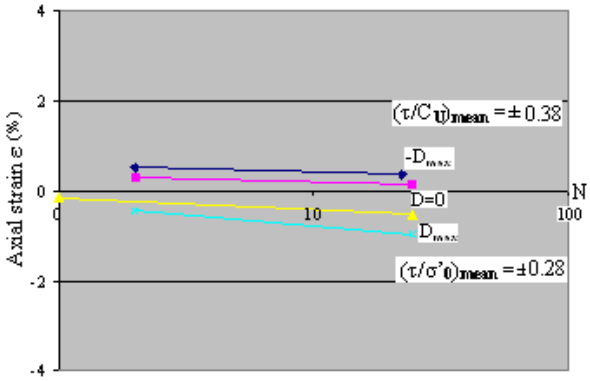

Fig 3.31.a Axial strain vs number of cycles for test B.1

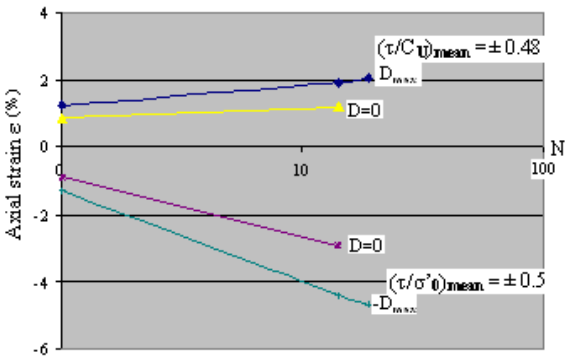

Fig 3.31.b Axial strain vs number of cycles for test B.2

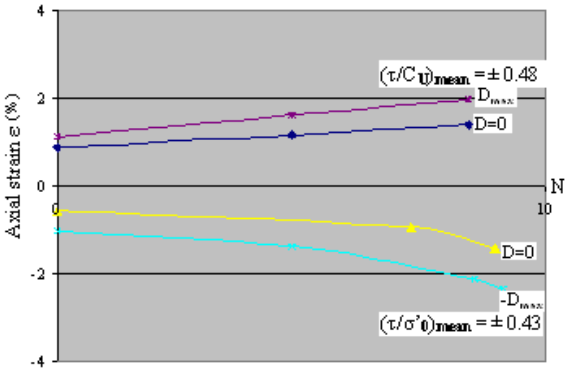

Fig 3.31.c Axial strain vs number of cycles for test B.3

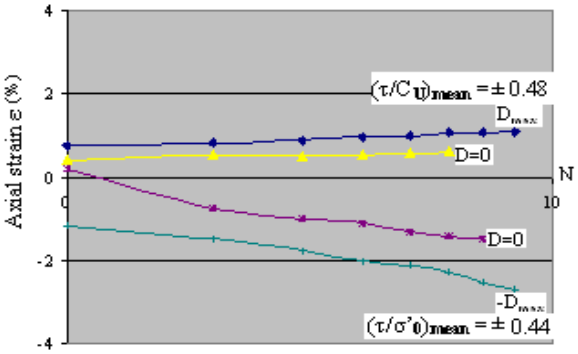

Fig 3.31.d Axial strain vs number of cycles for test B.4

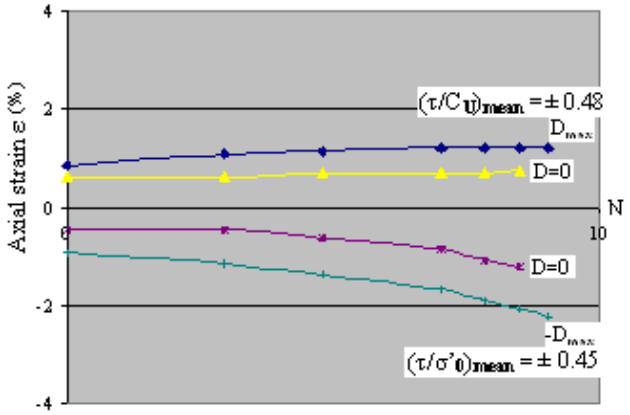

Fig 3.31.e Axial strain vs number of cycles for test B.5

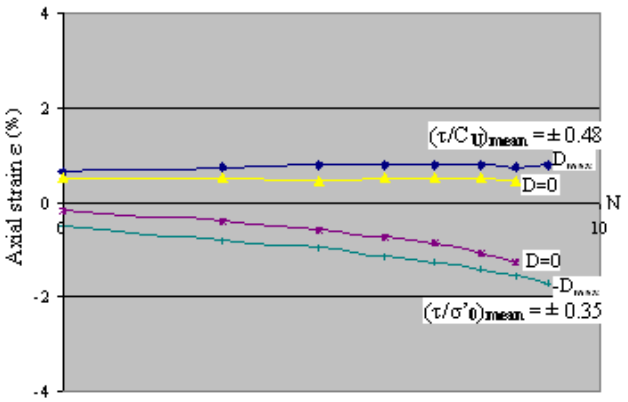

Fig 3.32.a Axial strain vs number of cycles for tests C.1

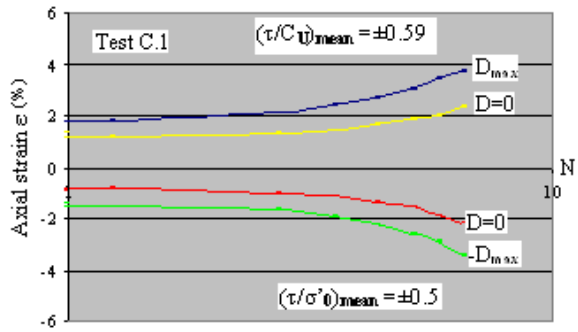

Fig 3.32.b Axial strain vs number of cycles for tests C.2

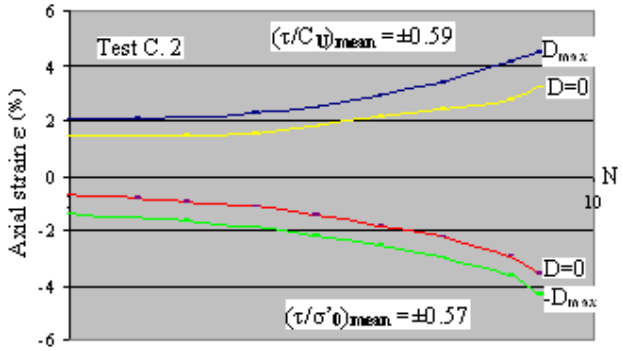

Fig 3.32.c Axial strain vs number of cycles for tests C.3

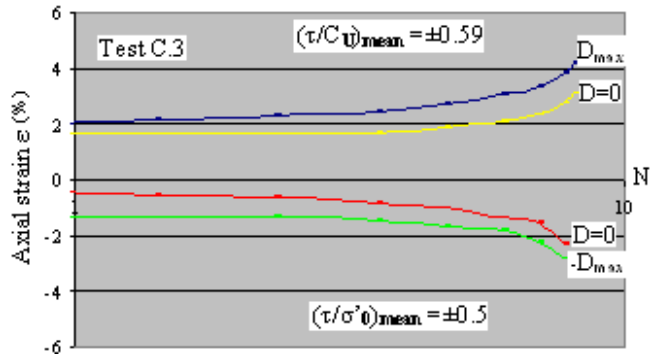

Fig 3.32.d Axial strain vs number of cycles for tests C.4

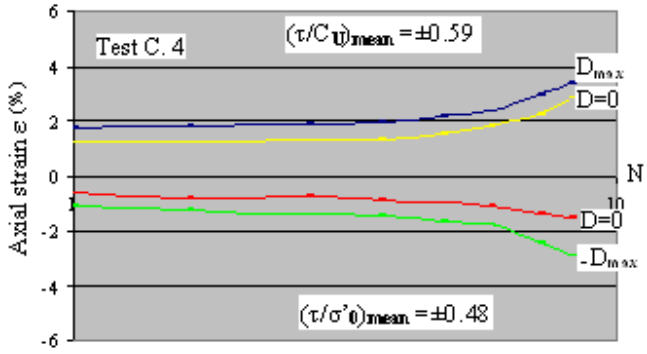

B. Pore pressure behaviour under cyclic loading

As explained in section 3.2.1, the author believes that accurate mid-height pore pressures relevant to failure conditions were consistently measured, while base pore pressures might have been erroneous, particularly in tests with high τ/Cu, as in tests of series C.

Figures 3.33 to 3.36 and Figures 3.37 (a,b) to 3.40 (a,b) show semi-logarithmic plots of excess mid and base pore pressures (ΔU_M and ΔU_B) at maximum deviator stress in tension and compression versus number of cycles (N) for all cyclic tests.

Also shown in Figures 3.33, 3.38 (a) and 3.40 (a) are plots of ΔU_{MC} and ΔU_{BC} (excess mid and base pore pressures corrected for variations in mean total stress by factors of -D/3 in

compression and + D/3 in tension) versus N for tests A.1, B.4 and C.3 respectively. It should be noted that ΔU_M and ΔU_B for tests A.1 to A.3 and B.1 were only obtained for the first and last cycles.

It is seen, in Figures 3.37(a,b) to 3.40(a,b), that during the first cycle the "compression" excess pore pressures measured at the middle and base of the specimens increased sharply. This was generally followed by a steady increase in ΔU_M and a decrease in U_B during the next few cycles, before the latter started to increase again.

Similarly, in tension, the sharp decrease in ΔU_M and ΔU_B during the first cycle is generally followed by a further slight decrease before both ΔU_M and ΔU_B

For one test from each series (i.e. A.1, B.4 and C.3) the values of excess mid and base pore pressure at $\pm D_{max}$ were corrected for mean total stress variation and plotted against the number of cycles, as shown in Figures 3.33, 3.38 (a) and 3.40 (a).

It is seen that the corrected excess peak mid and base pore pressure curves converge.

However, the convergence of the base pore pressure curves was significantly less than those of the mid pore pressure curves. Table 3.6 shows a comparison between the theoretical change in mean total stress (2D/3) and the observed mid and base pore pressure double amplitudes during the first and last cycles for all cyclic tests.

Generally larger double amplitudes of base pore pressures than 2D/3 are observed; however, good correlation of double amplitude of U_M with the change in mean total stress (2D/3) is seen. It can be deduced from the above observations that pore water pressures measured at mid-height were of a higher quality than those measured at the base.

Fig 3.33 Excess mid-base PWP vs number of cycles for tests A.1

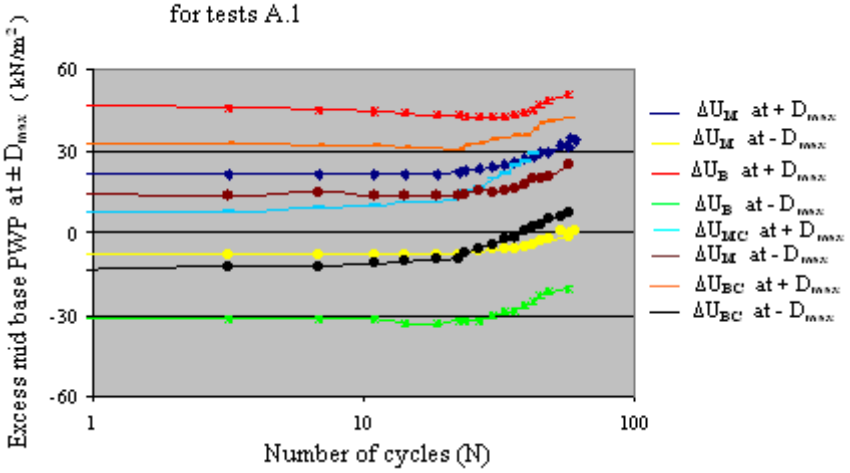

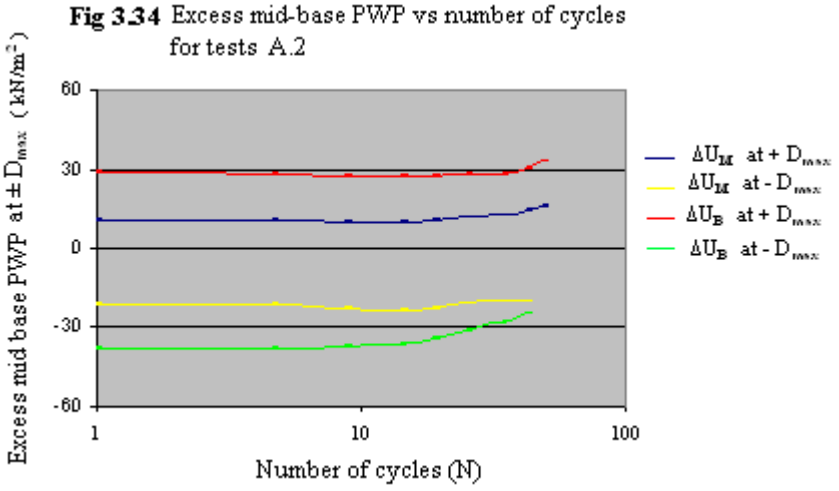

Fig 3.34 Excess mid-base PWP vs number of cycles for tests A.2

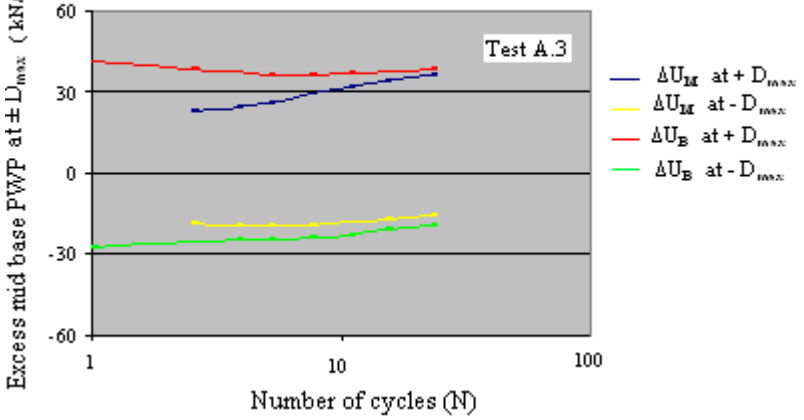

Fig 3.35 Excess mid-base PWP vs number of cycles for tests A.3

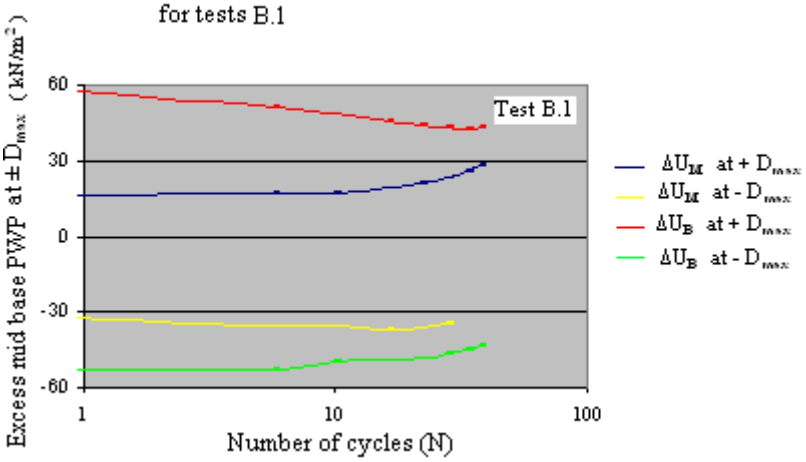

Fig 3.36 Excess mid-base PWP vs number of cycles for tests B.1

Fig 3.37.a Excess mid-base PWP vs number of cycles for tests B.2

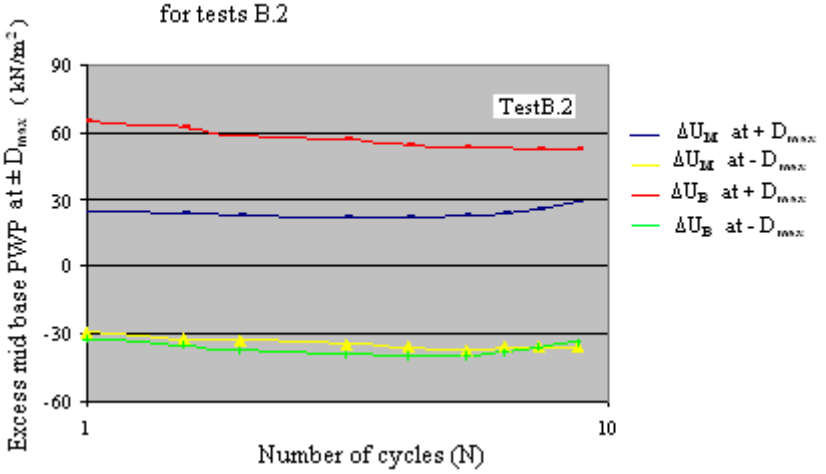

Fig 3.37.b Excessmid-base PWP vs number of cycles for tests B.3

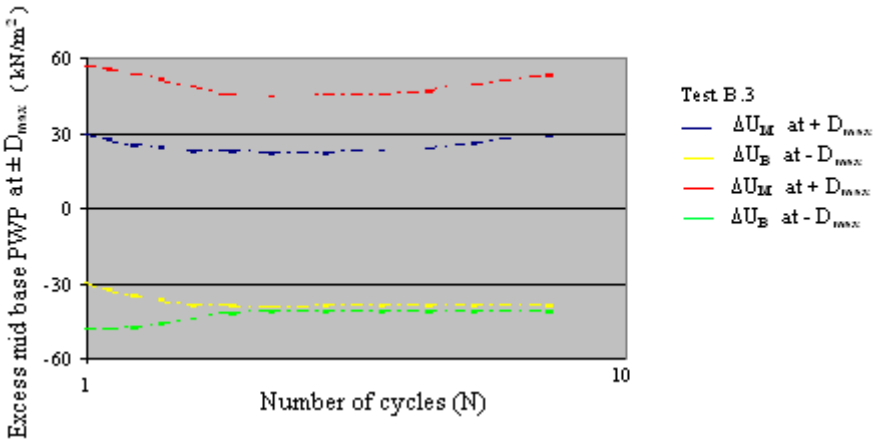

Fig 3.38 a Excess mid-base PWP vs number of cycles for tests B.4

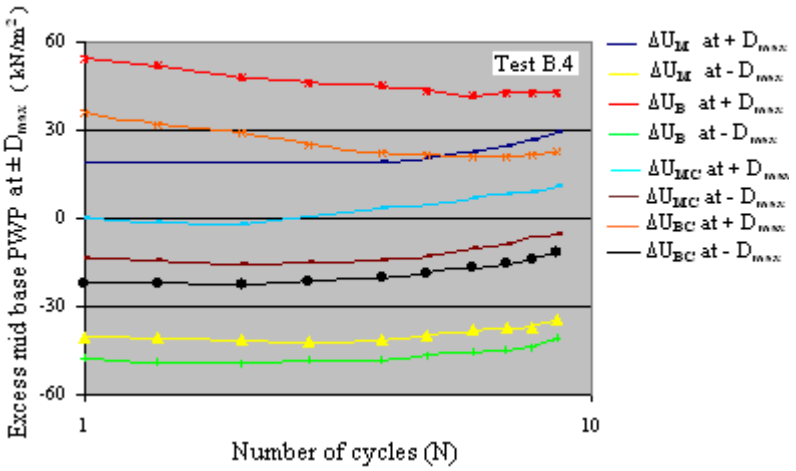

Fig 3.38.b Excess mid-base PWP vs number of cycles for tests B.5

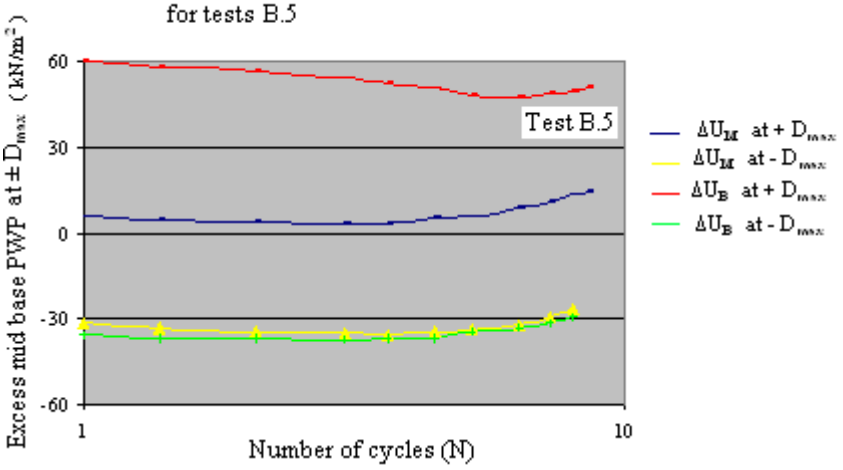

Fig 3.39.a Excess mid-base PWP vs number of cycles for tests C.1

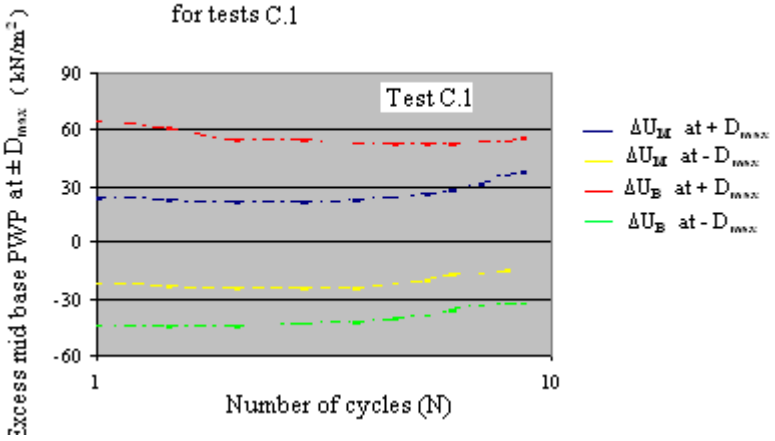

Fig 3.39.b Excess mid-base PWP vs number of cycles for tests C. 2

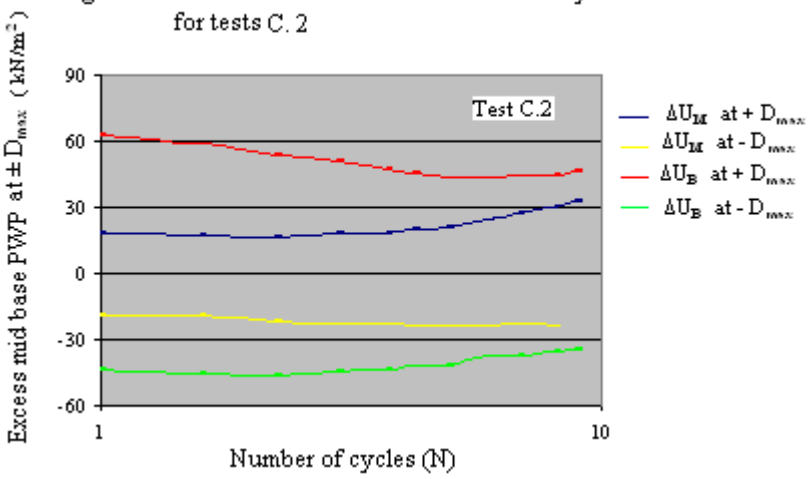

Fig 3.40.a Excess mid-base PWP vs number of cycles for test C.3

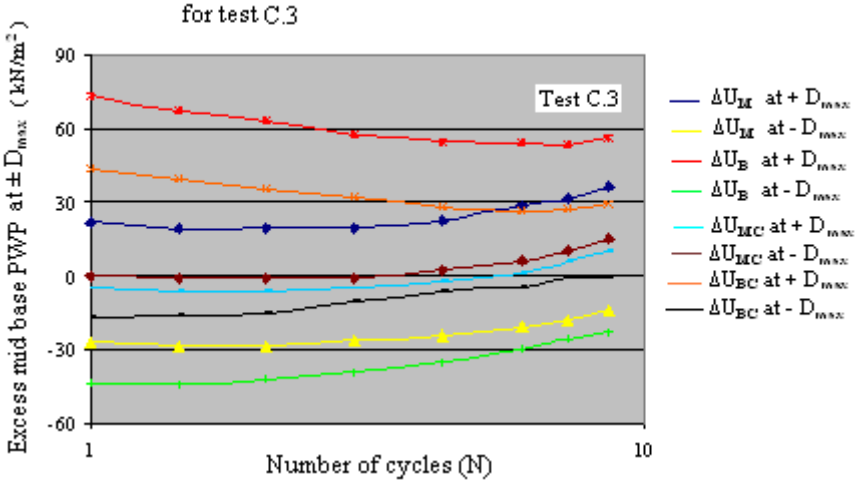

Fig 3.40.b Excess mid-base PWP vs number of cycles for tests C.4

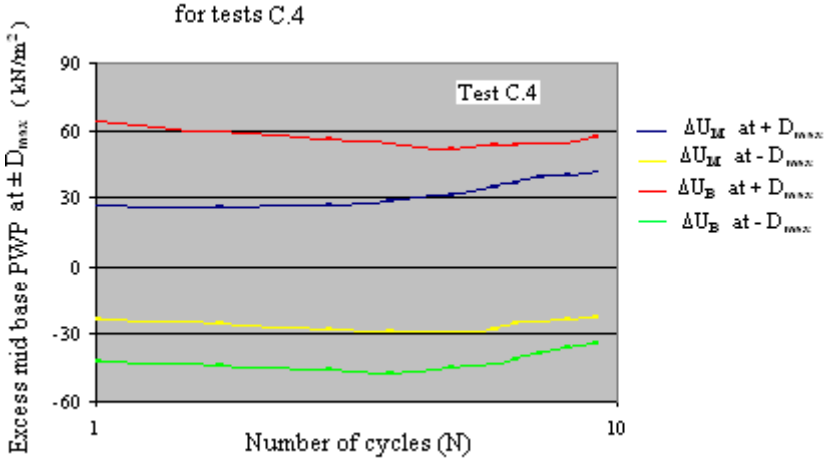

Khaffaf (1978) (15) applied correction factors of - D/3 and D/3 to his maximum and minimum base pore pressure values. He obtained divergent results, with the "corrected' minimum values of U_B often exceeding those of the "corrected" maximum ones. He attributed that to frequency effect (1/3Hz) stating that "clay did not have sufficient time to generate the full pore pressure throughout the sample".

However, the author believes that the response time of the Bell and Howell transducer used by Khaffaf was not fast enough for correct measurements at this rate of testing even if the clay had generated full pore pressures.

It was observed in tests B.2 to B.3 and C.1 to C.4 that while the double amplitude of U_B decreases with N, the double amplitude of U_M increases with N.

Similar behaviour was observed in tests A.1 to A.3 and B.1 when comparisons between pore pressures in the first and last cycles (with constant cell pressure) were made. This behaviour is illustrated in Fig.3.41, were plots of double amplitude of U_M and U_B versus N for one test from each series are presented. Plots of $(\Delta U_M)_{mean}^{(3)}$ and $(\Delta UB)_{mean}^{(3)}$ versus the number of cycles for the latter tests (i.e. Â.1, B.4 and C.3) are presented in Fig 3.42.

It is seen that generally $(\Delta U_M)_{mean}$ increases with the number of cycles. Similarly, after

a drop in the base pore pressure level in the first few cycles, $(\Delta U_B)_{mean}$ increases with the number of cycles.

Fig 3.41 Double amplitude mid-base PWP vs number of cycles for tests A.1, B.4 and C.3

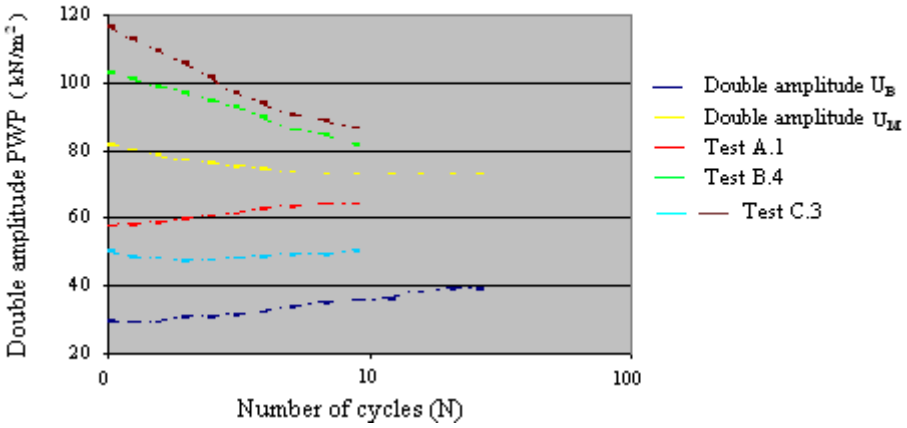

Fig 3.42 Mean excess mid-base PWP vs number of cycles for tests A.1, B.4, C.3.

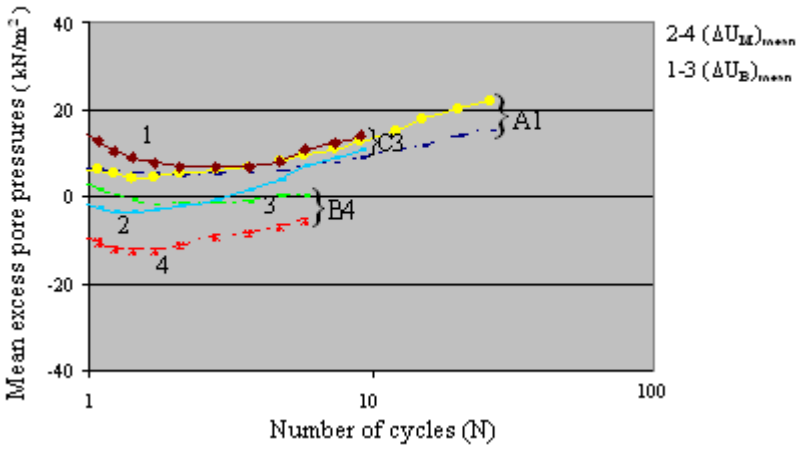

C Axial strain, deviator stress pore pressure versus time

Plot of axial strain, deviator stress, mid and base pore pressures versus time for the fist and last cycle (with constant cell pressure) for tests A.1, B.4 and C.3 are presented in figures 6.43 to 6.48

Tests A.1, B.4 and C.3 were taken as representative of each series of tests (i.e. A, B and C). From the examination of the data, the following observations were made:

-In test A.1, which had $\tau/Cu = \pm 0.3$ and $\tau/\sigma_o' = \pm 0.31$ in compression, ϵ_{max} and $+D_{max}$ occurred at the sae time (see figure 6.43).
However, with an increase in the number of cycles, ϵ_{max} occurred after D_{max} (see figure 6.44).

-In the remaining tests (i.e.B.4 and C.3, $| \pm \epsilon_{max} |$ occurred slightly after $+D_{max}$ and $-D_{max}$ respectively (see figure 6.45 to .6.48).

Bearing in mind the low frequency (0.00026 Hz) use in this investigation, the author believes that the latter behaviour may be due to creep effects. Creep is defined as the ability of the clay to continue deforming over a period of time under sustained load. Table 3.7 shows the creep strains developed during the first and last cycle (with constant cell pressure for all cyclic tests). The author believes would comment that that these strains were in fact an indication of creep effect.

The creep effect in cyclic loading tests was also reported by P.W. Rowe (1974) (31). He reported that, due to creep, clays give lower cyclic strengths with lower frequencies. He also suggested that, for similar reasons, rectangular pulse shape would give lower strengths than peaked pulses as the maximum loads are sustained for a much greater proportion of a cycle.

It is believed that at low cyclic stress ratios , and particularly during the first cycle where only small strains develop, creep effects can be either non existent or very small(as in compression during the first cycle of tests A.1 to A.3 and B. (see table3.7)

The author believes that as clay softening increases with the number of cycles, the effect of creep would become more apparent, as is the case in tests C.2, C.3, and C.4 (see table3.7).

However, it can also be deduced from table3.7, that for some tests (for example A.3and B.4) the amount of creep strain has been reduced. The author believes that the latter observations contradict the principal that creep effect increases with clay softening.

These contradictions are believed to be mainly due to the difficulties involved in accurately measuring such very small amounts of strain.

D.C Proctor and Khaffaf (1984) (16) suggested that load-controlled cycling performed at a stress level below a certain value of τ/Cu would have no weakening effect.

As pore pressure generation is strain dependent, pore pressures are expected to be affected by creep (i.e. due to the stress paths, pore water pressure will continue to increase in compression and decrease in tension after the maximum deviator stress was reached).

It was observed that in the first cycle of series A and B (e.g. Figures 3.43 and 3.45), U_{Mmax} and D_{max} occurred at the sane time.

With increasing number of cycles, U_{Mmax} occurred slightly after D_{Max}, except for test A.3 which was the only test where both U_{Mmax} and D_{max}, U_{Mmin} $(-D_{max})$ occurred at the same time.

In tests of series C (see Figures 3.47 and 3.48) U_{Mmax} occurred before D_{max}.

In tension, however, U_{Mmin} in all cyclic tests (except test A.3) occurred slightly after $(-D_{max})$ as seen in Figures 3.43 to 3.48

Plots of U_{MC} and U_{BC} (mid and base pore pressures corrected by factor of –D/3 in compression and +D/3 in tension) versus time for tests A.1, B.4 and C.3 are presented in Figures 3.43 to 3.48

It can be seen that the maximum value of U_{MC} is reached at approximately the middle of the cycle (D=0).

The standard reversed triaxial test is conducted under the conditions of variable mean total stress, i.e. while the axial load is varied, the cell pressure is maintained constant throughout a test.

In order to investigate the effects of the change in the mean total stress on the behaviour of the Cowden Clay, each test was terminated by a cycle in which the cell pressure was varied either in phase with the axial load, as in test A1, Figure 3.49, or out of phase, as in tests B.4 and C.3, Figures 3.50 and 3.51

The apparatus used to produce such variable cell pressure is described in **section 2.6**

Figures 3.49 to 3.51 show the variation of mid and base pore pressures; variation of the cell pressure, deviator stress and axial strain with time for the last cycle of tests Al, B, 4 and C.3 respectively.

For comparison purposes mid and base pore pressures and axial strain data from a previous cycle (where the cell pressure was constant) are also presented in Figures 3.49 to 3.51

It can be seen in Figure 3.49 for test A.1 (in phase test) that U_M and U_B have increased in the last cycle, whereas, in Figures 3.50 and 3.51 for out of' phase tests B.4 and C.3, mid and base pore pressures have been considerably reduced.

The author would comment that it appears that cycling the cell pressure in or out of phase with the deviator stress would result in affecting the amplitude of pore pressure without resulting in any effect on the permanent pore pressure.

These remaining differences in pore water pressures in the last cycle of tests B.4 arid C.3 may, in part, be due to some unwanted variation in mean total stress brought about by differences in amplitude between the deviator stress and the cell pressure (see Figures 3.50, 3.51), believed to be due to the following two main reasons:

1 - Synchronisation: it was found to be extremely difficult to obtain a perfect synchronisation of the servo-hydraulic system used for the application of the axial load and the rotating mercury system to apply the variable cell pressure, as both devices were independently controlled.

2 - Accuracy: although the maximum applied deviator stresses were constant, the maximum cyclic shear stresses ($\pm\tau_{max)}$ were asymmetric because of the area change This asymmetry gradually increased with increasing displacement, whereas the maximum and minimum amplitude of the cell pressure remained constant.

The author believes that the latter problems could be solved by the use of a servo-controlled water pressure system. Such equipment has recently been acquired by the Department of Civil Engineering, University of Manchester.

Furthermore, the use of a computer for the control of the two devices (servo-hydraulic system and servo-water system) would certainly give better results.

A comparison of the developed axial strains during the last two cycles, (with and without cell pressure variation), figures 3.50 and 3.51 shows, a small increase in (ϵ_A) during the last cycle.

However, this increase in (ϵ_A) cannot be definitely attributed to the reduction in the mean total stress variation and could well be due to the softening induced by the extra cycle.

Fig 3.43 Deviat stres. pore pres. axial stra. vert-lat eff stres vs time

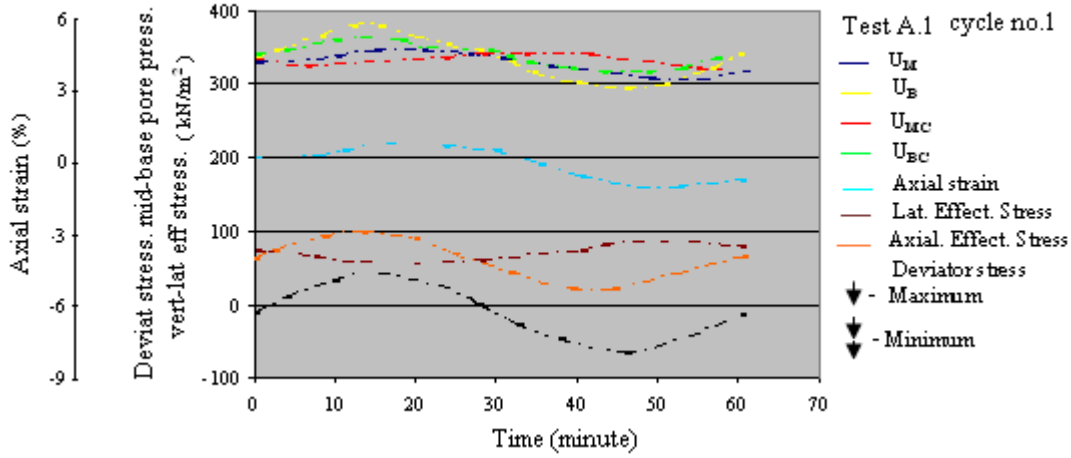

Fig 3.44 Deviat stres. pore pres. axial stra. vert-lat eff stres vs time

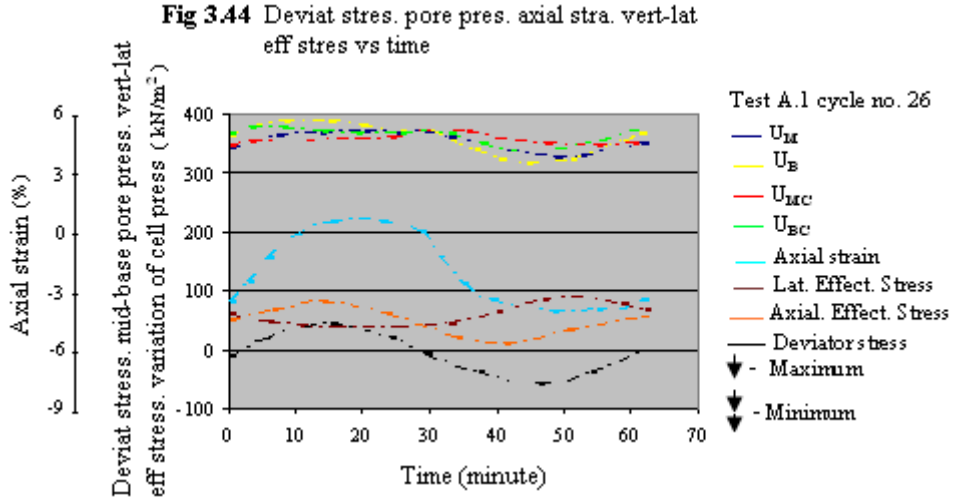

Fig 3.45 Deviat stres. pore pres. axial stra. vert-lat eff stres vs time

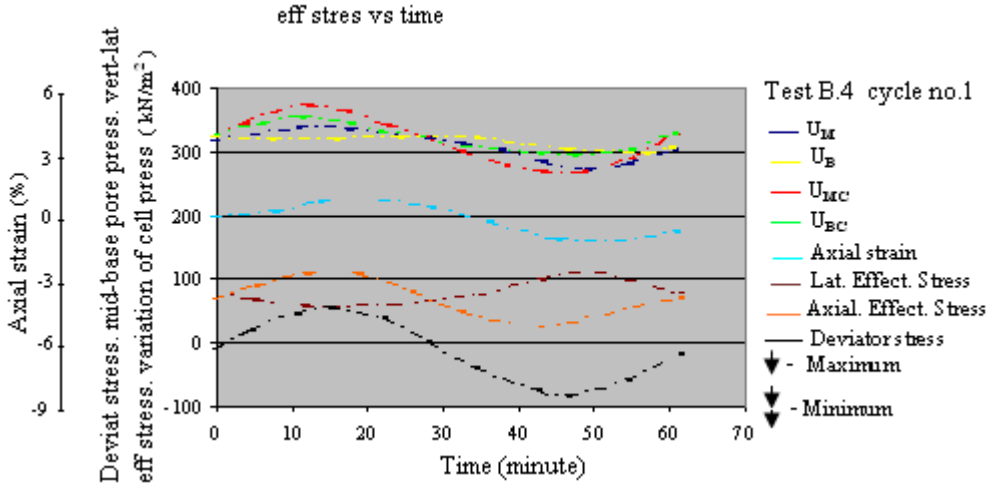

Fig 3.46 Deviat stres. pore pres. axial stra. vert-lat eff stres vs time

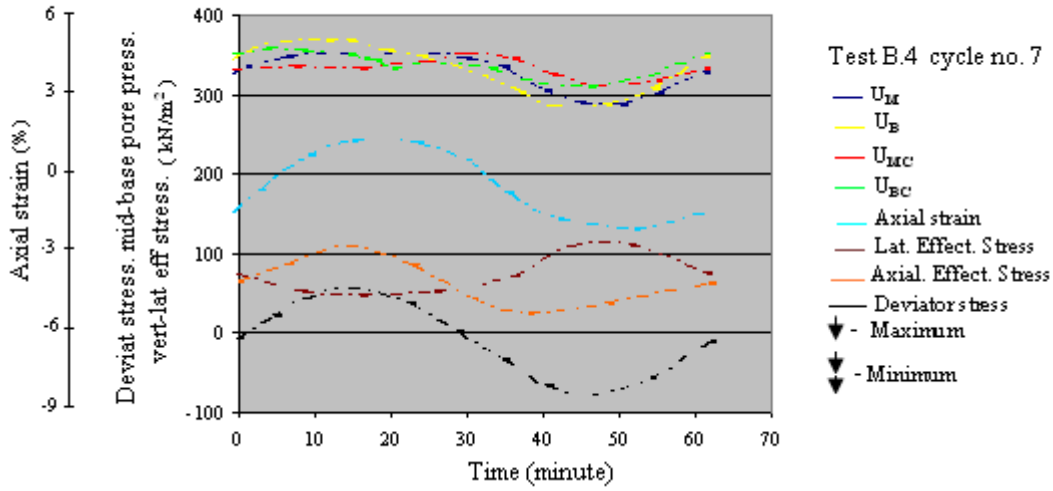

Fig 3.47 Deviat stres. pore pres. axial stra. vert-lat eff stres vs time

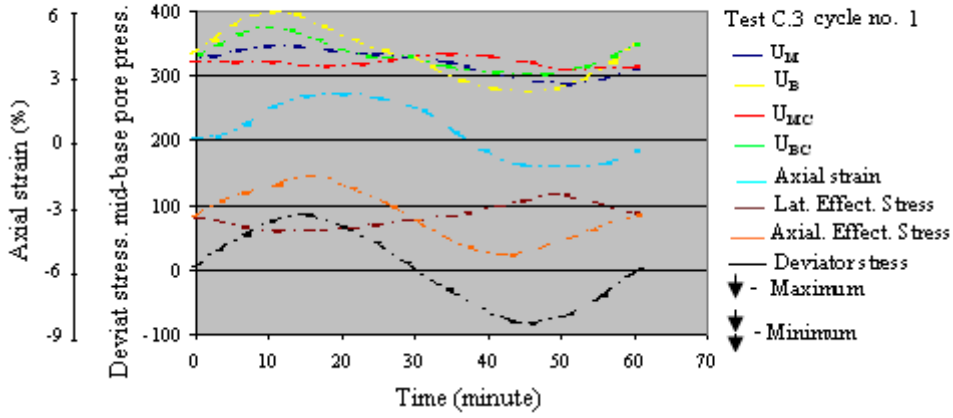

Fig 3.48 Deviat stres. pore pres. axial stra. vert-lat eff stres vs time

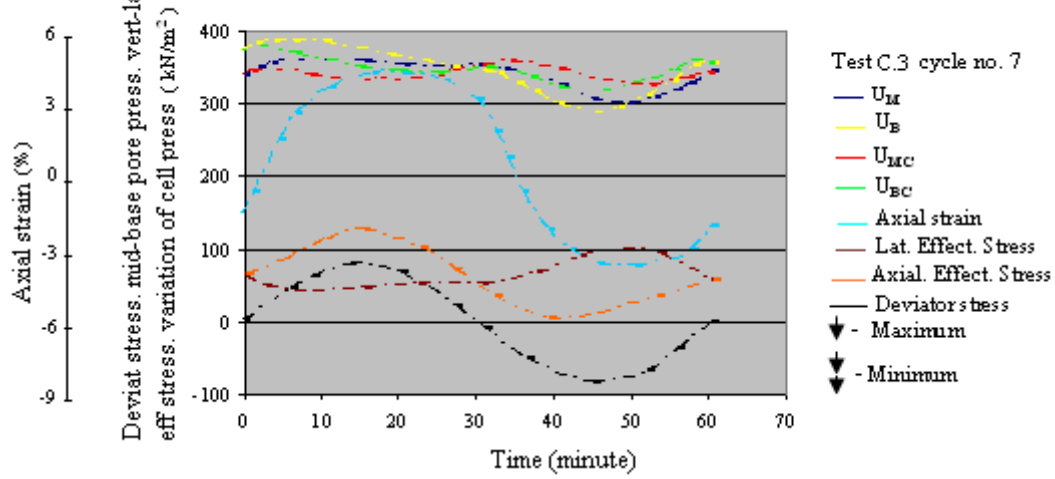

Fig 3.49 Deviat stres. pore pres. axial stra. vert-lat eff stres vs time

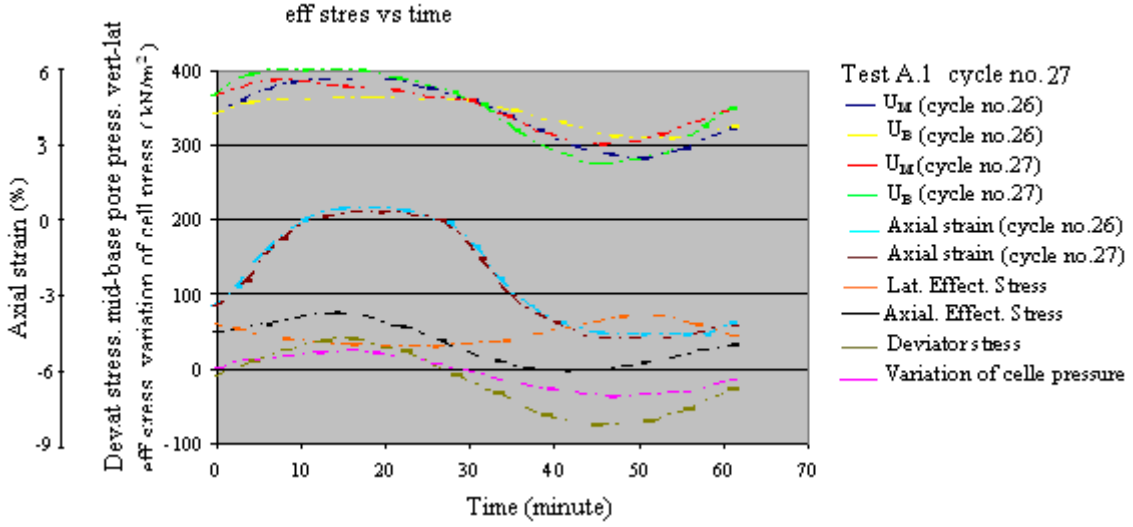

Fig 3.50 Deviat stres. pore pres. axial stra. vert-lat eff stres vs time

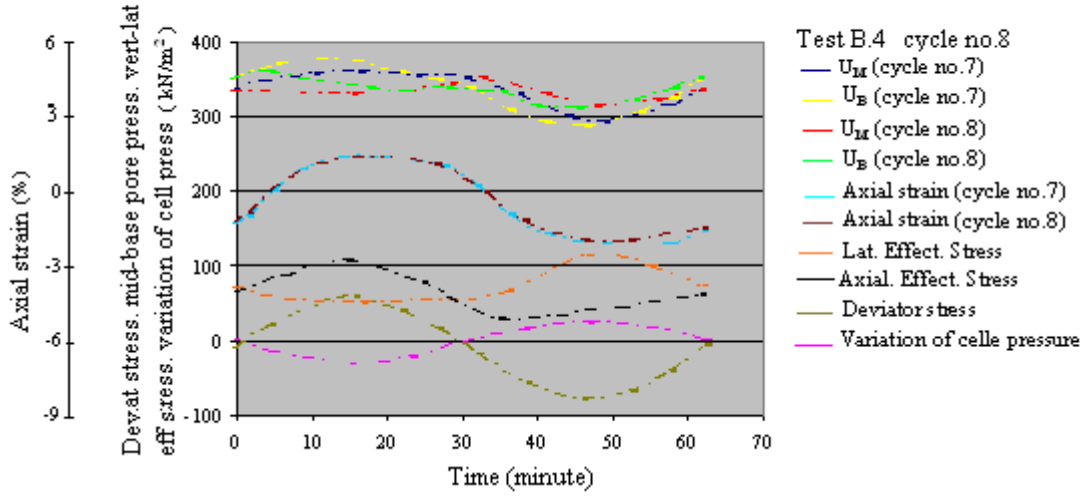

Fig 3.51 Deviat stres. pore pres. axial stra. vert-lat eff stres vs time

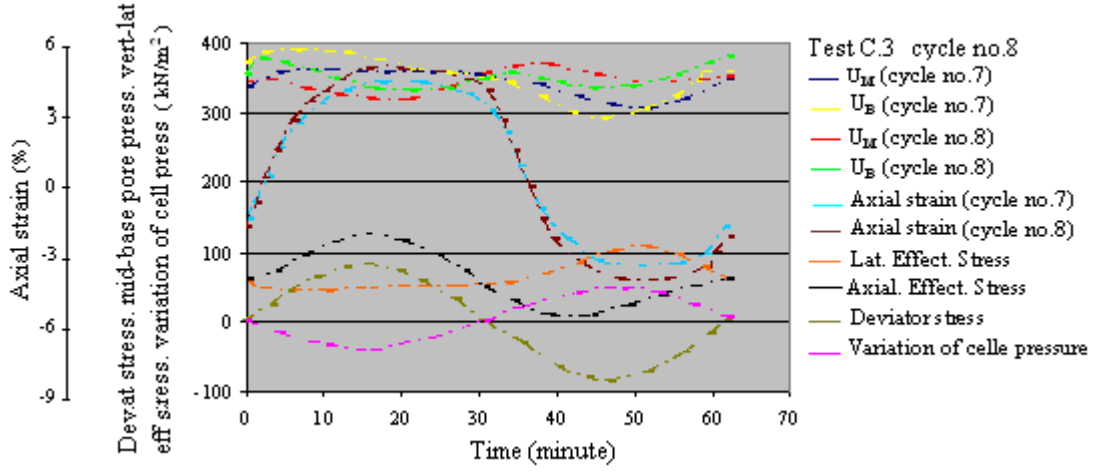

Kvalastad et al (1980) (32) performed two series of cyclic reversed triaxial tests, one with variable axial load and constant cell pressure and one with axial load and cell pressure varied out of phase in order to keep constant the octahedral normal stress (σ_{oct}) defined as $(\sigma_1 + 2\sigma_3)/2$.

The samples were overconsolidated (OCR = 4) and tested by superimposing the cyclic shear stress upon a permanent compressive shear stress in order to avoid failure in tension.

They reported that the effect of the octahedral normal stress on the overall cyclic behaviour of the Drammen clay is insignificant.

On the other hand, they observed that the effect of cyclic octahedral normal stress on the number of cycles to reach a certain permanent shear strain, (0.3%), is dependent on the shear stress amplitude. In fact, for a maximum shear stress τ_{max}= 30 - 32 kN/m^2 during cyclic loading, the clay becomes more resistant against cyclic loading if the octahedral normal stress (σ_{oct}) is constant, the resistance increasing with increasing ratio τ_P/τ_C[7].

It should be noted that this observation contradicts Kvalstad's earlier statement.

In tests with τ_{max}= 39 - 73 kN/m^2, they observed the reverse behaviour, namely keeping σ_{oct} constant makes the clay less resistant to cyclic loading. This is also in contradiction with Kvalstad's earlier statement.

Due to the inconclusive nature of the results reported in the present study, the author suggests that further investigation of the effects of the change in mean total stress during cyclic loading should be carried out before any definite conclusions are drawn.

D Effective stress analysis

Also shown in Figures 3.43 to 3.49 are the plots of axial and lateral effective stresses (σ_{ax}' and σ_{lat}' derived from mid pore pressure measurements versus time for tests A.1, B.4 and C.3.

It can be seen that the maximum axial effective stress and D_{max} occur almost at the

same time, while $(\sigma_{ax}')_{min}$ occurs before $(-D_{max})$. In the first cycle of tests A.1 and B 4, shown in figures 3.43 and 3.45, the minimum lateral effective stress occurred at the same time, while in the last cycle (Figures 3.43 and 3.46), $(\sigma'_{lat})_{min}$ occurred after D_{max}.

For test C.3, Figures 3.47 and 3.48, (σ_{lat}') occurred before D_{max}. The maximum lateral effective stress for tests A.1, B.4 and C.3 occurred after $-D_{max}$

In Figures 3.52 (a) to 3.63 (a) plots of shear stress $(\sigma'_{ax} - \sigma'_{lat})/2$ versus mean effective stress $(\sigma'_{ax} + \sigma'_{lat})/2$ for a few cycles from each cyclic test are presented. It is seen that the shape of the effective stress path varies with increasing shear stress ratio $(\tau/Cu)_{mean}$ (see Figures 3.52 to 3.60).

Andersen et al (1980) (6), Figure 3.64, carried out undrained load-controlled triaxial cyclic tests on undisturbed plastic Drammen clay which had the following average characteristics:

Natural water content	= 52%
Clay content (fraction smaller than 0.002 mm)	= 45% - 55%
Specific gravity	= 2.76 t/m^3
Plastic limit	= 28%
Liquid limit	= 55%
Plasticity index	= 27%

The clay was isotropically preconsolidated in the laboratory beyond the in-situ stress to a vertical preconsolidation stress of 4oo kN/m^2 .

The condition of no lateral strain was approximated by applying a horizontal stress to 0.5 times the vertical stress (i.e. $K_0 = 0.5$).

The clay was then unloaded to various consolidation pressures in order to produce overconsolidation ratios of 1, 4, 10 and 50.

The loading frequency was 1/10Hz. Also shown in Figure 3.64 are the effective failure envelopes obtained from static compression and tension tests run at a strain rate of 0.05 %/minute.

Andersen et al assumed that the normally consolidated samples generate failure envelopes with C' = 0, whereas, for the overconsolidated samples C' was determined assuming that Ø' is the same for the normally consolidated samples.

Andersen et all reported that the most significant problems they encountered were.

- The existence of stress concentrations caused by end restraint due to friction between the clay and the end platens
- Accurate measurement of rapid cyclic pore water pressure changes.

The author believes that the latter two problems may be more pronounced for cyclic tests. Consequently, the author believes that the pore water pressures measured by

Andersen et al may be erroneous and that both the effective static failure envelopes and the cyclic effective stress paths may have been affected.

The effective stress paths in Figures 3.60 (a) to 3.63 (a) for the symmetrical tests of series C which had $(\tau/Cu)_{mean} = \pm 0.59$, are similar to those obtained by Takahashi et all (1980), Figure 3.65, which had $\tau/Cu = \pm 0.75$ and a loading period of 10 to 480 minutes.

Plots of mean effective stress $(\sigma'_{ax} + \sigma'_{lat})/2$ obtained at the end of each cycle (tests of series A and B were loaded about an initial tensile deviator stress) versus the number of cycles for all cyclic tests are presented in Figures 3.52 (b) to 3. 63 (b).

It is seen that, with the increasing number of cycles, the effective stress paths migrate towards the origin. In fact, the direction of migration of the stress path for compression/tension tests is initially away from the origin but subsequently reverses. A similar observation was made by Takahashi et al (1980) (20).

They suggested that this behaviour was a characteristic of overconsolidated samples.. This is demonstrated in Figure 3.56, where plots of $(\sigma'_{ax} + \sigma'_{lat})/2$ versus the number of cycles for three samples with overconsolidation ratios of 1, 4 and 7 are shown

.

The author believes that this behaviour may be due to the tendency for volume increase associated with overconsolidated samples which would result in a decrease in pore pressure and an increase in the mean effective stress during the first cycle. However, as the number of cycles increases, the tendency for volume increase reduces and, due to reversed shearing, the pore water pressure level rises again resulting in a gradual decrease in the mean effective stress.

As a result of the sampling process, the samples used in the present investigation were also overconsolidated [(8)], (see table 6.4 for OCRs). Figures 3.63 (a and b) for the tension/compression test C.4 show that, with increasing number of cycles, the effective stress path migrates towards the origin from the start.

It can be seen in Figures 3.52 to 3.63 that, particularly in tension, the effective stress paths travel beyond the effective failure envelopes inferred from the slowest monotonic tests (i.e. 0.0l2%/min).

Also presented in the latter figures are the “tentative effective failure envelopes” inferred from the effective stress ratios of the single monotonic tests run at the strain rates of 0. 06 %/min and 0. 3 %/min (see Fig.3.23)

It can be deduced that no effective stress path passed the effective failure envelope anticipated from the monotonic tests as long as the equivalent [9] strain rate of the cyclic test (see table 3.8) was not higher than the strain rate of the monotonic tests from which the effective failure envelope was anticipated.

Fig 3.52.a Effective stress paths for test A.1 (compre/tension)

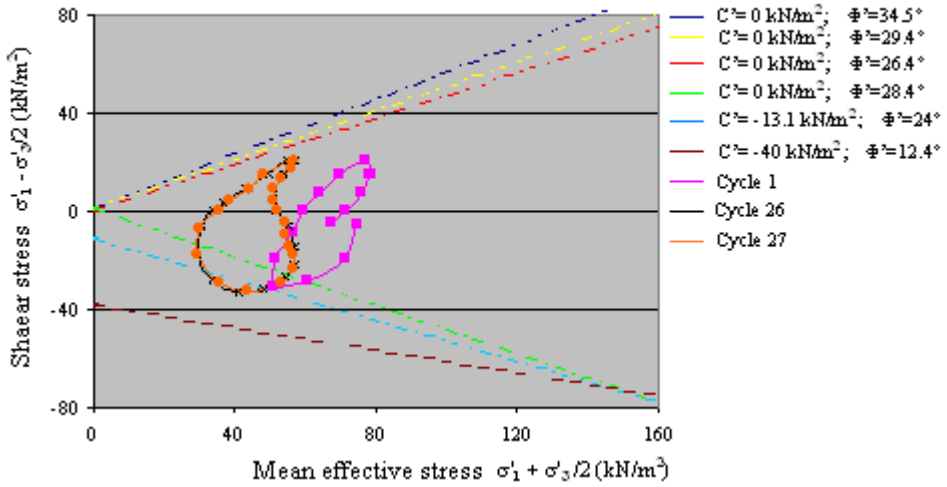

Fig3.52.b Mean effective stress at end of each cycles vs N

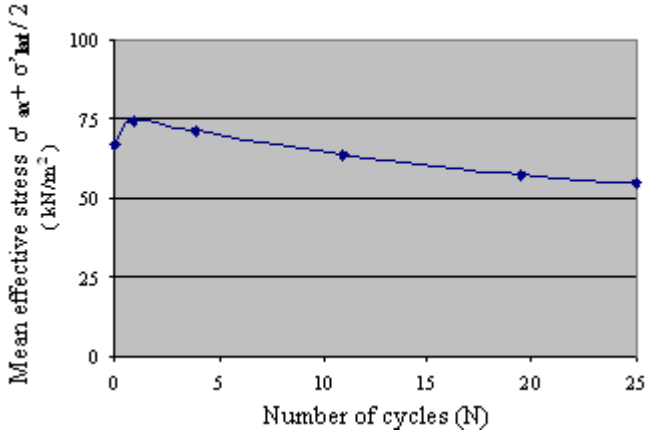

Fig 3.53.a Effective stress paths for test A.2 (compre/tension)

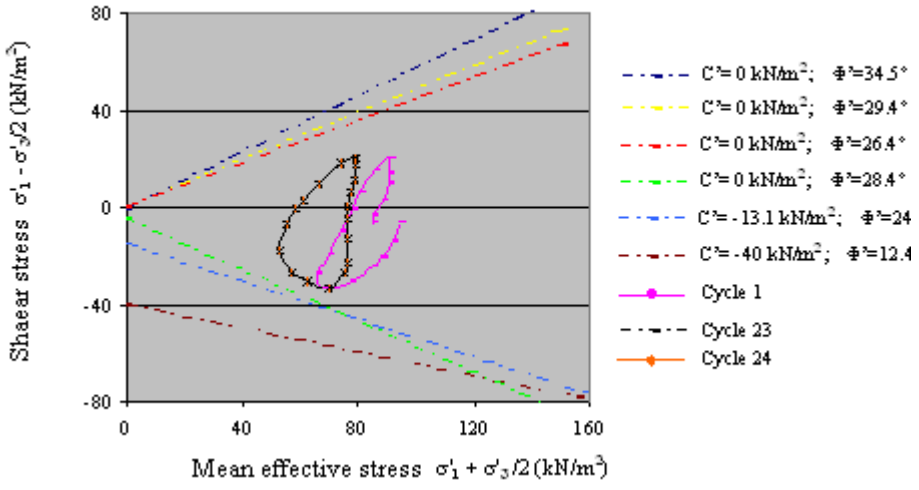

Fig 3.53.b Mean effective stress at end of each cycles vs N

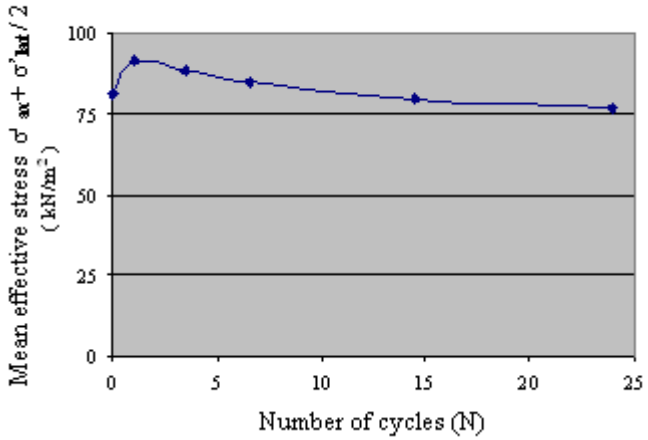

Fig 3.54.a Effective stress paths for test A.3 (compre/tension)

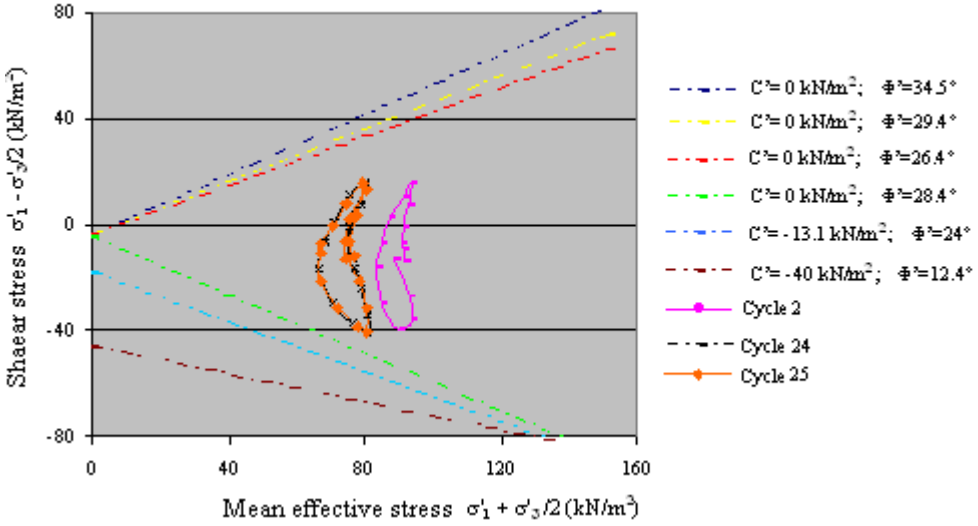

Fig 3.54.b Mean effective stress at end of each cycles vs N

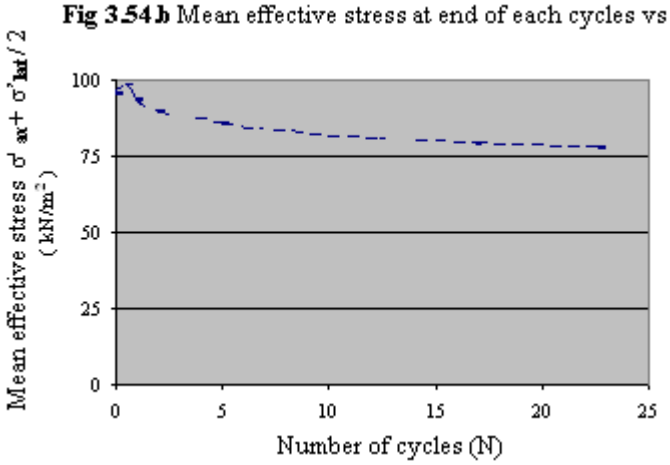

Fig 3.55.a Effective stress paths for test B.1 (compre/tension)

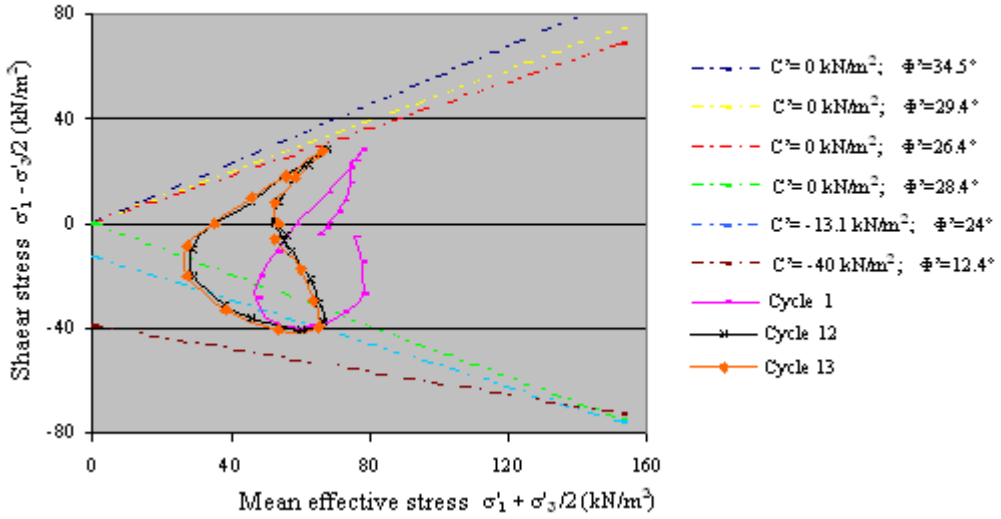

Fig 3.55.b Mean effective stress at end of each cycles vs N

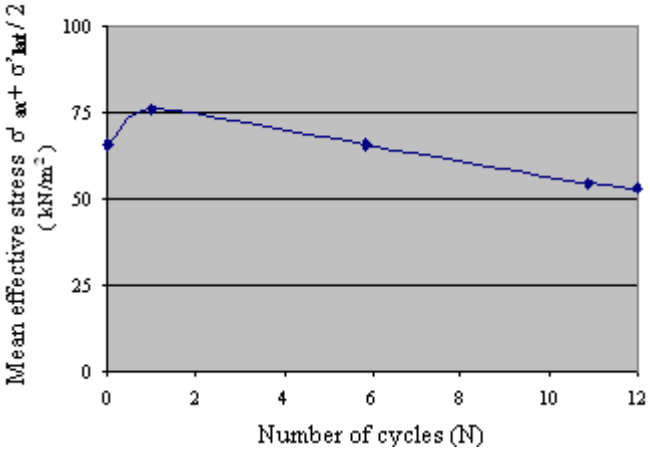

Fig 3.56.a Effective stress paths for test B.2 (compre/tension)

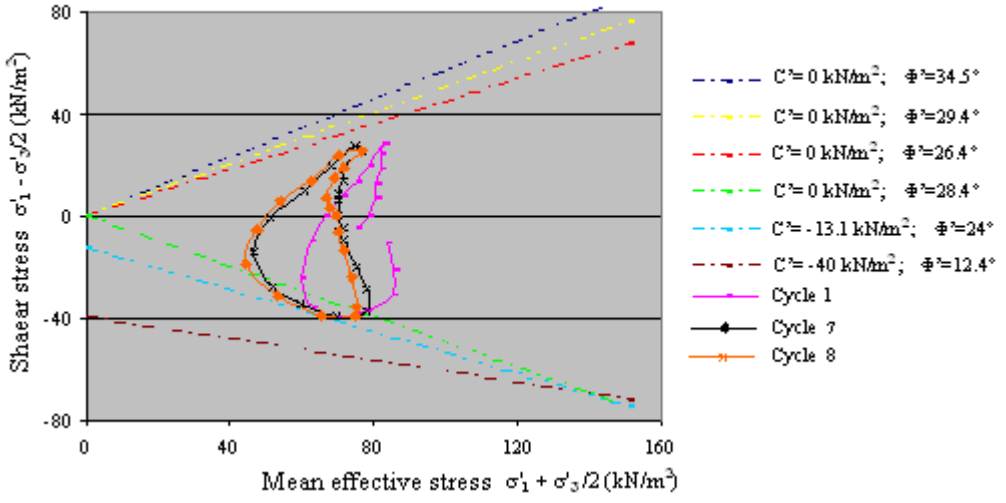

Fig 3.56.b Mean effective stress at end of each cycles vs N

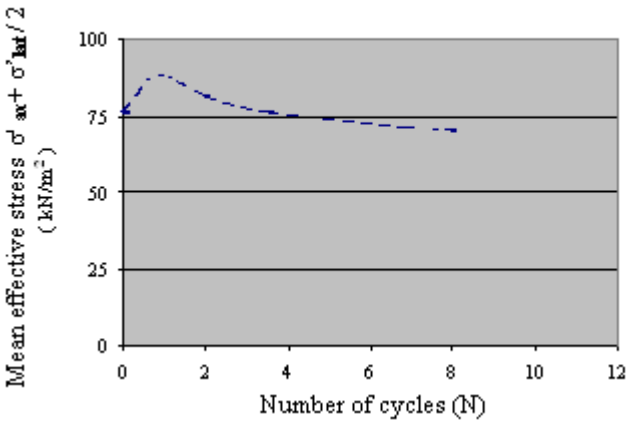

Fig 3.57.a Effective stress paths for test B.3 (compre/tension)

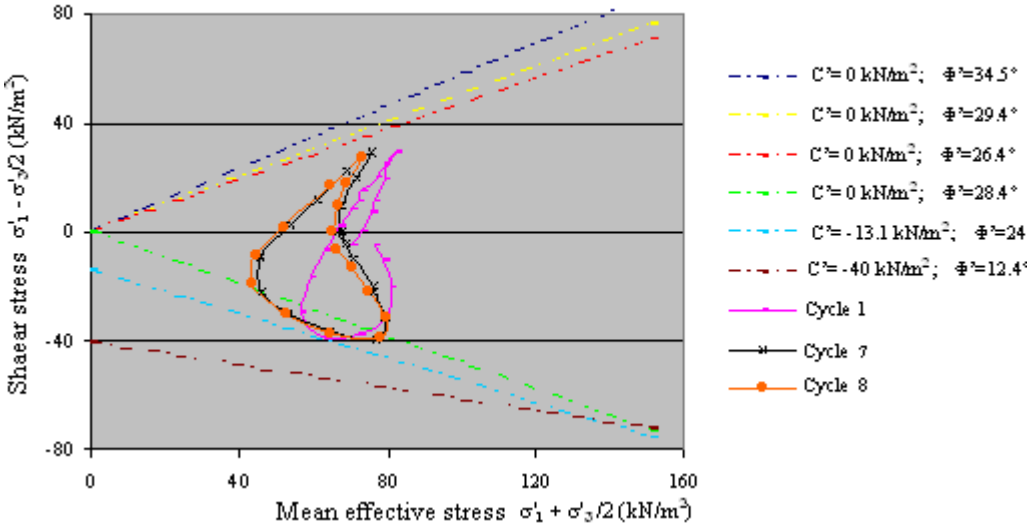

Fig 3.57.b Mean effective stress at end of each cycles vs N

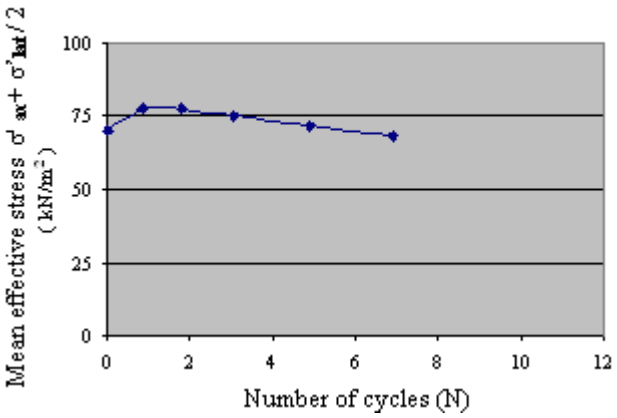

Fig 3.58.a Effective stress paths for test B.4 (compre/tension)

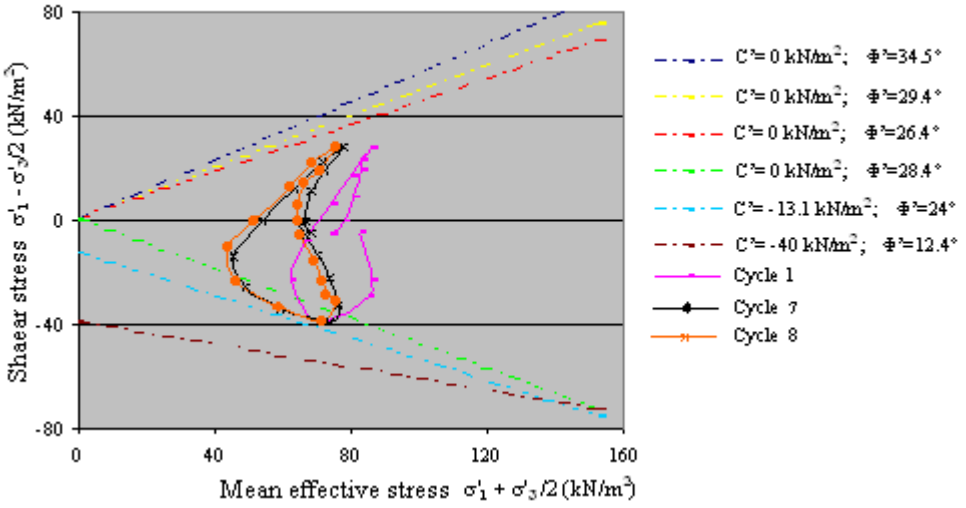

Fig3.58.b Mean effective stress at end of each cycles vs N

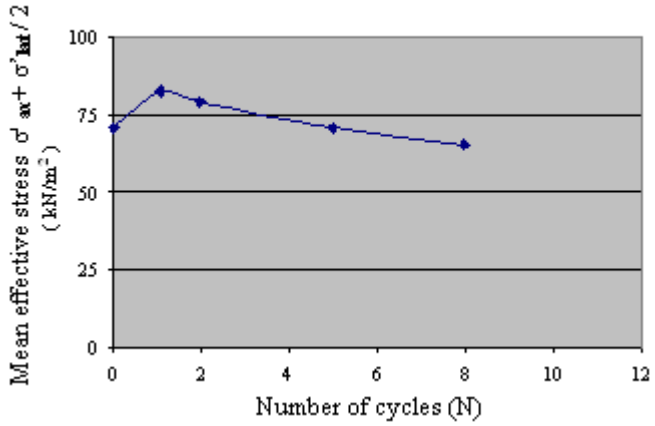

Fig 3.59.a Effective stress paths for test B.5 (compre/tension)

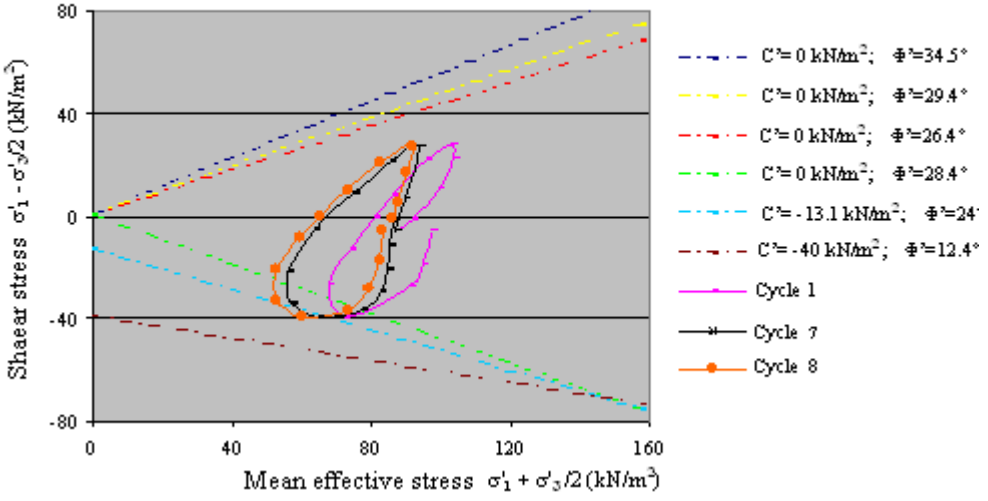

Fig 3.59.b Mean effective stress at end of each cycles vs N

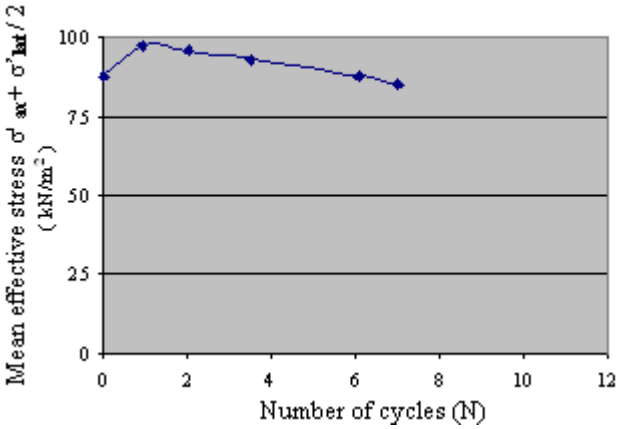

Fig 3.60.a Effective stress paths for test C.1 (compre/tension)

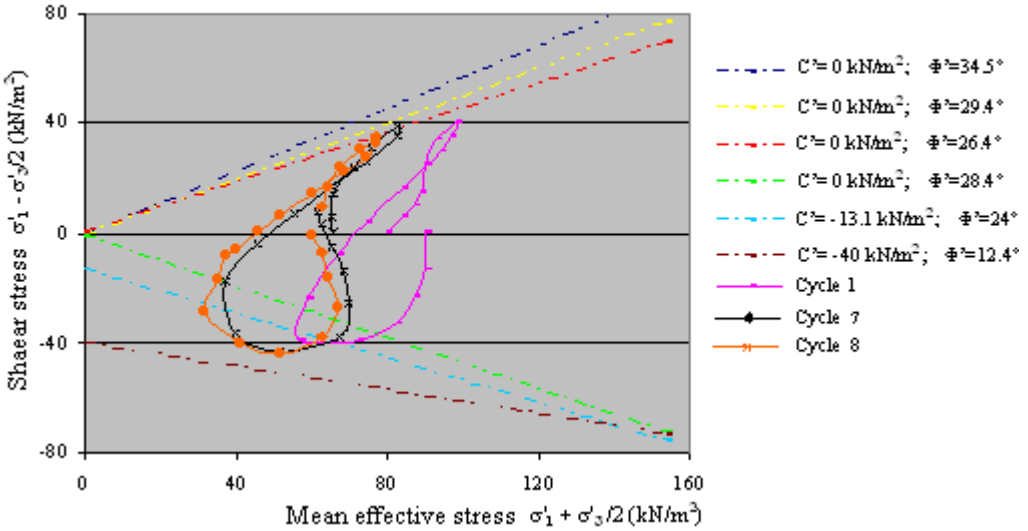

Fig 3.60.b Mean effective stress at end of each cycles vs N

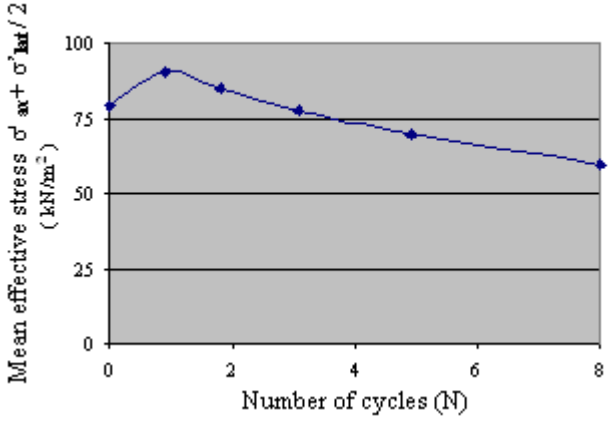

Fig 3.61.a Effective stress paths for test C.2 (compre/tension)

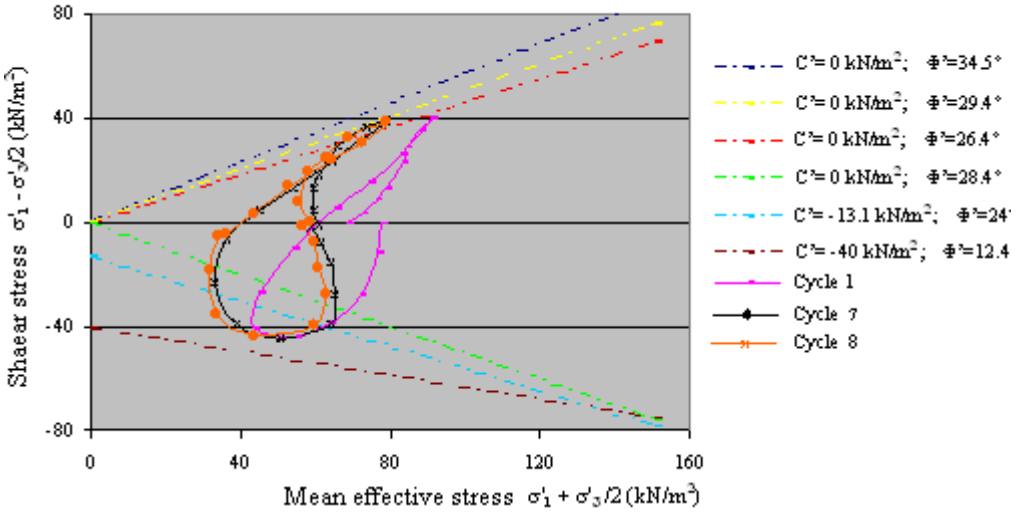

Fig 3.61.b Mean effective stress at end of each cycles vs N

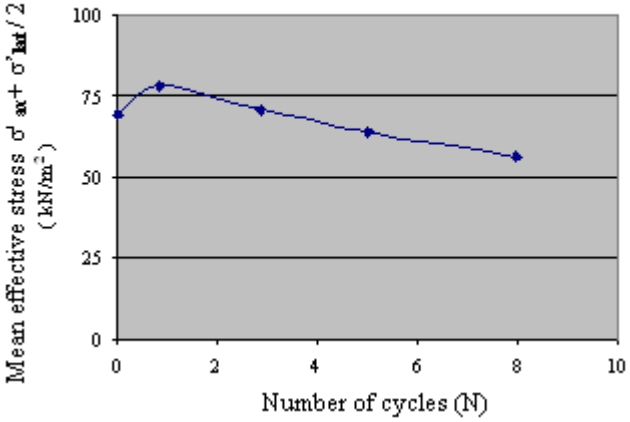

Fig 3.62.a Effective stress paths for test C.3 (compre/tension)

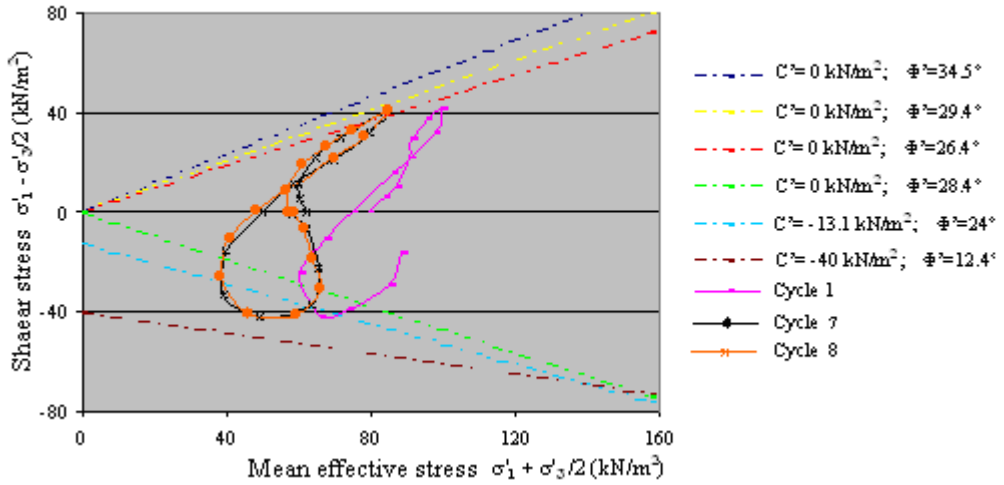

Fig 6.62.b Mean effective stress at end of each cycles vs N

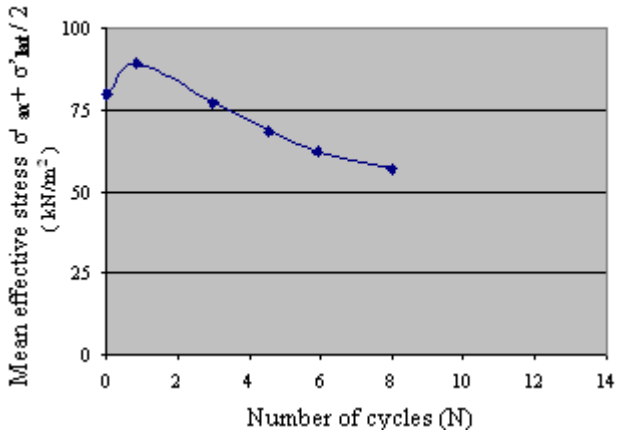

Fig 3.63.a Effective stress paths for test C.4 (compre/tension)

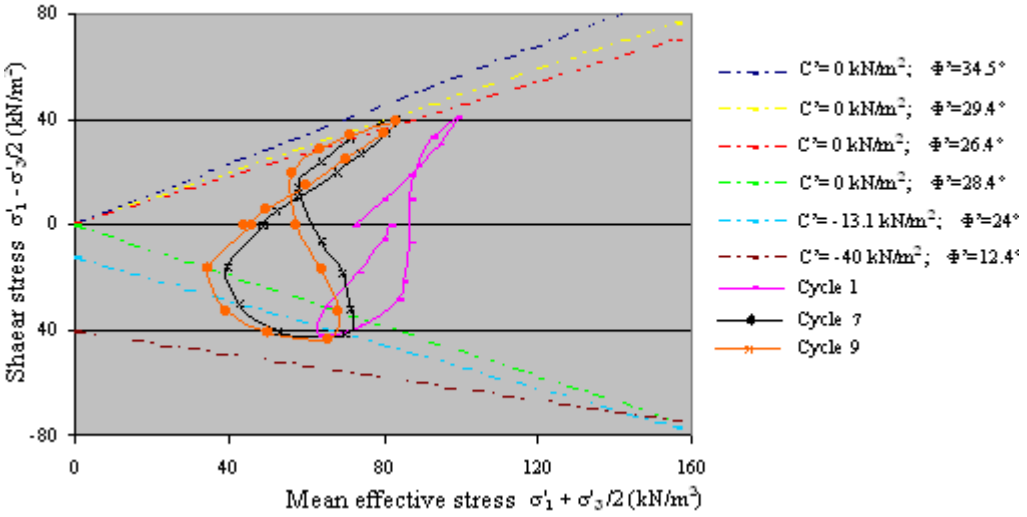

Fig 3.63.b Mean effective stress at end of each cycles vs N

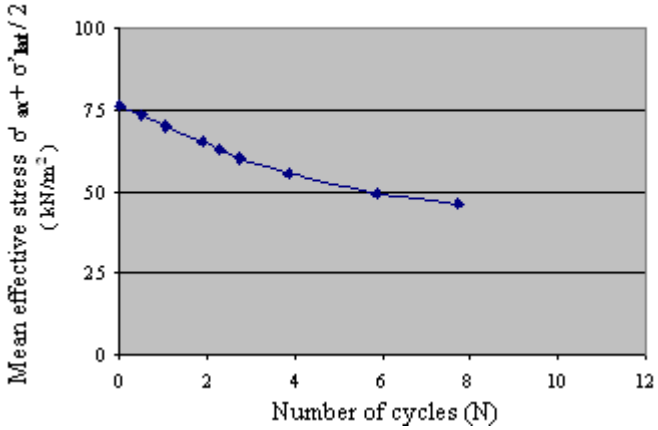

Fig 3.64 Effective stress paths for typical reversed stress-controlled triaxial test (after Andersen et Al 1980)

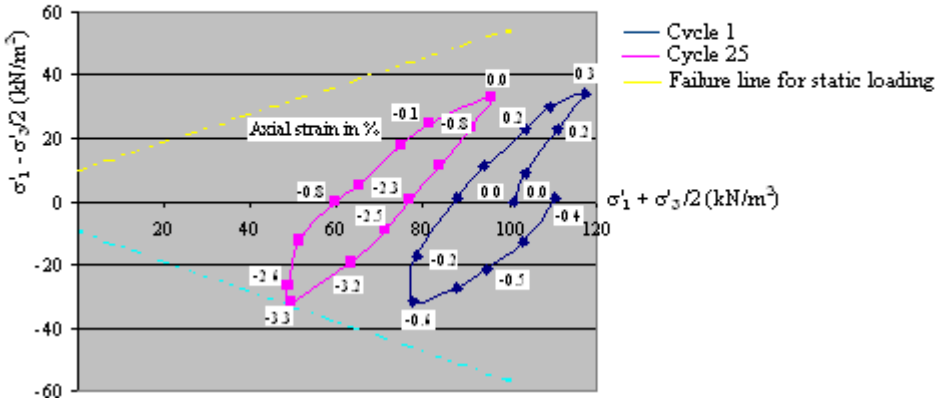

Fig 6.65 Effective stress paths for stress controlled triaxial tests with different total stress ratios and frequencies (after Takahashi et Al 1980)

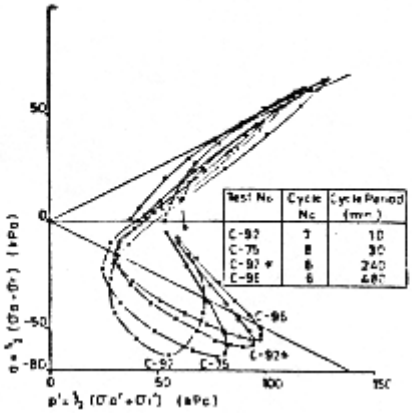

Fig 3.66 Mean effective stress after each cycle vs number of cycles (after Takahashi et Al 1980)

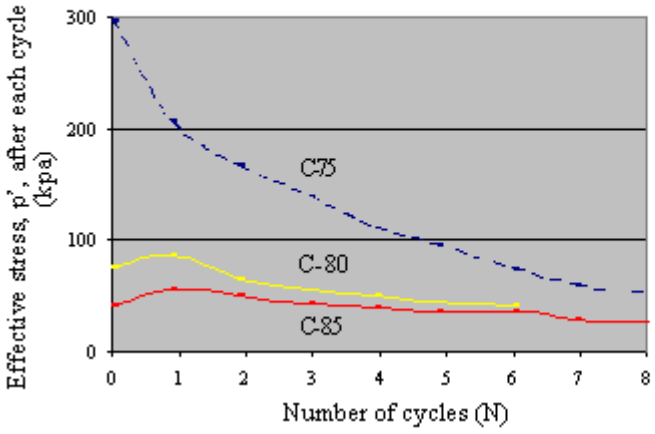

Test No	OCR	Cyclic stress Ratio
C-75	1	0.75
C-80	4	0.75
C-85	7	0.65

3.1.4 Monotonic tests on cyclically loaded samples

Even if failure was not reached as a result of cyclic loading, the clay samples suffered permanent pore pressures and deformations. In order to investigate the effects of undrained cyclic loading on the undrained shear strength, all tests of series B and C were subjected to post-cyclic monotonic loading.

Samples of tests B.1.C to B.5.C and C.3.C, C.4.C, were loaded in compression while samples of tests C.1.T and C.2.T were subjected to tensile loading. Details of these tests are given in Table 3.9.

It is seen in Table 3.9 that only samples with a reduction in the initial effective stress of approximately 50% or more, as well as having suffered residual axial strains higher than 2%, show a decrease in the undrained shear strength. The reduction in the maximum deviator stress varies between 3% and 17%.

Plots of the effective tress paths for tests B.1.C to B.5.C and C.1.T, C.2.T, C.3.C and C.4.C, as well as those for tests Comp.1, and Tens.1 (without cyclic loading history) and their respective effective failure envelopes are presented in Fig.3.67. It should be noted that all tests mentioned above were carried out at a strain rate of 0.012%/minute. It is seen in Fig.3.67 that both in compression and tension, the effective stress paths exceed the effective failure envelope from tests without cyclic loading.

It appears from the effective failure envelopes for the post-cyclic tests that except for a small increase in c' from 0 to 3.2 and 13. 1 kN/m^2 in compression and tension respectively, Ø' has not been affected and that the level of the applied cyclic stresses was not high enough to affect Ø'.

The author believes that even if no drainage has been permitted, the effective stress reduction during the undrained cyclic loading may have the same effect as if the effective stresses had been reduced by a real unloading of normal stresses. In other words, the cyclic loading may have caused an apparent overconsolidation of the soil.

Fig 3.67 Effective stress paths for post cyclic monotonic tests

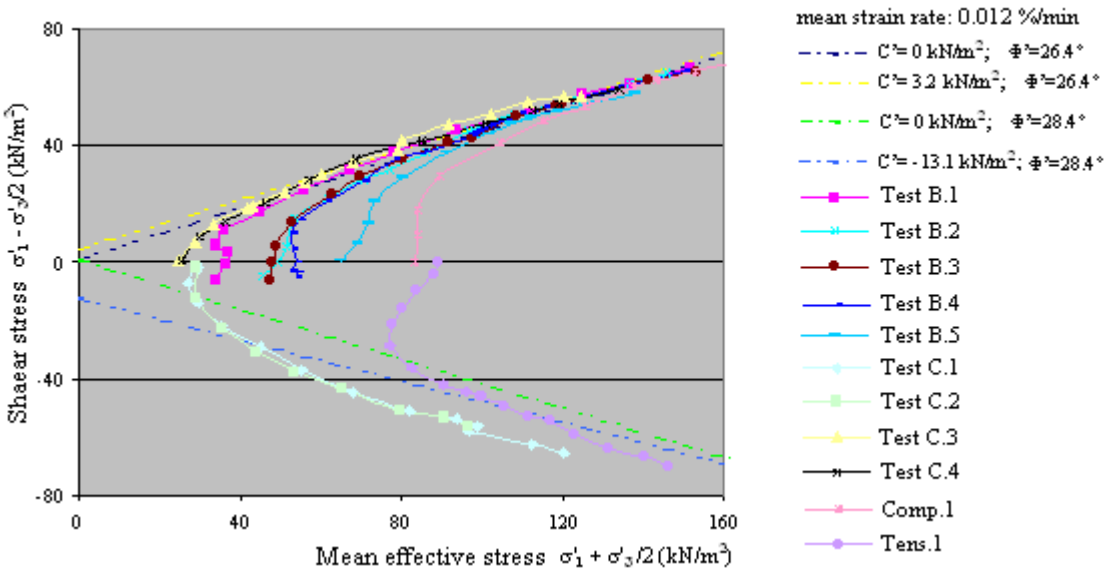

3.2 Conclusions

a) Monotonic tests

- Under monotonic (compression and tension) loading the normalised shear strength ($D_{max}/\sigma_{0'}$) at failure increased with increasing strain rate.

- The effective failure envelope inferred from the slowest monotonic compression and extension tests had C'=0; Ø'= 23°.4 in compression, and C'= 0, Ø'= 28.4° in extension .
- The limited amount of data indicate that increasing strain rate may affect C' and Ø'.

- Accurate mid-height pore water pressures relevant to failure conditions were consistently measured.

- Expressed in terms of the initial effective stress, the excess pore pressure at failure decreased with increasing strain rate. In terms of effective stress, the increase in shear strength with increasing strain rate may be partly explained by the reduction of pore pressure at failure and partly by strain rate effects on C' and 0' parameters.

b) Cyclic tests

- The higher the initial effective stress ratio τ/σ_0'the smaller the number of cycles required to reach a specified ϵ_{da}

- Except for the first cycle, the stiffness measured in compression was similar to that measured in tension. During the first cycle of the compression/ tension tests, the samples were much stiffer in compression than in tension. The opposite behaviour appears to occur under tension/compression loading this behaviour may be due to structural anisotropy resulting from the consolidation process and the direction of initial loading.

- The initial migration of the effective stress path away from the origin (also observed by Takashi et al (1980) (20) is believed to be due to the tendency for volume increase associated with over-consolidated samples, which would result in a decrease in pore pressure and an increase in the mean effective stress during the first cycle. However, with an increasing number of cycles, the tendency for volume increase reduces and, due to reversed shearing, the pore water pressure level rises again, resulting in a gradual decrease in the mean effective stress.

- The fact that the effective stress paths for the cyclic tests travel beyond the effective failure envelopes inferred from slow monotonic tests appears to be related to differences in rate of loading.

- Mean excess pore pressure increases with the number of cycles

- Good correlation of the double amplitude of the mid-height pore pressure with the theoretical change in mean total stress 2D/3 is observed.

Table3.1: Summary of the monotonic compression tests

		Test Code			
		Comp.1	Comp.2	Comp.3	Comp.4
Strain rate	%/min	0.012	0.012	0.06	0.3
Œdometer Consolidation pressure	kN/m^2	600	600	600	600
Cell pressure	kN/m^2	500	500	400	400
Moisture content	%	19.7	19.6	18.8	18.9
B_M	kN/m^2	0.95	1	1	1
B_B	kN/m^2	0.9	1	1	1
OCR		4.9	5.1	6.0	6.1
Initial Effective Stress	kN/m^2	81.9	77.9	66.3	65.5
$(\epsilon_A)_{Dmax}$	%	8.4	8.52	12.0	10.5
Dmax	kN/m^2	141.0	139.0	139.7	151.3
$Dmax/\sigma_o'$		1.72	1.78	2.1	2.31

C_u = mean value of the undrained shear strength obtained from tests Comp.1 and Comp.2

$C_u = {}_{Dmax\,/\,2} = 70\ kN/m^2$

Table.3.2: Summary of the monotonic tension tests

		Test code			
		Tens.1	Tens.2	Tens.3	Tens.4
Strain rate	%/min	0.012	0.012	0.06	0.3
Œdometer consolidation pressure	kN/m^2	600	600	600	600
Cell pressure	kN/m^2	500	500	400	400
moisture content	%	19.6	19.6	18.9	18.9
B_M	kN/m^2	0.95	1	1	1
B_B	kN/m^2	0.95	1	0.97	0.98
OCR		4.5	4.1	4.5	6.1
Initial effective Stress	kN/m^2	89.0	96.7	89.5	65.6
$(\epsilon_A)_{Dmax}$	%	-13.4	-8.25	-18.00	-20.2
Dmax	kN/m^2	-139.3	-139.1	-148.9	-136.2
$Dmax/\sigma_o'$		-1.56	-1.44	-1.66	-2.07

Cu = mean value of the undrained shear strength obtained from tests Tens.1, Tens.2

$Cu = {}_{Dmax\,/\,2}$ ב 70 kN/m^2

Table3.3: $\Delta U_{MC}/ \sigma_o'$ at the end of shearing for all monotonic tests

Test Code	Type of Test	σ_o'	τ / σ_o'	τ / Cu	Cycle No.1		Cycle No.2		Cycle No.7	
					ϵ_A at +Dmax	$\epsilon_{A\ at}$ -Dmax	$\epsilon\varepsilon_A$ at +Dmax	ϵ_A at -Dmax	ϵ_A at +Dmax	ϵ_A at -Dmax
		kN/m^2			%	%	%	%	%	%
C.1	Comp/Tens	81.4	±0.5	±0.59	1.88	-1.35	2.09	-1.84	3.47	-4.51
C.2	Comp/Tens	72.5	±0.57	±0.59	2.05	-1.46	2.38	-1.9	4.03	-4.58
C.3	Comp/Tens	81.3	±0.5	±0.59	2.04	-1.2	2.41	-1.56	4.15	-3.63
C.4	Comp/Tens	85	±0.48	±0.59	1.80	-1.11	2.07	-1.61	3.81	-4.37

Table 3.5: Axial strain at maximum$\pm_{D\,max}$ for tests of series C

		Test code							
		Comp.1	Comp.2	Comp.3	Comp.4	Tens.1	Tens.2	Tens.3	Tens.4
σ_o'	kN/m^2	81.9	77.9	66.3	66.5	89	96.7	89.5	65.6
Strain rate	%/min	0.012	0.012	0.06	0.3	0.012	0.012	0.06	0.03
D/3	kN/m^2	45.8	45.0	46.2	48.4	-45.7	-43.4	-49.6	-45.4
ΔU_M	kN/m^2	-19	-13.6	-25.7	-29.4	-121.1	-125.4	-138.2	-133
ΔU_{MC}	kN/m^2	-64.8	-58.6	-71.9	-77.8	-75.5	-82	-88.6	-87.6
$\Delta U_{MC}/\ _o$'		-0.79	-0.75	-1.08	-1.17	-0.85	-0.85	0.99	-1.33

ΔU_{MC} is the excess pore pressure corrected for the change in mean total stress ($\pm$D/3)
$\Delta U_{MC} = \Delta U_M \pm$ D/3

Table3.3: $\Delta U_{MC}/ \sigma_o'$ at the end of shearing for all monotonic tests

		Test code							
		Comp.1	Comp.2	Comp.3	Comp.4	Tens.1	Tens.2	Tens.3	Tens.4
σ_o'	kN/m^2	81.9	77.9	66.3	66.5	89	96.7	89.5	65.6
Strain rate	%/min	0.012	0.012	0.06	0.3	0.012	0.012	0.06	0.03
D/3	kN/m^2	45.8	45.0	46.2	48.4	-45.7	-43.4	-49.6	-45.4
ΔU_M	kN/m^2	-19	-13.6	-25.7	-29.4	-121.1	-125.4	-138.2	-133
ΔU_{MC}	kN/m^2	-64.8	-58.6	-71.9	-77.8	-75.5	-82	-88.6	-87.6
$\Delta U_{MC}/\sigma_o'$		-0.79	-0.75	-1.08	-1.17	-0.85	-0.85	0.99	-1.33

ΔU_{MC} is the excess pore pressure corrected for the change in mean total stress (±D/3)
$\Delta U_{MC} = \Delta U_M \pm D/3$

Table 3.4: Summary of cyclic loading tests

Test Code	Moisture Content	OCR	Cu	τ/ Cu		Δ τ / Cu In Comp. &Tens.	$(\tau / Cu)_{mean}$	B		σ_o'	τ / σ_o'		(τ / σ_o')	Cell press. "in" or"out" Of phase during last cycle	Total Nbre. of cycles
	%		kN/m^2	Comp.	Tens.	%		mid	base	kN/m^2	Comp.	Tens.			
A.1	18.8	5.9	70	0.3	-0.46	53.3	±0.38	1	1	67.7	0.31	-0.47	±0.39	In	27 24
A.2	19.8	5.0	70	0.3	-0.46	53.3	±0.38	1	1	79.7	0.26	-0.4	±0.33	Out	25
A.3	17.3	4.2	70	0.3	-0.46	53.3	±0.38	1	1	95.6	0.22	-0.35	±0.28	Out	13
B.1	18.3	6.0	70	0.4	-0.57	42.5	±0.48	0.97	0.92	67.1	0.42	-0.58	±0.5	In	8
B.2	18.8	5.0	70	0.4	-0.57	42.5	±0.48	0.97	0.92	79.7	0.36	-0.49	±0.43	In	8
B.3	18.5	5.2	70	0.4	-0.57	42.5	±0.48	1	1	79.3	0.37	-0.52	±0.44	Out	8
B.4	18.8	5.2	70	0.4	-0.57	42.5	±0.48	1	0.98	76.1	0.38	-0.52	±0.45	Out	8
B.5	19.2	4.1	70	0.4	-0.57	42.5	±0.48	1	0.98	97.4	0.29	-0.41	±0.35	In	8
C.1	18.5	4.9	70	0.59	-0.59	42.5	±0.59	1	0.98	81.4	0.5	-0.5	±0.50	In	8
C.2	19.7	5.5	70	0.59	-0.59	42.5	±0.59	1	1	72.5	0.57	-0.57	±0.57	In	8
C.3	18.4	4.9	70	0.59	-0.59	42.5	±0.59	1	0.97	81.3	0.5	-0.5	±0.5	Out	9
C.4	18.4	4.7	70	0.59	-0.59	42.5	±0.59	1	0.98	85.0	0.48	-0.48	±0.48	in	

Table 3.6: A Comparison between the calculated change in mean total stress and the observed middle and base pore pressure double amplitude

Test Code	σ_o'	τ/ Cu		τ / σ_o'		Cycle No.	2D/3	Double Amplitude Of U_M	Double Amplitude Of U_B	Cycle No.	2D/3	Double Amplitude Of U_M	Double Amplitude Of U_B
	kN/m^2	Comp.	Tens	Comp.	Tens		kN/m^2	kN/m^2	kN/m^2		kN/m^2	kN/m^2	kN/m^2
A.1	67.7	0.3	-0.46	0.31	-0.47	1	35.4	29.4	81.5	26	36.1	41.1	71.0
A.2	79.7	0.3	-0.46	0.26	-0.4	1	35.4	32.4	67.8	23	35.6	43.1	58.1
A.3	95.6	0.3	-0.46	0.22	-0.35	2	35.5	40.4	64.5	24	35.6	53.4	54.8
B.1	67.1	0.4	-0.57	0.42	-0.52	1	45.5	48.3	112.1	12	46.1	62.7	87.3
B.2	79.7	0.4	-0.57	0.36	-0.49	1	45.1	55.3	112.1	7	45.8	64.3	88.1
B.3	76.3	0.4	-0.57	0.37	-0.52	1	45.5	52.5	105.5	7	45.7	67.3	90.7
B.4	76.1	0.4	-0.57	0.38	-0.52	1	45.6	57.5	102.5	7	45.8	64.8	83.0
B.5	97.4	0.4	-0.57	0.29	-0.41	1	45.5	37.8	96.9	7	45.6	43.5	82.1
C.1	81.4	-0.59	-0.59	0.5	-0.5	1	54.8	45.7	108.5	7	55.5	52.8	86.5
C.2	72.5	-0.59	-0.59	+0.57	-0.57	1	55.0	38.7	108.1	7	55.3	55.7	82.5
C.3	81.3	-0.59	-0.59	+0.5	-0.5	1	54.9	50.0	115.3	7	55.0	51.3	85.3
C.4	85.0	-0.59	-0.59	+0.48	-0.48	1	55.0	50.1	101.3	7	55.3	64.9	92.1

2D/3 is defined as $\frac{|D_{max}| + |-D_{max}|}{3}$

.

Table 3.7: Values of creep strain

Test Code	σ_o'	τ/σ_o'		τ / C_u		Cycle No.	$\lvert \epsilon_{max} \rvert - \lvert \epsilon_{+Dmax} \rvert$	$\lvert \epsilon_{min} \rvert - \lvert \epsilon_{-Dmax} \rvert$	Cycle No.	$\lvert \epsilon_{max} \rvert - \lvert \epsilon_{+Dmax} \rvert$	$\lvert \epsilon_{Emin} \rvert - \lvert \epsilon_{-Dmax} \rvert$
	kN/m^2	Comp.	Tens	Comp.	Tens		%	%		%	%
A.1	67.7	0.31	-0.31	0.3	-0.46	1	0.00	0.05	26	0.03	0.04
A.2	79.7	0.26	-0.4	0.3	-0.46	1	0.00	0.03	23	0.01	0.01
A.3	95.6	0.22	-0.35	0.3	-0.46	2	0.00	0.00	24	0.00	0.00
B.1	67.1	0.42	-0.58	0.4	-0.57	1	0.03	0.06	12	0.03	0.04
B.2	79.7	0.36	-0.49	0.4	-0.57	1	0.04	0.02	7	0.02	0.03
B.3	76.3	0.37	-0.52	0.4	-0.57	1	0.04	0.03	7	0.01	0.02
B.4	76.1	0.38	-0.52	0.4	-0.57	1	0.02	0.02	7	0.02	0.02
B.5	97.4	0.29	-0.41	0.4	-0.57	1	0.00	0.02	7	0.01	0.02
C.1	81.4	0.5	-0.5	0.59	-0.59	1	0.03	0.09	7	0.02	0.05
C.2	72.5	0.57	-0.57	0.59	-0.59	1	0.02	0.06	7	0.04	0.1
C.3	81.3	0.5	-0.5	0.59	-0.59	1	0.02	0.04	7	0.04	0.06
C.4	85.0	0.48	-0.48	0.59	-0.59	1	0.04	0.04	7	0.05	0.06

$\lvert \epsilon_{max} \rvert - \lvert \epsilon_{+Dmax} \rvert$ and $\lvert \epsilon_{min} \rvert - \lvert \epsilon_{-Dmin} \rvert$ are the axial strains developed after D_{max} was reached in compression and tension respectively.

Table 3.8: Mean strain rates during the first and last cycles (with constant cell pressure) of all cyclic tests

Test Code	σ_o'	τ / C_u		Cycle No.	Mean strain rate in compression	Mean strain rate in tension	Cycle No.	Mean strain rate in compression	Mean strain rate in tension
	kN/m^2	Comp.	Tens		%/ min	%/min		%/ min	% /min
A.1	67.7	0.31	-0.46	1	0.038	0.08	26	0.253	0.235
A.2	79.7	0.31	-0.46	1	0.0175 >0.012 (1)	0.045 > 0.0012	23	0.075 > 0.06	0.074 > 0.06
A.3	95.6	0.31	-0.46	2	0.04	0.043	24	0.07	0.072
B.1	67.1	0.4	-0.57	1	0.11	0.136	12	0.343 > 0.3	0.542 > 0.3
B.2	79.7	0.4	-0.57	1	0.085 > 0.06 (2)	0.11	7	0.201	0.187
B.3	76.3	0.4	-0.57	1	0.047	0.091 > 0.06	7	0.17	0.112 > 0.06
B.4	76.1	0.4	-0.57	1	0.055 > 0.012	0.087	7	0.17 > 0.06	0.16
B.5	97.4	0.4	-0.57	1	0.046	0.063	7	0.112	0.11
C.1	81.4	0.59	-0.59	1	0.12	0.37	7	0.22	0.44
C.2	72.5	0.59	-0.59	1	0.13	0.187	7	0.415 > 0.3 (3)	0.482 > 0.3
C.3	81.3	0.59	-0.59	1	0.13 > 0.06	0.17 > 0.06	7	0.37	0.43
C.4	85.0	0.59	-0.59	1	0.15	0.07	7	0.425	0.43

(1), (2), (3): are the three strain rates used in monotonic loading tests

Table 3.9: Monotonic tests after cyclic loading

Test Code	Mode of testing	$\Delta \sigma_o'$ (1)	$(\tau / \sigma_o')_{mean}$	$(\tau / Cu)_{mean}$	σ_o' before cycling	σ_o' before cyclic loading	OCR	No of cycles	Strain rate	ϵ_{AP}	Assume D_{max} without Cyclic loading	(ϵ_A) at failure	D_{max}	ΔD_{max} (2)
		%			kN/m^2	kN/m^2			% min	%	kN/m^2	%	kN/m^2	%
B.1.C	Comp.	-49.6	± 0.5	± 0.48	67.1	33.8	11.8	13	0.012	-3.76	140	16.4	135.4	-3.3
B.2.C	Comp.	-42.9	± 0.43	± 0.48	79.7	45.5	8.8	8	0.012	-1.87	140	14.8	143.1	+2.2
B.3.C	Comp.	-38.8	± 0.44	± 0.48	76.3	46.7	8.6	8	0.012	-2.0	140	14.4	140	0
B.4.C	Comp.	-29.6	± 0.45	± 0.48	76.1	53.6	7.5	8	0.012	-1.66	140	15.3	143	+2.1
B.5.C	Comp.	-34.5	± 0.35	± 0.48	97.4	63.8	6.3	8	0.012	-1.06	140	16.7	153	+9.3
C.1.T	Comp.	-63.4	± 0.5	± 0.59	81.4	29.8	13.4	8	0.012	-4.34	-140	-15.9	-130.6	-6.7
C.2.T	Comp.	-58.6	± 0.57	± 0.59	72.5	30.0	13.3	8	0.012	-4.84	-140	-15.8	-126.5	-9.6
C.3.C	Comp.	-70.4	± 0.5	± 0.59	81.3	24.1	16.6	8	0.012	-2.4	+140	18	126	-10
C.4.C	Comp.	-74.1	± 0.48	± 0.59	85.0	22.0	18.2	9	0.012	+3.84	+140	18	115.8	-17.2

(1) $\Delta \sigma_o'$ is the reduction in the initial effective stress due to cyclic loading.

$$\Delta \sigma_o' = \frac{\sigma_o'_{(after\ cyclic)} - \sigma_o'_{(before\ cyclic)}}{\sigma_o'_{(before\ cyclic)}} \times 100$$

(2) ΔD_{max} is the reduction or increase in the D_{max} due to cyclic loading

(3)

$$\Delta D = \frac{\pm D_{max\ (after\ cycling)} - D_{max\ (without\ cycling)}}{\pm D_{max\ (without\ cycling)}} \times 100$$

Test Code	Mode of testing	$\Delta \sigma_o'$ (1)	$(\tau / \sigma_o')_{mean}$	$(\tau / Cu)_{mean}$	σ_o' before cycling	σ_o' before cyclic loading	OCR	No of cycles	Strain rate	ϵ_{AP}	Assume D_{max} without Cyclic loading	(ϵ_A) at failure	D_{max}	ΔD_{max} (2)
		%			kN/m^2	kN/m^2			% min	%	kN/m^2	%	kN/m^2	%
B.1.C	Comp.	-49.6	± 0.5	± 0.48	67.1	33.8	11.8	13	0.012	-3.76	140	16.4	135.4	-3.3
B.2.C	Comp.	-42.9	± 0.43	± 0.48	79.7	45.5	8.8	8	0.012	-1.87	140	14.8	143.1	+2.2
B.3.C	Comp.	-38.8	± 0.44	± 0.48	76.3	46.7	8.6	8	0.012	-2.0	140	14.4	140	0
B.4.C	Comp.	-29.6	± 0.45	± 0.48	76.1	53.6	7.5	8	0.012	-1.66	140	15.3	143	+2.1
B.5.C	Comp.	-34.5	± 0.35	± 0.48	97.4	63.8	6.3	8	0.012	-1.06	140	16.7	153	+9.3
C.1.T	Comp.	-63.4	± 0.5	± 0.59	81.4	29.8	13.4	8	0.012	-4.34	-140	-15.9	-130.6	-6.7
C.2.T	Comp.	-58.6	± 0.57	± 0.59	72.5	30.0	13.3	8	0.012	-4.84	-140	-15.8	-126.5	-9.6
C.3.C	Comp.	-70.4	± 0.5	± 0.59	81.3	24.1	16.6	8	0.012	-2.4	+140	18	126	-10
C.4.C	Comp.	-74.1	± 0.48	± 0.59	85.0	22.0	18.2	9	0.012	+3.84	+140	18	115.8	-17.2

(1) $\Delta \sigma_o'$ is the reduction in the initial effective stress due to cyclic loading.

$$\Delta \sigma_o' = \frac{\sigma_o'_{(\text{after cyclic})} - \sigma_o'_{(\text{before cyclic})}}{\sigma_o'_{(\text{before cyclic})}} \times 100$$

(2) ΔD_{max} is the reduction or increase in the D_{max} due to cyclic loading

(3)

$$\Delta D = \frac{\pm D_{max\ (\text{after cycling})} - D_{max\ (\text{without cycling})}}{\pm D_{max\ (\text{without cycling})}} \times 100$$

Table 3.9: Monotonic tests after cyclic loading

CHAPTER4

A SHEET PILE WALL ANALYSIS, DISCUSSION OF RESULTS AND CONCLUSIONS

4.1 Current methods of analysis for geotechnical problem

Different methods of analysis of a geotechnical engineers can be grouped into the following categories:

- Theoretical closed form analysis;
- Simple analysis such as lower or upper bound solutions;
- Numerical analysis.

For a particular geotechnical structure, it is possible to satisfy the four requirements for a general solution:

- Equilibrium (i.e. well known equation of Timoshenko);
- Compatibility (i.e. no overlapping of material and no generation of holes);
- Material constitutive behaviour (i.e. description of material);
- Behaviour in terms of stress-strain relationship);

Then an ‘exact theoretical’ solution can be obtained. But as soil a highly complex non linear material, full analytical solutions to geotechnical problems are usually not available.

Therefore approximations must be introduced. Geotechnical engineers normally resort to three main design analysis methods to solve their geotechnical problems. These are the:

1) Simple analysis approach,
2) Simplified numerical approach (beam-spring)
3) Full numerical analysis approach

1) Simple analysis:

In a simple analysis the constraints on satisfying the basic solution requirements are not fully met, but mathematics is still used to obtain an approximate analytical solution. Examples of such 'simple analyses are limit equilibrium method, upper bound theory etc.

All these methods essentially assume the soil is at failure and/or a specific failure mechanism is assumed, but differ in the manner in which they arrive at a solution.

2) Simplified numerical approach

A more comprehensive way of introducing approximations in solving geotechnical problems is through numerical approximations. Using this approach, all requirements of a theoretical solution are considered, but may only be satisfied in an approximate manner, hence the 'simplified numerical approach'.

The simplified numerical approach used to model soil-structure interaction behaviour approximates the soil as a set unconnected vertical and horizontal spring, or as a set of linear elastic interaction factors, and represents structural supports (e.g. props, anchors…) by simple springs. This is commonly known as the "beam-spring" approach.

3) Full numerical approach

In the full numerical approach, attempts are made to satisfy all theoretical requirements, include realistic soil constitutive models and boundary conditions that realistically simulate field conditions. Approaches based on finite difference, boundary element and finite element methods are those widely used. These methods essentially involve computer simulation of the history of the boundary value problem from green field conditions, through construction and in the long term. Their ability to accurately reflect field conditions essentially depends on the ability of the constitutive model to represent real soil behaviour and correctness of the boundary conditions imposed.

4.2 Soil model

Natural soils are complex and variable. None of the currently available soil Constitutive models can reproduce all aspects of real soil behaviour; therefore the choice of soil model will depend on several factors:

- Which soil features govern the behaviour of a particular geotechnical problem;
- The type of soil to model;
- The analysis conditions;
- The availability of soil data from which the parameters should be derived;

4.3 Description of the most commonly used models

In the following, the soil models that are most commonly used in finite element analyses are presented.

The first group consists of the elastic material models, of both linear and non linear type. The second group is the elastic-plastic models and includes the models of Tresca, von Mises, Mohr Coulomb (with and without stress hardening), Drucker-Prager and Cam clay. Although there are many other advanced soil models available for use in finite element analyses, they are not covered under the context of this report.

4.3.1 Elastic material models (Figure 4.1)

The basic assumption of elastic behaviour is that the directions of principal incremental stress and incremental strain coincide. Elastic constitutive models can take many forms: isotropic or anisotropic, linear or non linear.

The isotropic linear elastic models involve two elastic stiffness parameters: Young's modulus and Poisson's ratio, or shear modulus and effective bulk modulus. For geotechnical engineering it is often convenient to use bulk modulus K and shear modulus G. The reason for this is that the behaviour of soil under changing mean (bulk) stress is very different to that under changing deviatoric (shear) stress. For instance, under increasing mean stress the bulk stiffness of the soil will usually increase, whereas under increasing deviatoric stress the shear stiffness will reduce. Furthermore, in the formulation of the isotropic elastic model, the two modes of deformation are decoupled: changes in mean stress $\Delta p'$ do not cause distortion (shear strain) and changes in deviatoric stress do not cause volume change .

The linear elastic model is very limited for the simulation of soil behaviour. It is primarily used for stiff massive structures in the soil (structural elements e.g. retaining walls, slabs etc.
In reality, the stress-strain behaviour of soil becomes nonlinear, particularly as failure conditions are approached. Therefore, nonlinear elastic models, in which the material parameters vary with stress and/or strain level are a substantial improvement over the linear models, whereas they still fail to model some of the important facets of real soil behaviour. In particular they cannot reproduce the tendency to change volume when sheared. Also, because of the assumption of coincidence of principal incremental stress and strain directions, they cannot accurately reproduce failure mechanisms.

Fig 4.1 Elastic model. (a) Linear elastic model, (b) Non-linear elastic model (bilinear and hyperbolic) (Potts and Zdravkovic, 1999)

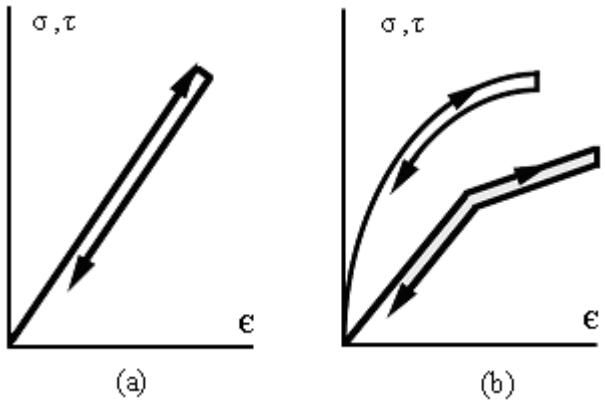

Duncan and Chang model

In this formulation, the stress-strain curve is hyperbolic in the shear stress, $(\sigma_1-\sigma_3)$, versus axial strain space and the soil modulus is a function of the confining stress and the shear stress that a soil is experiencing. This nonlinear material model is attractive since the soil properties it requires can be obtained quite readily from triaxial tests or the literature. Depending on the stress state and stress path, three soil moduli are required; namely, the initial modulus, E_i the tangential modulus, E_t, and the unloading-reloading modulus, E_{ur} (see figure 4.2).

4.3.2 Elastic-plastic material models

Fig 4.2 Non linear stress-strain behaviour

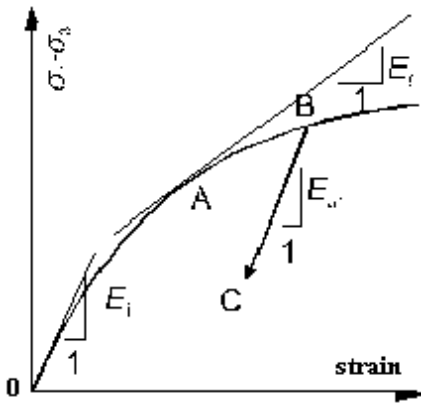

Elastic plastic theory provides probably the best framework available in which to formulate constitutive models that can realistically simulate real soil behaviour. It assumes elastic behaviour prior to yield and can therefore utilise the benefits of both elastic and plastic behaviour. Elastic-

plastic models are based on the assumption that the principal directions of accumulated stress and incremental plastic strain coincide. They require the following piece of information for their definition: a yield function which separates purely elastic from elastic-plastic behaviour; a plastic potential (or flow rule) which prescribes the direction of plastic straining, and (optional) a set of hardening/softening rules which describe how the state parameters (for example strength) vary with plastic strain (or plastic work).

In uniaxial situations, the yield stress indicates the onset of plastic straining. In a multi-axial situation a yield function is defined instead, which is a scalar function of stress and state parameters {k}: F ({σ}, {k}) =0.

Figure 4.3 gives examples of yield function with the Mohr Coulomb and Von Mises failure conditions (common plasticity rules used respectively to describe drained and undrained situations).

Fig 4.3. (a) Mohr Coulomb and (b) Von Mises failure criteria

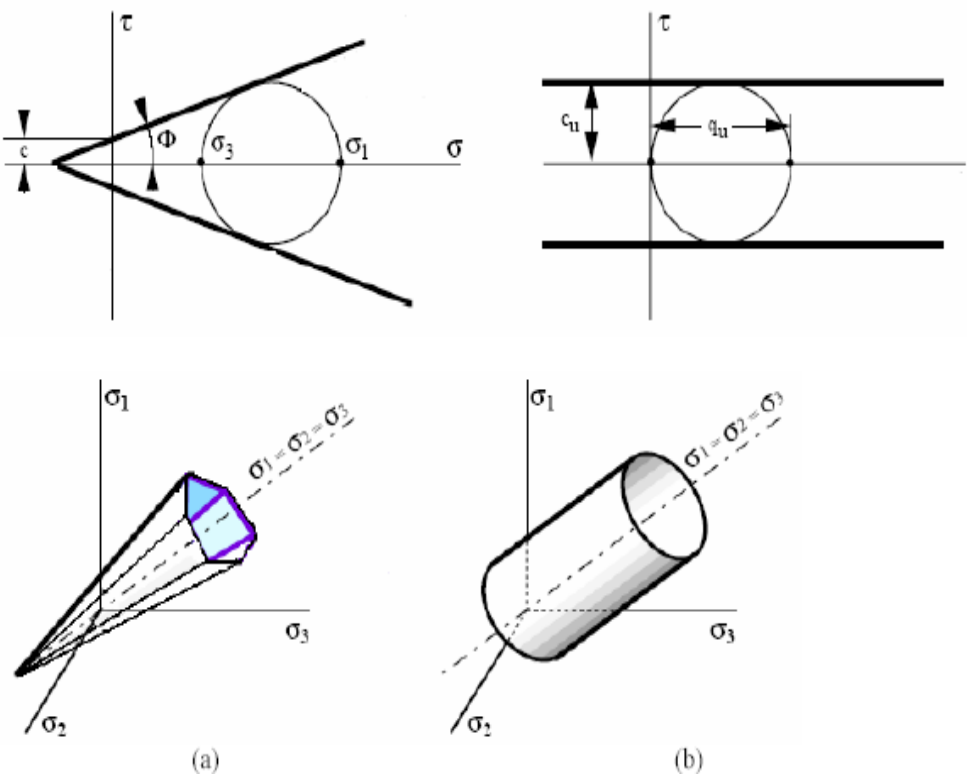

The yield function defines the state of stress at which material response changes from elastic to plastic. In general, the surface is a function of the stress state {σ } and its size also changes as a function of the state parameters {k}, which can be related to hardening/softening parameters.

In real soil plastic strain occurs even before reaching "failure". Strain hardening and softening models introduce plastic strains before reaching the ultimate yield surface.

The plastic strains modify the yield surface during hardening or softening. The Figure 4.4 illustrates the three main forms of elastic-plastic behaviour. They can be compared with some of the more common features of soil behaviour. For example if the curve corresponding to the elastic plastic strain hardening model is replotted with the stress axis horizontal and the strain axis vertical, it bares some resemblance to the behaviour observed in an œdometer test. Soil behaviour on a swelling line is often assumed to be reversible and therefore is akin to behaviour on an elastic unload-reload loop. The behaviour on the virgin consolidation line is irreversible and results in permanent strains. It is therefore similar to behaviour along the strain hardening path.

Similarity also exists between the strain softening behaviour and the shear stress-shear strain behaviour observed in a direct or simple shear test on dense sand. To simulate the behaviour of real soil it is necessary to have a model that involves both strain hardening and softening.

Fig 4.4 Elasto-plastic models- illustration

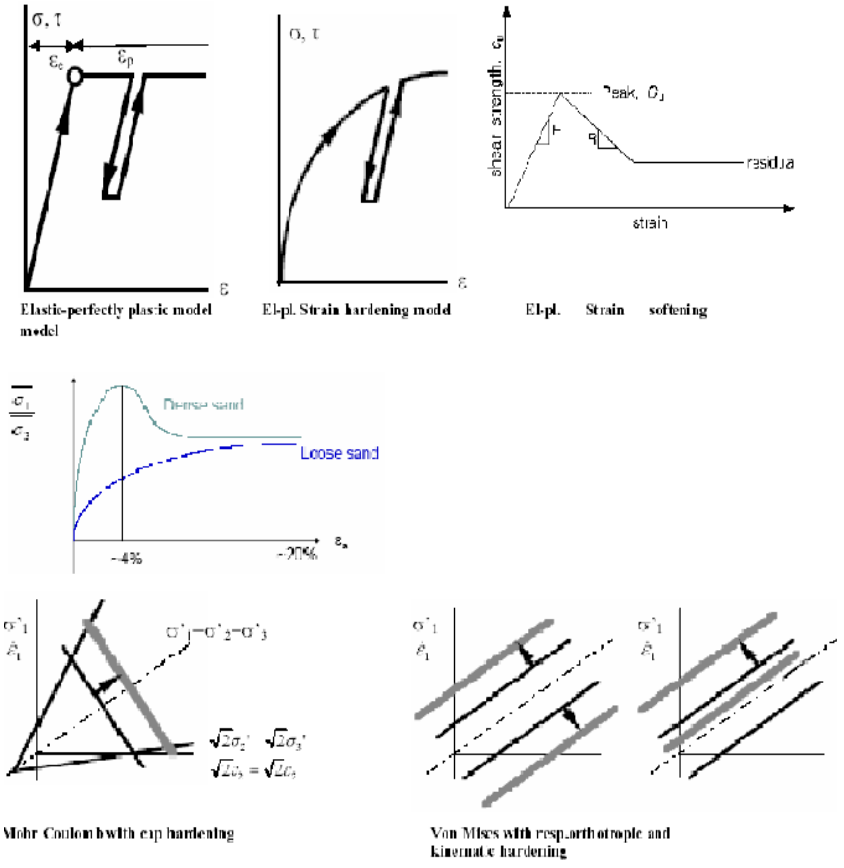

In the multi-axial case it is necessary to have some means of specifying the direction of plastic straining at every stress state. This is done by means of a flow rule that relates strain increments to stress increments after the onset of initial yielding. The flow rule can be expressed as follows: $\Delta\varepsilon^p = \Lambda \frac{\partial p(\{\sigma\},\{m\})}{\partial \sigma}$ where $d\varepsilon^p$ is the incremental plastic strain, P is the plastic potential function and Λ is a scalar multiplier.

The plastic potential function is of the form $P(\{\sigma\},\{m\})=0$ where {m} is essentially a vector of state parameters the values of which are immaterial, because only the differentials of P with respect to the stress components are needed in the flow rule.

Due to the complex nature of soil it has not been possible, to date, to develop an elastic plastic model that can capture all the facets of real soil behaviour and be defined by a limited set of input parameters that can be readily obtained from simple laboratory tests. There are therefore many such models currently in the literature. These range from simple to extremely complicated models.

4.3.3 Simple elastic-plastic constitutive models (elastic perfectly plastic models)

Tresca and van Mises elastic perfectly plastic models are expressed in terms of total stresses and apply to undrained soil behaviour, while the Mohr Coulomb and Drucker-Prager models are expressed in terms of effective stresses, and are therefore more suited for solving most geotechnical problems.

The implicit assumption of the Tresca and Mohr Coulomb models is that yield and strength are independent of the intermediate principal stress σ_2. There is little experimental data available to accurately quantify the effect of the intermediate principal stress on soil behaviour. The limited data that does exist suggests that both yield and failure functions plot as smoothed surfaces (no corners) in the deviatoric plane, with a shape somewhere between that of the hexagons and circles (assumptions of Tresca / Mohr-Coulomb and von Mises / Drucker Prager). As conventional soil mechanics is based on the Tresca and Mohr Coulomb models, it seems sensible to use these models in preference to the von Mises and Drucker Prager models. This has the advantage that the finite element analysis is then compatible with conventional soil mechanics, but has the disadvantage that the software has to deal with the corners of the yield and plastic potential surfaces.

To increase the flexibility of the models, it is also possible to replace the linear elastic with nonlinear elastic behaviour, by allowing the elastic constants to vary with stress and/or strain level.

- **Tresca model**

If a conventional triaxial test is performed, it is common to plot the results in terms of the vertical and horizontal stresses σ_v (') and σ_h (') If testing saturated clay, the Mohr's circle of stress at failure is often plotted in terms of total stress and may look like that given in figure 4.5.

If two similar samples are tested at different cell pressures, without allowing any consolidation, conventional soil mechanics theory suggests that the Mohr's circles
For finite element analysis, it is more convenient to rewrite this equation in terms of the stress invariants p (mean effective stress), J (deviatoric stress), θ (Lode's angle)

$$p' = \tfrac{1}{3}(\sigma'_1 + \sigma'_2 + \sigma'_3)$$

$$F(\{\sigma\},\{K\}) = j\cos\theta - S_u = 0 \text{ where}$$

$$J = \tfrac{1}{6}\sqrt{(\sigma'_1 - \sigma'_2)^2 + (\sigma'_2 - \sigma'_3)^2 + (\sigma'_1 - \sigma'_3)^2}$$

$$\theta = \tan^{-1}\left[\frac{1}{\sqrt{3}}\left(2\frac{(\sigma'_2 - \sigma'_3)}{(\sigma'_1 - \sigma'_3)} - 1\right)\right]$$

Fig 4.5 Mohr's circles of total stress (Potts and Zdravkovic, 1999)

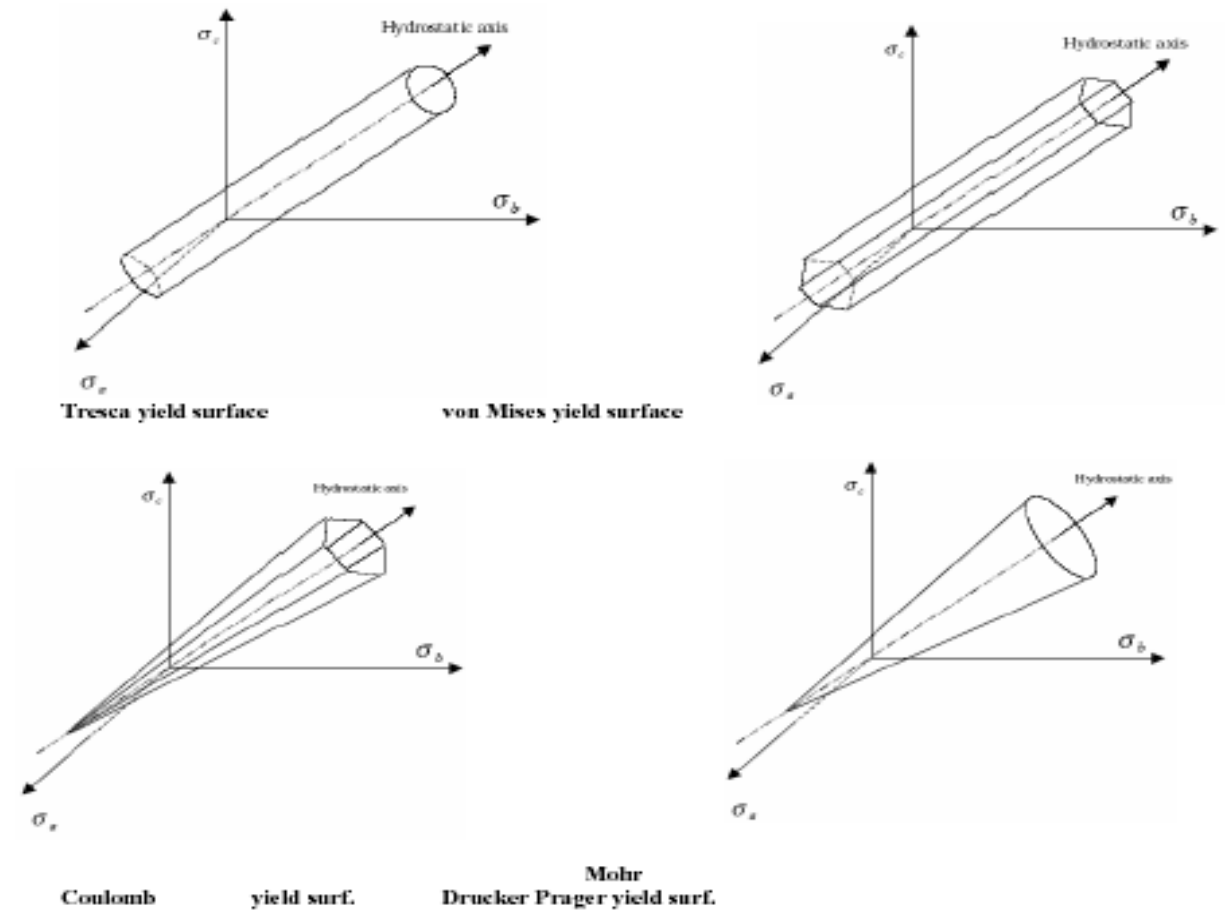

Fig 4.6 Mohr's circles of total stress (Potts and Zdrakovic 1999).

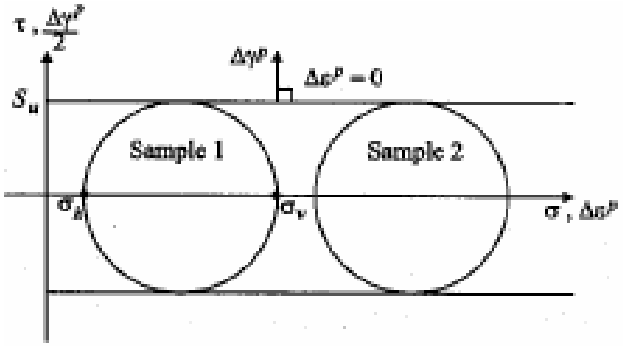

In principal total stress space this yield function plots as a regular hexagonal cylinder, which has the space diagonal as its line of symmetry. This model is perfectly plastic, therefore there is no hardening/softening law required and the state parameter $\{k\}=S_u$ is assumed constant (independent of plastic strain).

As the model is intended to simulate the undrained behaviour of saturated clay, it should predict zero volumetric strains. Since the soil is purely elastic (below the yield surface) or purely plastic (on the yield surface), both the elastic and plastic components of the volumetric strain use be zero. It can be shown that an associated plastic flow i.e. $p(\{\sigma\},\{m\}) = F(\{\sigma\},\{K\})$ satisfies the no plastic volumetric strain condition. Besides, as there should be no elastic volumetric strains, $\mu \sim 0.5$. The model can therefore be defined by specifying the undrained strength S_u and the undrained Young's modulus E_u.

- **Von Mises model**

When plotted in 3D principal total stress space, the Tresca yield surface has corners. In particular, the intersection of the surface with a deviatoric plane (i.e. a plane normal to the space diagonal) produces a regular hexagon which has its corners at triaxial compression and extension points. These corners imply singularities in the yield function which can cause difficulties in numerical analysis.

Therefore applied mathematicians have often simplified the yield function expression so that it plots as a circular cylinder in principal stress space, instead of a hexagonal cylinder. However, there are ways that the numerical difficulties due to the singularities in the Tresca yield function can be overcome, and the Tresca model is thought to be more appropriate than von Mises because it is based on the same assumptions as conventional soil mechanics .

Fig 4.7 Von Mises and Tresca yield surfaces
in principal stress space

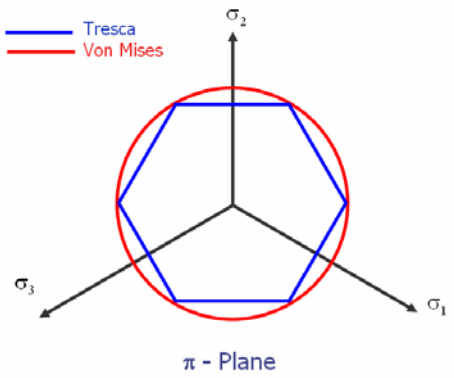

- **Mohr Coulomb model**

If the results of laboratory tests are plotted in terms of effective stresses, the Mohr's circles of stress at failure are often idealised as shown in figure 4.4
It is s usual to assume that the tangent of the failure circles from several tests, performed

Fig 4.8 Morh's circles of effective stress

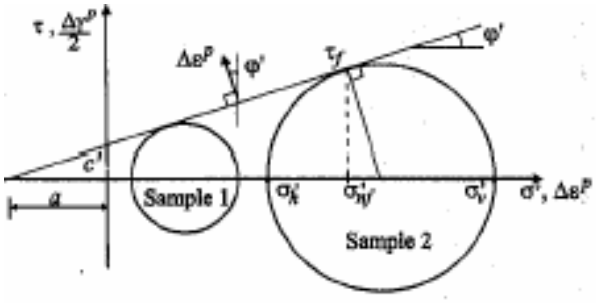

with different initial effective stresses is straight. This line is called the Coulomb failure criterion and can be expressed as $\tau_f = c' + \sigma'_{nf} \tan\varphi'$ where τ_f and σ'_{nf} are the shear and normal effective stresses on the failure plane, and the cohesion *c'* and the angle of shearing resistance φ' are material parameters.

Using the Mohr's circle of stress and noting that $\sigma_1 = \sigma_v$ and $\sigma_3 = \sigma_h$ the equation can be rewritten as $\sigma_1' - \sigma_3' = 2c'\cos\varphi' + (\sigma_1' + \sigma_3')\sin\varphi'$. This is often called the Mohr Coulomb failure criterion and in the present model is adopted as the yield function $F(\{\sigma'\}\{K\}) = \sigma_1' - \sigma_3' - 2c'\cos\varphi' - (\sigma_1' + \sigma_3')\sin\varphi'$ or in terms of stress invariants

$$F(\{\sigma'\}\{K\}) = J - \left(\frac{c'}{\tan\varphi'} + p'\right)g(\theta) = 0 \quad \text{where} \quad g(\theta) = \frac{\sin\varphi'}{\cos\theta + \frac{\sin\theta\sin\varphi'}{\sqrt{3}}}$$

In principal effective stress space the yield function plots as an irregular hexagonal cone. If S_u is substituted for c' and φ' is set to zero, the Tresca yield function is obtained.

As the Mohr Coulomb model is assumed to be perfectly plastic, there is no hardening/softening law required; the state parameter $\{K\} = \{c', \varphi'\}$ is assumed constant, independent of plastic strain.

Similar to the Tresca model, an associated flow rule with $p(\{\sigma\},\{m\}) = F(\{\sigma\},\{K\})$ could be adopted for the plastic potential function, but there is two drawbacks to this approach. Firstly the magnitude of the plastic volumetric strains (the dilation) is much larger than that observed in real soils, and secondly, once the soil yields it will dilate for ever. Real soil, which may dilate initially on meeting the failure surface, will often reach a constant volume condition (zero incremental plastic volumetric strains) at large strains.

The first drawbacks can be partly rectified by adopting a non-associated flow rule, where the plastic potential function is assumed to take a similar form to that of the yield surface, but with φ' replaced by dilatation υ (more often noted ψ)

$$p(\{\sigma'\},\{m\}) = J - (a_{pp} + p')g_{pp}(\theta) = 0$$

where $$g(\theta) = \frac{\sin\varphi'}{\cos\theta + \frac{\sin\theta\sin\varphi'}{\sqrt{3}}}$$

and a_{pp} is the distance of the apex of the plastic potential cone from the origin of principal effective stress space. It is akin c'/tanφ' in the yield function.

Fig 4.9 Relationship between the yield and plastic potential functions

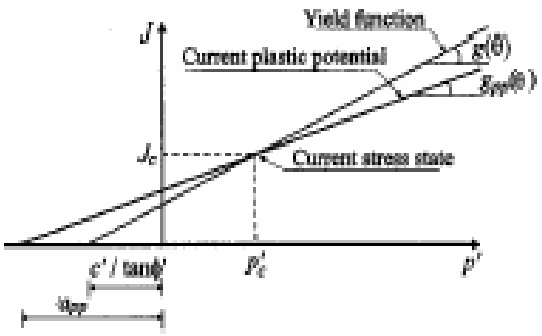

While the yield surface is fixed in p'- j- θ space, the plastic potential surface moves so as to pass through the current stress state.

If, ν = φ' associated conditions arises. However ν = φ' results in non-associated conditions, and ν reduces less dilation is generated. If ν = 0°, zero plastic dilation (no plastic volume strain) occurs.

Consequently, by prescribing the angle of dilation υ the predicted plastic volumetric strains can be controlled.

- **Drucker-Prager model**

As the Tresca model, the Mohr Coulomb yield function has corners when plotted in principal effective stress space. In order to simplify numerical difficulties, earlier pioneers sought simplifications. One way to overcome the corner problem is to modify the yield function so that it plots as a cylindrical cone. This form of the yield function is often called the Drucker-Prager yield function.

4.3.4 An elastic strain hardening/softening Mohr Coulomb model

To improve the Mohr Coulomb model, the strength parameters c' and φ' and the angle of dilation ν can all be allowed to vary with the accumulated plastic strains. One example model assuming the variation of c' and φ' with accumulated deviatoric plastic strain E^p_d is given in figure 4.9. Strain hardening occurs in zone 1, behaviour is perfectly plastic in zone 2 and strain softening occurs in zone 3. The angle of dilation is assumed to be proportional to the angle of shearing resistance φ' in zones 1 and 2 whereas in zone 3 it is assumed to reduce from the peak value assumed in zone 2 to a residual value ν_r in the same manner as φ' reduces (i.e. either linearly or exponentially).

Fig 4.10 Hardening rules

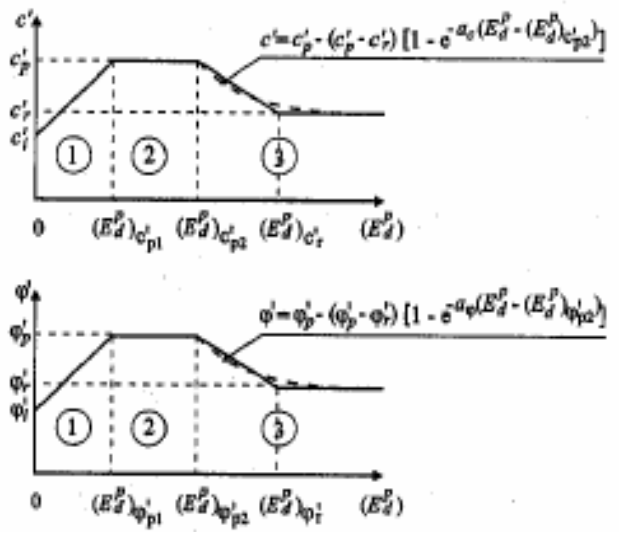

4.3.5 Cam Clay and Modified Cam Clay models (critical state models)

Cam Clay and Modified Cam Clay models were originally developed for triaxial loading conditions. The models are essentially based on the following assumptions:

- A piece of clay, which is subjected to slow, perfectly drained isotropic $(\sigma_1' = \sigma_2' = \sigma_3')$ compression, moves along a trajectory in the *v*-ln*p*' plane (*v* =specific volume $1+e,\ p' = (\sigma_1' + \sigma_2' + \sigma_3')/3)$ which consists of a virgin consolidation line and a set of swelling lines. Initially, on first loading, the soil moves down the virgin consolidation ligne

Fig 4.11 Behaviour under isotropic compression

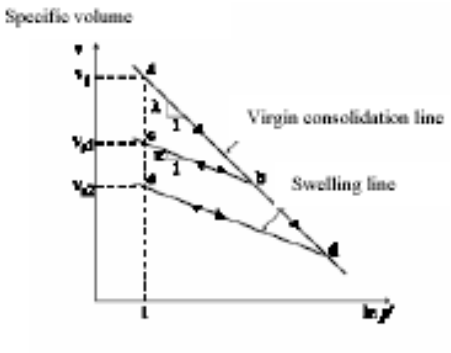

Fig 4.12 Yield surface

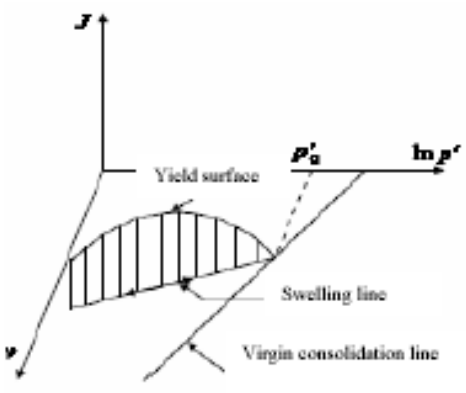

The virgin consolidation line and the swelling lines are assumed to be straight in $\upsilon - \ln p'$ space and are given by the following equations: $v + \lambda(\ln p') = v_1 \qquad v + k(\ln p') = v_s$

The values of k, λ and v_1 are characteristics of the particular type of clay, whereas the value of v_s *is* different for each swelling line. Volume change along the virgin consolidation line is mainly irreversible or plastic, while volume change along a swelling line is reversible or elastic.

The behaviour under increasing triaxial shear stress, $q = \sigma_v' - \sigma_h' = \sqrt{3J}$ (where $j = \left[(\sigma_1' - \sigma_2')^2 + (\sigma_2' - \sigma_3')^2 + (\sigma_1' - \sigma_3')^2\right]^{0.5*}(1/6)$) is assumed to be elastic until a yield value of q is reached, which can be obtained from the yield function $F(\{\sigma'\},\{K\}) = 0$.

Behaviour is elastic along swelling lines and therefore the yield function plots above each swelling line. For respectively Cam clay and modified Cam clay the yield surface are assumed to take the form:

$$F(\{\sigma'\},\{K\}) = \left(\frac{J}{p'.M_j}\right) + \ln\left(\frac{2.7183p'}{p_0'}\right) \qquad \text{(Original Cam clay)}$$

$$F(\{\sigma'\},\{K\}) = \left(\frac{J}{p'.M_j}\right)^2 - \left(\frac{p'_0}{p'} - 1\right) = 0 \qquad \text{(Modified Cam Clay)}$$

Fig 4.13 Projection of yield surface surfaces onto J-p' plane

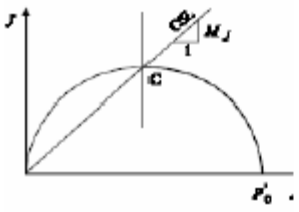

Fig 4.14 State boundary

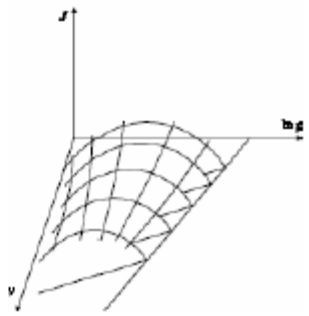

where p' is the mean effective stress, J is the deviatoric stress, M_J is another clay parameter, and p_o' is the value of p' at the intersection of the current swelling line with the virgin consolidation line. The projection of these curves onto the J-p' plane is shown in Figure 4.12 where it can be seen that the modified Cam clay yield surface plots as an ellipse. The parameter p_o' essentially controls the size of the yield surface and has a particular value for each swelling line.

As there is a yield surface for each swelling line, the yield function defines a surface in *v-J-p*' space, called the Stable State Boundary Surface. If the *v-J-p*' state of the clay plots inside this surface, its behaviour is elastic, whereas if its state lies on the surface it is elastic plastic. It is not possible for the clay to have a *v-J-p*' state that lies outside this surface.

Hardening/softening is isotropic and is controlled by the parameter p_o' which is related to the plastic volumetric strain, ε_v^p by

$$\frac{dp'_0}{p'_0} = d\varepsilon_v^p \frac{v}{\lambda - k} \qquad \text{(Hardening rule)}$$

When the soil is plastic (i.e. On the Stable State Boundary Surface), the plastic strain increment vector is taken normal to the yield curve. Consequently, the model is associated, with the plastic potential $P(\{\sigma'\},\{m\})$ being equal to the yield function.

In the original formulation, no elastic shear strains are considered. To avoid numerical problems and to achieve a better modelling inside the state boundary surface, elastic shear strains are usually computed from an elastic shear modulus, *G*, which is an additional model parameter. In the above form, both the Cam Clay and modified Cam Clay models require 5 material parameters: $v1$, k, λ, M_J and *G*. Sometimes an elastic Poisson's ratio, μ, is specified instead of *G*.

4.4 Material properties

4.4.1 The construction of the excavation

The construction is carried out in order to construct a tunnel. The excavation is 30m wide and the final depth is 20m. It extends in longitudinal direction for a large distance, so that a plane strain model is applicable. The sides of the excavation are supported by 30 m long diaphragm walls, which are braced by horizontal struts at an interval of 5.0 m, (fig 4.15)

The upper 40 m of the subsoil consists of clay, which is modelled as a homogeneous layer. The bottom of the problem to be analysed is taken at 40 m below the ground surface. Since the geometry is symmetric, only one half (the left side) is considered in the analysis. The excavation process is simulated in three separate excavation stages. The diaphragm wall is modelled by means of a plate. The interaction between the wall and the soil is modelled at both sides by means of interfaces. The interfaces allow for the specification of a reduced wall friction compared to the friction in the soil. The trust is modelled as a spring element for which the normal stiffness is a required input parameter

4.4.2 Material properties

The properties of the clay and the interfaces are shown in table 4.1. The strength reduction factor interface R_{inter} was taken as 0.5. This parameter factor relates the strength of the soil to the strength in the interfaces, according to the equations:

$$\tan \varphi_{interface} = R_{inter} \,.\, \tan \varphi_{soil} \quad \text{and} \quad C_{inter} = R_{inter} \,.C_{soil}$$

Where: $C_{soi}l = C_{ref}$

Hence, the latter value of R_{inter} gives a reduced interface friction and interface compared to the friction angle in the adjacent soil

The material properties of the diaphragm wall and the strut(anchor) are respectively shown in table 4.2 and table 4.3.

Fig 4.15 Geometry model of the situation
Of a submerged excavation

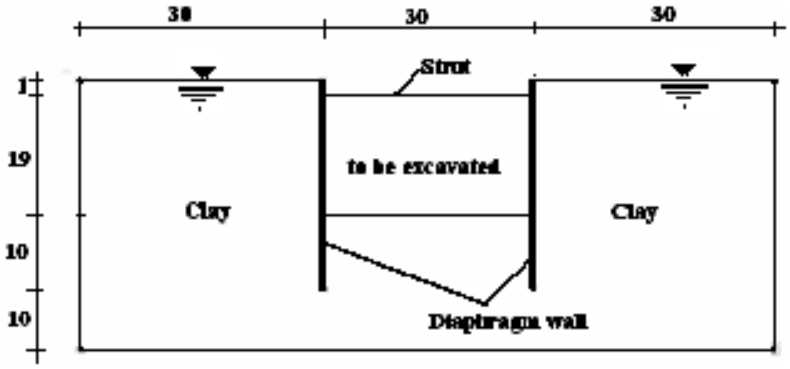

Tab 4.1 Material properties of the clay and the interfaces

Parameter	Name	Clay layer	Unit
Material model	Model	Mohr-Coulomb	-
Type of material behaviour Soil	Type	Undrained	-
Unit weight below phreatic level	γ_{sat}	18	kN/m^3
Permeability in horiz. direction	k_x	0.001	m/day
Permeability in vert. direction	k_y	0.001	m/day
Young's modulus (constant)	E_{ref}	10000	kN/ m^2
Poisson's ratio	v	0.35	-
Cohesion (monotonic loading)	c_{ref}	0.0	kN/m^2
Cohesion (monotonic loading)	c_{ref}	3.2	-
Friction angle(monotonic loading)	Ø	26°4 Monotonic	°
Friction angle(monotonic loading)	Ø	26°4 Cyclic	°
Strength reduction factor inter	R_{inter}	0.5	-

Tab 4.2 Material properties of the diaphragm wall (plate)

Parameter	Name	Value	Unit
Type of Behaviour	Material	Elastic	
Normal stiffness	EA	$7.5.10^6$	kN/m
Flexural rigidity	EI	$1.0.10^6$	$kN/m^2/m$
Equivalent thikness	d	1.265	m
Weight	w	10.0	kN/m/m
Poisson's ratio	v	0.0	-

Tab 4.3 Material properties of the strut (anchor)

Parameter	Name	Value	Unit
Type of Behaviour	Material type	Elastic	
Normal Stiffness	EA	2.10^6	kN
Spacing out of plane	L_s	5.0	m
Maximum force	$F_{max;comp}$	1.10^{15}	kN
	$F_{max;tens}$	1.10^{15}	kN

4.5 Discussion of results

4.5.1 Introduction

In practice, the construction of an excavation is a process that can consist of several phases as follows:

The wall is installed to the desired depth

Some excavation is carried out to create space to install an anchor or a strut.

The soil is gradually removed to the final depth while special measures are usually taken to keep the water out of the excavation .Struts will also be provided to support the retaining wall .

The excavation as considered in this work is to be carried out in three phases.

In this work, a comparison of the behaviour of retaining structures (i.e. sheet pile wall) under monotonic and cyclic loading was carried out.

To achieve that, a parametric study of the behaviour of the latter structure was carried out.

The commercial software “Plaxis” used in this research allows for a fully automated mesh generation procedure, in which the geometry is divided into elements of the basic type and compatible structural elements, if applicable.

The specifications of the sheet pile wall cause the analysis to be implemented in plane strain conditions. A case which is usually applied for all structures having uniform cross section and stress state in the direction perpendicular to the surface .

In other respects, due to eventual relation between the soil failure and pore pressure changes, the type of the analysis has been effective stresses.

Since the duration of the earthquake loading is small, the analysis has been done under undrained conditions.

For the sake of simplicity, the model has been made in one step in static conditions.

The Mohr coulomb model has been applied.

The properties of the clay in which the sheet pile is embedded, the sheet pile (retaining structure) and the used strut (anchor) are successively given in tables 4.1, 4.2 and 4.3.

4.5.2 Parametric study

The analyses were made for the case of sheet pile wall under undrained conditions using the shear strength parameters c' and Φ' obtained from monotonic and cyclic undrained triaxial tests (table 3.1).

To make the comparison easy, the results obtained, using shear strength parameters of monotonically and cyclically loaded soil, plots and diagrams are presented side by side.

- **Initials conditions**

Once the mesh has been generated, the finite element is complete.

Before starting the calculations, however, the initial conditions must be generated.

In general, the initial conditions comprise the initial groundwater conditions, the initial geometry configuration and the initial effective stress state.

The water weight is set to 10 kN/m^3. The water pressures are fully hydrostatic.

In "Plaxis", the full weight of the soil is applied for the generation of initial stresses.
The analysis require the generation of initial effective stresses by means of the K_o-procedure.

The K_o procedure may only be used for horizontal layered geometries with a horizontal ground surface and, if applicable, a horizontal phreatic level.

The default value of K_o is based on Jacky's formula: $K_o = 1 - \sin Ø$

4.5.3 Main results

1. Mesh deformation
2. Vertical and horizontal displacements (soil)
3. Plastic points
4. Active and excess pore pressure in the soil and interface
5. Effective horizontal stresses
6. Horizontal displacement of the sheet pile
7. Bending moment of the sheet pile

A. Mesh deformation

Fig 4.16 (a) Mesh deformation

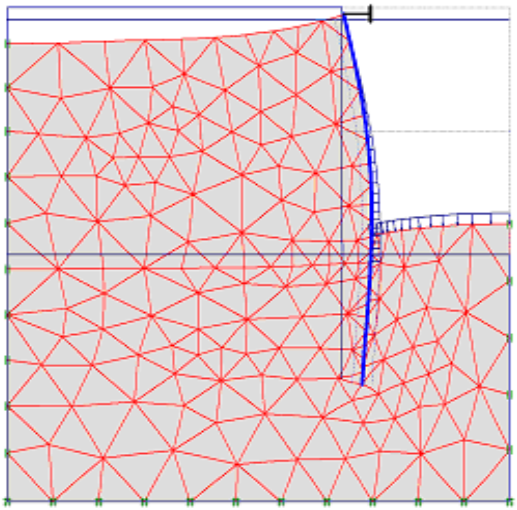

A) Monotonic
Extreme total displacement**:** 131.18 x 10^{-3}m

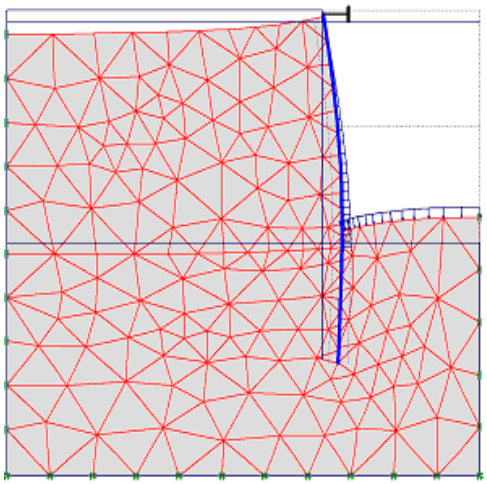

B) Cyclic
Extreme total displacement 148,46x 10^{-3} m

Fig 4.16 (b) Positions of points A, B, C, D, E and F

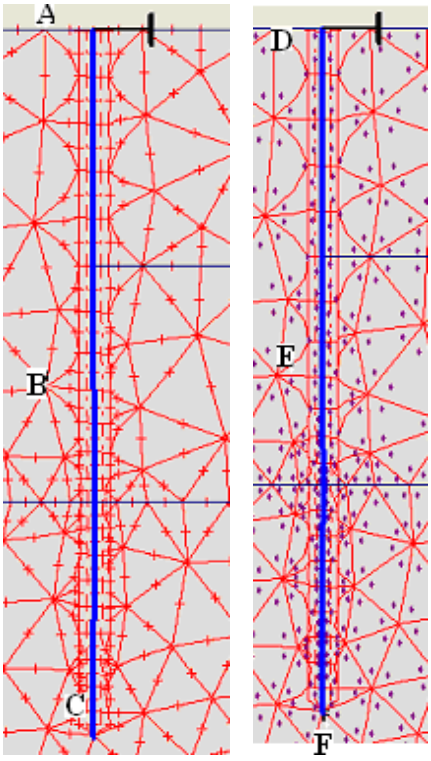

When the geometry of the model was complete, the finite element model (or mesh) was generated.

The mesh generation takes full account of the position of points and lines in the geometry model, so that exact position of layers and structure is accounted for in the finite element mesh. The generation process is based on a triangle principle that search for optimised triangles.

Figure 4.16 shows the deformation meshes of the massif of the soil of the excavation taken into account in the calculations both under monotonic and cyclic loading.

The deformed meshes clearly show settlements of the backfills and limited heaves at the bottom of the excavations.

It can be seen that a maximum total displacement observed under monotonic condition (147×10^3 m) is greater than that observed under cyclic condition (110.5×10^3 m)

Points A, b, C and D are location in the massif of clay where displacements and stresses were computed.

B. Vertical and horizontal displacements (soil)

Shadings of vertical and horizontal displacements are successively shown in figures 4.17 and 4.18.

The most improved zones are coloured in red (for vertical displacement) and in blue (for horizontal displacement).

It can be seen in table below that, vertical displacements that occurred in the backfill as well as at the bottom of the excavation were larger under monotonic than those occurred under cyclic condition.

The vertical displacements in the backfill have caused settlements while under the excavation they caused limited heave at the bottom of the excavation.

Most of the deformations were caused by the horizontal movement of the sheet pile wall, which pushed the soil up. The horizontal displacement are concentrated at the middle and the toe of the sheet pile and

It can bee seen in table 4.4 that a small increase in the cohesion induced by cyclic loading, has resulted in 11.4% and 13.2%decrease in maximum vertical and horizontal displacement respectively

Fig 4.17 Vertical displacement

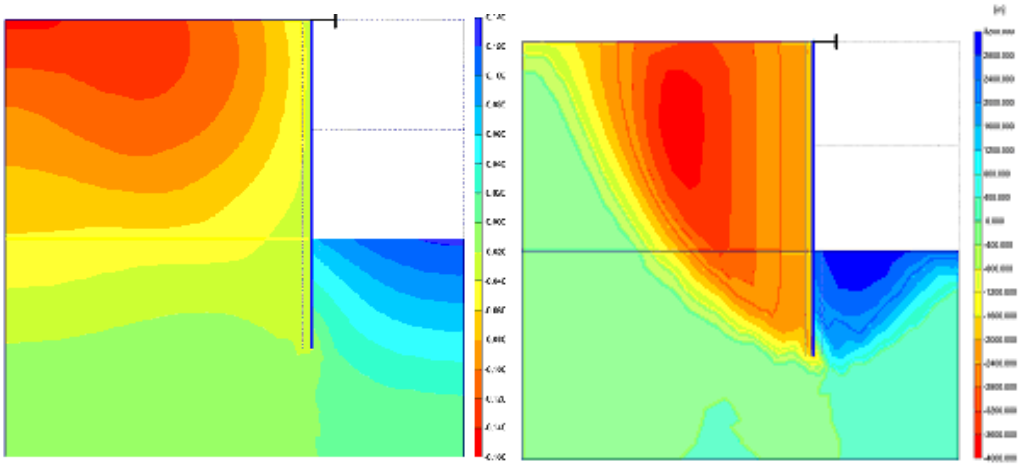

A) Monotonic
Extreme vert/displ: 145.07x 10^{-3} m

B) Cyclic
Extreme vert/displ: 128.53x10^{-3}m

Table 4.4 Maximum vertical & horizontal displacement

	Maximum displacements in 10^{-3} m			
	Vertical		Horizontal	
	Backfill	Bottom of excavation	Backfill	Bottom of excavation
Monotonic	145.07	145.07	132.40	132.40
Cyclic	128.53	128.53	115.04	115.04
Decrease in %	11.4	11.4	13.2	13.2

Fig 4.18 Horizontal displacement

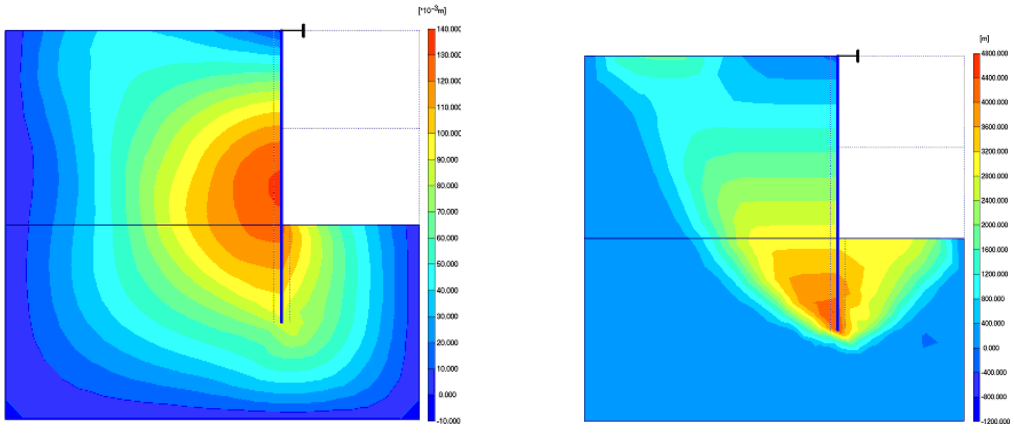

A)

Monotonic
Extreme horiz/displ: 132.40x10^{-3} m

B) Cyclic
Extreme horiz/displ: 115.04x 10^{-3}m

C. Plastic points

Mohr- coulomb and tension cut-off points are shown in figure 4.19.

It can be seen, that under monotonic conditions, while a high concentration of Mohr-Coulomb points is observeved at the lower end of the sheet pile wall, a less concentration of Mohr-Coulomb points is observed in the soil behind the sheet pile wall as well as in the soil in which the strut is fixed.

Meanwhile, under cyclic conditions, a very small areas of the soil behind the sheet pile developed scattered Mohr Coulomb points.

It can also be observed, that tension cut-off points are almost inexistent under both monotonic and cyclic loading conditions

Fig 4.19 Plastic points

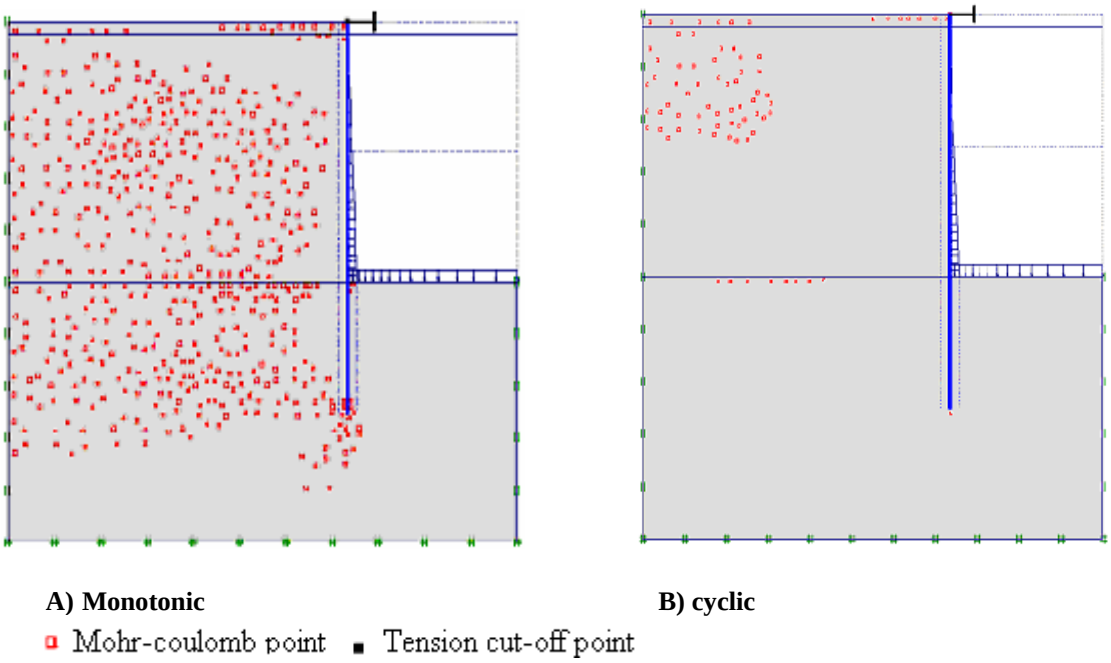

D. Pore and excess pore pressures.

Pore pressure and excess pore water pressure contours under both monotonic and cyclic conditions are respectively presented in figures 4.20 and 4.21

Under both modes of loading, high values of pore and excess pore pressures are developed at the toe of the sheet pile. This is due to the fact that this part of the sheet pile has undergone important horizontal displacements inducing a rise in pore pressure.

Maximum values of pore and excess pore pressures are shown in table 4.5
In terms of pore pressure (Table 4.5), cyclic loading

Table 4.5 Maximum pore water pressures

	Maximum pore pressure (kN/m^2) x 10^3
	Pore pressure
Monotonic	418.4
Cyclic	403.09
Decrease in %	3.65

It can be deduced from tables 4.5 and 4.6 that maximum pore and excess pore pressures developed under monotonic condition are higher than those developed under cyclic condition. This is in contradiction with the well established principal that cyclic loading will induce a supplementary pore pressure.

Fig 4.20 Active pore water pressure

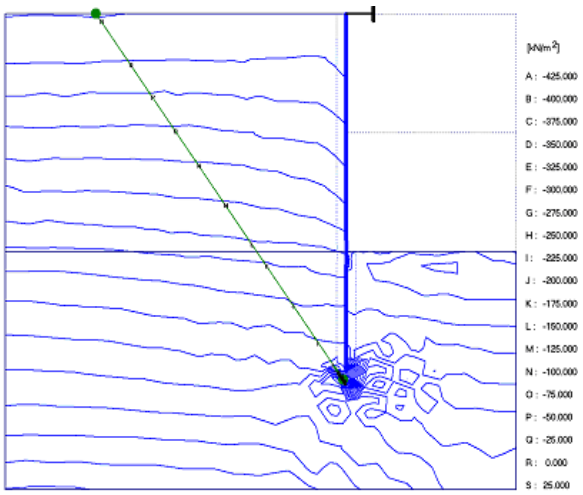

A) Monotonic
Maximum value: $418.4 kN/m^2$

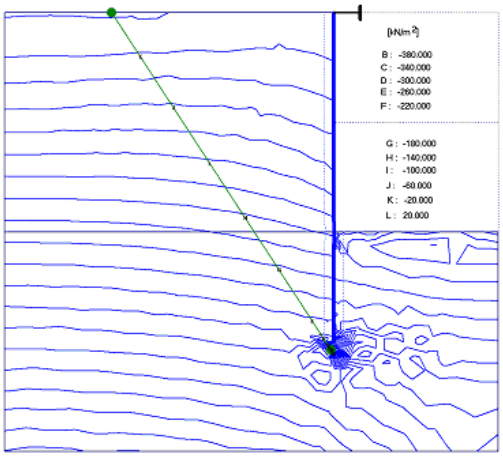

B) Cyclic
Maximum value: $403.09 kN/m^2$

Fig 4.21 Excess Pore water pressures

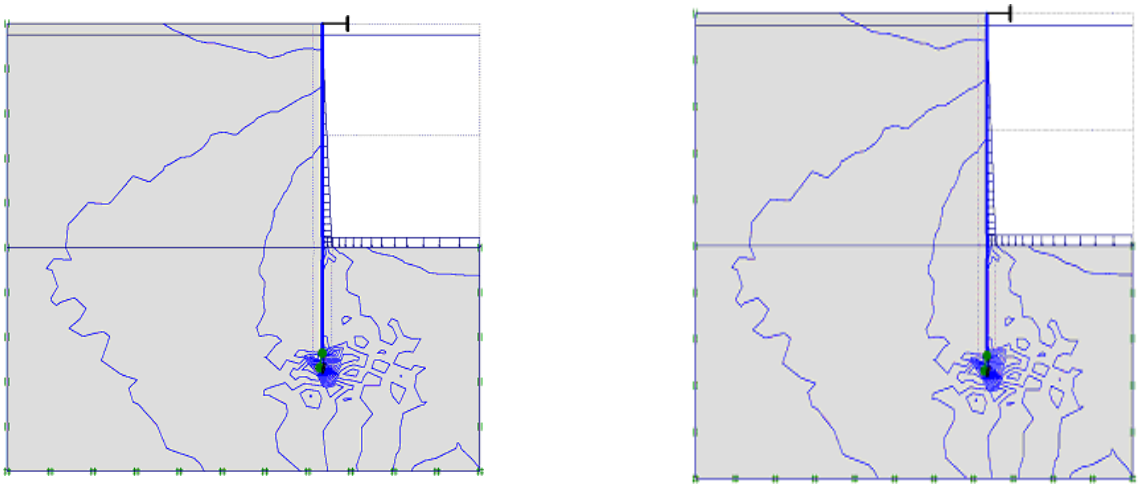

A) Monotonic - Maximum value: 264.6kN/m^2 **B) Cyclic**- Maximum value: 240.18kN/m^2

A better comparison of pore pressure behaviour, under the two modes of loading, can be obtained from plots of excess pore water pressures at points D,E and F as shown in figure 4.22 (a,b,c).

In the latter figure, it can easily be observed that cyclic loading has induced higher excess pore pressures under cyclic loading (Table 4.6)

Table 4.6 Excess pore pressures at points D,E and F

	Excess pore pressures (kN/m^2)		
	Point D	Point E	Point F
Monotonic	4.0	39.0	6.0
Cyclic	6.0	47.0	18.5
Increase in %	50.0	20.15	208.3

Fig 4.22 Excess Pore water pressures **at** points D, E and F

a) **b)**

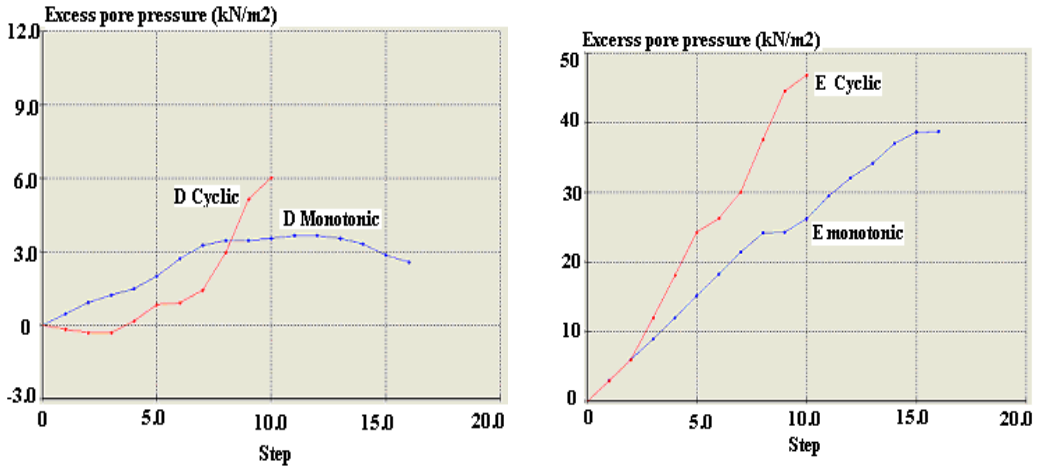

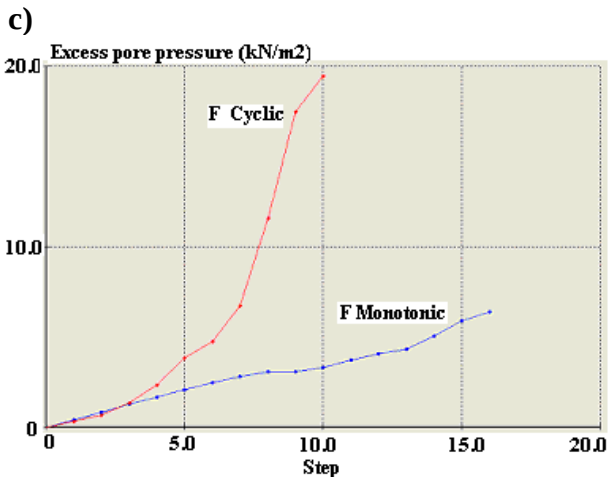

E. Horizontal displacement of the sheet pile

Fig 4.23 Horizontal-displacement vs. depth

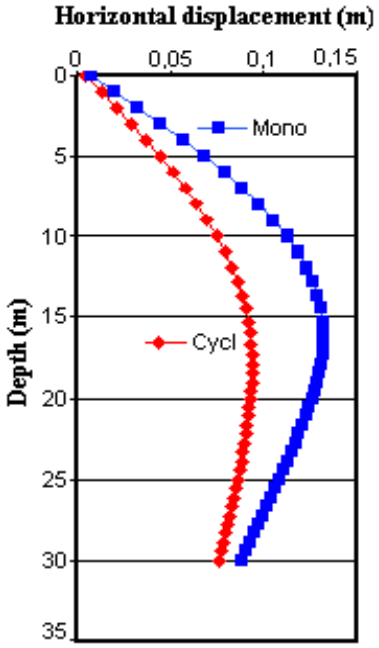

Plots of horizontal displacements versus the depth of the sheet pile are shown in figure 4.23.

It is seen that cyclic loading expressed by a small increase in the cohesion (3.2 kN/m^2) has resulted in a 45.4% decrease in the horizontal displacement in the mi-height of the sheet pile.

F. Effective horizontal stresses

Due to the low permeability of the clay soil, cyclic loading induces a pore pressure rise.

As the Influence of pore pressure on the overall behaviour of clay soil under cyclic loading is of a paramount importance, the stress analyses must carried out in terms of effective stress.

Curves of effective horizontal stresses versus steps of calculation for points D, E and F are presented in figure 4.24.

Maximum values of effective horizontal stress for the latter points are given in Table 4.7.

Table 4.7 Effective horizontal stresses at points D, E and F

	Effective horizontal stress (kN/m^2)		
	Point D	Point E	Point F
Monotonic	7.5	85.0	135
Cyclic	14	85.0	167
Increase in %	86.7	0.0	23.7

It can be seen in table 4.4, that at points D and E, cyclic loading has no great effect on the effective horizontal stresses .This is mainly due is due the small horizontal displacements experienced by the two points.

At point F where large horizontal displacements were observed, large values of the effective horizontal stresses were found under both modes of loading

Fig 4.24 Effective horizontal stress kN/m^2

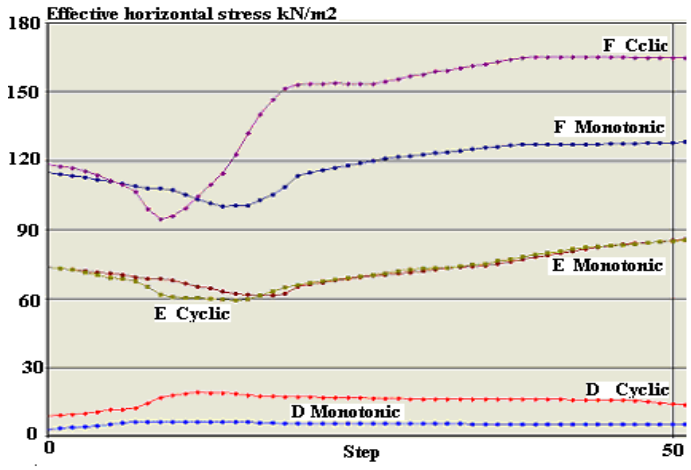

G. Bending moment of the sheet pile

Plots of the bending moments against the depth of the sheet pile are shown in figure 4.25. The increase of 3.2kN/m^2 in the cohesion induced 44% decrease of bending moments developed at mid-height of the sheet pile.

Fig 4.25 Bending moment vs. depth

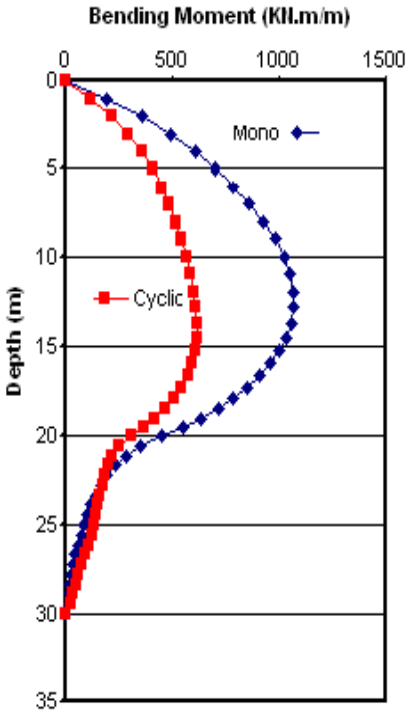

4.6 Conclusion

In this second part of this research work, a parametric study has been carried out.

The effects of the variation of the cohesion of internal friction resulting from cyclic loading, on the behaviour of sheet pile wall have been observed.

An increase of the cohesion of 3.2 kN/m^2 has induced:

1- A large diminution of the plastic zones at the backfill and below the excavation tension cut of zone has nearly disappeared under cyclic loading.
2- A diminution of vertical displacement resulting in settlements of the backfill and a reduction of the bottom of the excavation.
3- An increase in excess pore pressure is observed.
4- A decrease in horizontal sheet pile wall displacements.
5- A part from the ends.
6- of the sheet pile where no variation in the bending moments were observed, a large decrease in the bending moments were observed

CHAPTER 5:

GENERAL CONCLUSIONS

5.1 General Conclusions

a) Monotonic tests

- Under monotonic (compression and tension) loading the normalised shear strength ($D_{max}/\sigma_{0'}$) at failure increased with increasing strain rate.

- The effective failure envelope inferred from the slowest monotonic compression and extension tests had C'=0; Ø'= 23°.4 in compression, and C'= 0, Ø'= 28.4° in extension .
- The limited amount of data indicate that increasing strain rate may affect C' and Ø'.

- Accurate mid-height pore water pressures relevant to failure conditions were consistently measured.

- Expressed in terms of the initial effective stress, the excess pore pressure at failure decreased with increasing strain rate. In terms of effective stress, the increase in shear strength with increasing strain rate may be partly explained by the reduction of pore pressure at failure and partly by strain rate effects on C' and 0' parameters.

b) Cyclic tests

- The higher the initial effective stress ratio τ/σ_0'the smaller the number of cycles required to reach a specified ϵ_{da}

- Except for the first cycle, the stiffness measured in compression was similar to that measured in tension. During the first cycle of the compression/ tension tests, the samples were much stiffer in compression than in tension. The opposite behaviour appears to occur under tension/compression loading this behaviour may be due to

structural anisotropy resulting from the consolidation process and the direction of initial loading.

- The initial migration of the effective stress path away from the origin (also observed by Takashi et al (1980) (20) is believed to be due to the tendency for volume increase associated with over-consolidated samples, which would result in a decrease in pore pressure and an increase in the mean effective stress during the first cycle. However, with an increasing number of cycles, the tendency for volume increase reduces and, due to reversed shearing, the pore water pressure level rises again, resulting in a gradual decrease in the mean effective stress.

- The fact that the effective stress paths for the cyclic tests travel beyond the effective failure envelopes inferred from slow monotonic tests appears to be related to differences in rate of loading.

- Mean excess pore pressure increases with the number of cycles

- Good correlation of the double amplitude of the mid-height pore pressure with the theoretical change in mean total stress 2D/3 is observed.

The effects of the variation of the cohesion of internal friction resulting from cyclic loading, on the behaviour of sheet pile wall have been observed.

An increase of the cohesion of 3.2 kN/m^2 has induced:

1- A large diminution of the plastic zones at the backfill and below the excavation tension cut of zone has nearly disappeared under cyclic loading.

2- A diminution of vertical displacement resulting in settlements of the backfill and a reduction of the bottom of the excavation.
3- An increase in excess pore pressure is observed.
4- A decrease in horizontal sheet pile wall displacements.
5- A part from the ends.
6- of the sheet pile where no variation in the bending moments were observed, a large decrease in the bending moments were observed

5.2 Suggestions for future work

For the amount of data provided by the experimental work was limited, further investigation is needed to achieve a better understanding of the behaviour of retaining structures under cyclic loading.
The effects of the variation of the mean total stress on the pore pressure behaviour and clay softening under monotonic (compression and tension) as well as under cyclic loading must be investigated. This could be achieved if different series of monotonic and cyclic tests with the same initial effective stresses were carried out as follows:

a) Monotonic (compression/tension) tests with constant cell pressure.
b) Monotonic (compression/tension) tests with constant cell pressure.
c) Cyclic (compression/tension and tension/ compression) tests with constant cell pressure.
d) Cyclic (compression/tension and tension/ compression) tests with constant mean total stress.

Table3.5: Axial strain at maximum$\pm_{D\,max}$ for tests of series C

Test Code	Type of Test	σ_o'	τ / σ_o'	τ / Cu	Cycle No.1		Cycle No.2		Cycle No.7	
					ϵ_A at +Dmax	$\epsilon_{A\,at}$ -Dmax	$\epsilon\varepsilon_A$ at +Dmax	ϵ_A at -Dmax	ϵ_A at +Dmax	ϵ_A at -Dmax
		kN/m^2			%	%	%	%	%	%
C.1	Comp/Tens	81.4	±0.5	±0.59	1.88	-1.35	2.09	-1.84	3.47	-4.51
C.2	Comp/Tens	72.5	±0.57	±0.59	2.05	-1.46	2.38	-1.9	4.03	-4.58
C.3	Comp/Tens	81.3	±0.5	±0.59	2.04	-1.2	2.41	-1.56	4.15	-3.63
C.4	Comp/Tens	85	±0.48	±0.59	1.80	-1.11	2.07	-1.61	3.81	-4.37

REFERENCES

A THAMMATHIWAT et AL. *" behaviour of strenght and pore pressure of soft clay under cyclic loading".* Thammasat .Ing.J.Sc. Tech Vol 9 n° 4 page 21-28. 2004

ANDERSEN, K.H. *"Behaviour of clay subjected to undrained cyclic loading"*. Proc. 1st Int. Conf. on .Behaviour of Offshore Structures, Trondheim, Vol 1, 3926403. 1976.

ANDERSEN, K.H., POOL, J.S, BROWN, S.F., ROSENBRAND, W.F. *"Cyclic and static laboratory tests on Dramen clay"*, Proc. A.S.C.E, Vol 106, No UTS, 499-529. 1980

BARDEN, L. a McDERMOTT, R.J.W. *"Use of free ends in triaxial testing of clays"*. J. Soil Mech. Found. Div., A.S.C.E., 91, SM6, 1-23. 1965.

BERRE, T. and BJERRUM, L., *"Shear strength of normally consolidated clays"*. Proc; 8th Int .Conf. on Soil Mechanics and Foundation engineering, Moscow, Vol 11, 39—49. 1973.

BISHOP, A.W.and HENKEL, D.J. *"The measurements of soil properties in the triaxial test"*. Edward Arnold Ltd., London, England. 1967.

BJERRUM, L., *"Geotechnical problems involved in foundation structures in the North Sea"*. Geotechnique, Vol 23, No.3. 319-358. 1973.

BJERRUM, L., SIMON, N. and TORBOLAA, I. *"The effect of time on the shear strength of a soft marine clay"*. Proc. Brussels Conf. on Earth Pressure Problems, Vol 1, 148—158. 1958.

CASAGRANDE, A. and SHANNON, W. *"Research on stress deformation and strength characteristics of soils and soft rocks under transient 1oading"*. Pub. Harvard University Grad, Sch., Eng., Soil Mech., Series No.31. 1948.

CASAGRANDE, A. and SHANNON, W.L. *"Strength of soils under dynamic loads"*. Trans. Amer. Soc. Civ. Engs. 114, 755-772. 1949.

CRAIG, W.H. *"Strain rate and viscous effects in physical models"*. Proc. Conf .Soil Dynamics and Earthquake Eng., Southampton, 351-365. 1982.

CRAWFORD C.B. *"The influence of rate of strain on effective stresses in a sensitive clay"*, Soc. Testings Mat., Special Technical Pub. No. 254, 36-61. 1959.

FISHER, J.A., KOUTSOFTAS, D.C., LU, T.D. *"The behaviour of marine soils under cyclic loading"*. Proc. B.O.S.S. 76 Norwegian Inst. of Tech., Vol 2, 407-417. 1976.

G. LEFEBVRE, et AL. *" stability threshold for cyclic loading of saturated clay"*. Canad geotech journal. Vol 26 n° 1 page 122-131. (1989).

GRAHAM, J CROOKS, J.H.A., BELL, A.L. *"Time effects on the stress behaviour of natural clay"*. Géotechnique, Vol 33, Mc 3, 327-340. 1983.

HIGHT, D.W. *"A simple piezometer probe for the routine measurement of pore pressure in triaxial tests on saturated soils"*, Geotechnique, Vol 32, No 4, 396-401. 1982.

KACHACHI, G.B. *"The behaviour of clays under reversed undrained triaxial cyclic loading"*. MSc thesis, University of Manchester. 1983.

KACHACHI, J.A.A. *"The behaviour of normally and overconsolidated clays under cyclic loading"*. MSc thesis, University of Manchester. 1981.

KHAFFAF, J H. *"The behaviour of saturated undrained clay under cyclic loading conditions"*. MSc thesis, University of Manchester. 1975.

KHAFFAF, J.H. *"Weakening of undrained saturated c1a under cyclic triaxial stress"*. Ph.D Thesis, University of Manchester. 1978.

KIMURA, T., SAITOHK. *"Thee influence of disturbance due to sample preparation on the undrained strength of saturated cohesive Soil".* Soils and Foundations Vol 22, No 4, 109-120. 1982.

KOUTSOFTAS, D.C. *"Effect of cyclic loads on undrained strengths of two marine clays"* Proc.A.C.C.E., Vol 104, GT5, 609-619". 1978.

KVALSTAD, T.J., DAHBERG, R. *"Cyclic behaviour of clay as measured in laboratory"*. Int. Symp. of Soils under cyclic and transient loading, Swansea, 157-166. 1980.

L.CALLISTO et AL (1998). *" Mechanical behaviour of natural soft clay"*. Geotechnique Vol 48 n° 4 page 495-513.

LEE, K.L.,*"Cyclic loading triaxial tests on undisturbed samples of North Sea clay soil"*, Unpublished draft report. 1974.

M. HYODO,Y. YAMAMOTO and M. SUGIYAMA *" Undrained cyclic shear behaviour of clay with initial static shear stress".* built Environment (Japan) Vol 3. 1993.

OLSON, R.B. *"Discussion on shear strength of saturated remoulded clays"*. Proc. Conf. on shear strength of cohesive soils, Boulder, Colorado, (U.S.A.), 1043- 1049. 1960.

PROCTER, D.C., KHAFFAF, J.H. *"Cyclic triaxial tests on remoulded clays"*. Proc. A.S.C.E., Div., Geotechnique Engineering, Vol 110, No 17, 1431-1445. 1984.
RICHARDSON, A.M., WHITMAN, E.V., *"Effect of strain rate upon undrained shear resistance of saturated remoulded fat clays"*, Geotechnique, Vol No.4, 310-324. 1983.
ROWE, P.W. *"Sand liquefaction and clay softening with cyclic loading"*. Unpublished internal report, Engineering Department, university of Manchester. 1974.
ROWE, P.W., BARDEN, L. *"The importance of free ends in the triaxial test"*, J. Soil. Mech., Found, Div. A.S.C.E., Vol 90, 5141, 1-27. 1964.
S. TEACHAYORASINSKUN et AL. "Shear modulus and dumping of soft Bangkok clays". Canad geotech journal. Vol 39 n° 5 page 1201-1208. 2002
SEED, H.B., CHAN, C.K. *"Clay strength under earthquake loading conditions"*. J. Soil Mech. Found. Div., A.S.C.E., Vol 92, SM2, 53-78. 1966.
SHIMMING, B.B., HASS, H.J.H., SAXE, 11.0., *"Study of dynamic and static failure envelopes"*. J. of Soil Mech". Found. Div. A.S.C.E., Vol 92, 105-123. 1966.
TAKAHASHI, M., HIGHT, D.W. and VAUGHAN, P.R. *"Effective stress changes observed during undrained cyclic triaxial tests on c1ay"*. Int. Symp. on Soils under Cyclic and Transient Loading", Swansea, Vol 1, 201-209. 1980.
THIERS, G.R., SEED, 11.3. *"Cyclic stress-strain characteristics of clay"*. J. Soil Mech. Found. Div., A.S.C.E., 94, SM2, 555-569. 1968.
THIERS, G.R., SEED, H.B. *"Strength and stress-strain characteristics of clays subjected to seismic loading conditions"*, Symp. Â.S.T.M., STP45O, 3-36. 1969.
WHITMAN, E.V.*"Some consideration and data regarding the shear strength of clays"*, Colorado, 581- 614. 1960.